YEAR-END TECHNICAL REPORT
September 29, 2022 to September 28, 2023

Environmental Remediation Science and Technology

Date submitted:

December 8, 2023

Principal Investigator:

Leonel E. Lagos, Ph.D., PMP®

Florida International University Collaborators:

Yelena Katsenovich, Ph.D.
Ravi Gudavalli, Ph.D.
John Dickson, Ph.D.
Pieter Hazenberg, Ph.D.
Angelique Lawrence, M.S., GISP
Vadym Drozd, Ph.D.
DOE Fellows

Submitted to:

U.S. Department of Energy
Office of Environmental Management
Under Cooperative Agreement # DE-EM0005213

FIU | Applied Research Center
FLORIDA INTERNATIONAL UNIVERSITY

Addendum:

This document represents one (1) of five (5) reports that comprise the Year End Reports for the period of September 29, 2022 to September 28, 2023 prepared by the Applied Research Center at Florida International University for the U.S. Department of Energy Office of Environmental Management (DOE-EM) under Cooperative Agreement No. DE-EM0005213.

The complete set of FIU's Year End Reports for this reporting period includes the following documents:

Project 1: Chemical Process Alternatives for Radioactive Waste
Document number: FIU-ARC-2022-800012997-04b-007

Project 2: Environmental Remediation Science and Technology
Document number: FIU-ARC-2022-800013918-04b-006

Project 3: Waste and D&D Engineering and Technology Development
Document number: FIU-ARC-2022-800013919-04b-007

Project 4: DOE-FIU Science & Technology Workforce Development Initiative
Document number: FIU-ARC-2022-800013920-04b-011

Project 5: Long-Term Stewardship of Environmental Remedies: Contaminated Soils and Water and STEM Workforce Development
Document number: FIU-ARC-2022-800013922-04b-005

Each document will be submitted to OSTI separately under the respective project title and document number as shown above. In addition, the documents are available at the DOE Research website for the Cooperative Agreement between the U.S. Department of Energy Office of Environmental Management and the Applied Research Center at Florida International University: https://doeresearch.fiu.edu.

For Project 2: Environmental Remediation Science and Technology, the reports included in the Appendices are written in manuscript format with the intention of submitting them for publication in peer-reviewed journals. Posting these documents on the web would make them ineligible for publication due to a self-plagiarism issue, which could be identified by plagiarism detection software, such as Turnitin.

TABLE OF CONTENTS

LIST OF FIGURES

LIST OF TABLES

PROJECT 2 EXECUTIVE SUMMARY

This project focuses on research to support environmental remediation and long-term monitoring of contaminated sediment, surface water, and groundwater at the Hanford Site, Savannah River Site, Oak Ridge Reservation, and the Waste Isolation Pilot Plant (WIPP). The objective is to reduce the potential for contaminant mobility or toxicity in the surface and subsurface through the development and application of state-of-the-art environmental remediation technologies at DOE sites.

In FIU Year 3, FIU ARC provided research and technical support for contaminant remediation efforts at the Hanford Site under Task 1, at SRS under Tasks 2 and 3, at the WIPP under Tasks 5 & 6, and at the ORR under Task 7. The research involved laboratory-scale studies that utilized novel analytical methods and microscopy techniques for the characterization of various mineral samples. Tasks also included the implementation of hydrological models to predict the behavior and fate of existing and potential contaminants in the surface and subsurface. Photogrammetry techniques were also applied for the development of high-resolution digital elevation models (DEMs) to support hydrological model development.

DOE Fellows supporting this project include Kirstin Olson (Undergraduate, Environmental Engineering), Melissa Dieguez (Undergraduate, Biomedical Engineering), Aubrey Litzinger (Graduate, M.S., Environmental Engineering), Caridad Estrada (Undergraduate, Environmental Engineering), Carolina Trummer, (Undergraduate, Environmental Engineering), Hannah Aziz (undergraduate, Environmental Engineering), Melanie Sztybel (Undergraduate, Civil Engineering), Mariah Doughman (graduate, Ph.D., Chemistry), Phuong Pham (graduate, Ph.D., Chemistry) Carolyn Grace Cooke (graduate, Ph.D., Chemistry), and Stevens Charles (undergraduate, Civil Engineering).

The following ARC researchers are supporting this project and mentoring the DOE-EM Fellows: Yelena Katsenovich (Ph.D., Env. Engineering, Tasks 1.2, 1.3, 1.4 & 1.5, Project Manager), Ravi Gudavalli (Ph.D., Env. Engineering, Tasks 2.1 & 2.2, Research Scientist), John Dickson (Ph.D., Agricultural Chemistry and Soil Science/Environmental Soil Chemistry, Tasks 5 & 7, Sr. Research Scientist), Pieter Hazenberg (Ph.D., Hydrology and Quantitative Water Management, Tasks 3 & 6, Sr. Research Scientist), Angelique Lawrence (M.S., Environmental Science, Tasks 3 & 6, Research Specialist II), Vadym Drozd (Ph.D., Inorganic Chemistry, Task 1.4, Research Associate), Jose Rivera (B.S., Civil Engineering, Research Analyst), Leonel Lagos (Ph.D., PMP®, Mechanical Eng./Civil/Env. Engineering, PI).

Task 1: Remediation Research and Technical Support for the Hanford Site

DOE EM has a critical need to understand the biogeochemical processes influencing the behavior of contaminants (uranium (U), iodine (I), technetium (Tc), chromium (Cr), and nitrate (NO_3^-)) in Hanford Site's deep vadose zone, which can impact groundwater quality. These contaminants were accidentally released during the production of atomic weapons at the Hanford Site from 1944 through the late 1980s, leaving a legacy of radionuclide contamination in soil and groundwater. This legacy pose technically complex environmental cleanup challenges unique to EM. The radioactive waste at the Hanford Site contains about 195 million curies of radioactivity and 220,000 metric tons of chemicals contaminants. Among the 177 tanks onsite, sixty-seven have leaked about 3,800 cubic meters (1 million gallons) of liquids into the underlying sediment. In

addition to chemical waste remaining in tanks, significant contamination still persists in the soil, groundwater, and burial grounds (Gephart, 2003). Most of this residual waste is in or near the 200 Area, creating plumes that threaten groundwater quality due to potential downward migration through the unsaturated vadose zone (VZ) sediment. The fastest-moving contaminants in the subsurface are technetium-99, iodine-129, chromium, uranium, and nitrate (Gephart, 2003).

Task 1 component of this end-of-year report presents an overview of subtasks supporting the cleanup mission at the Hanford Site, complementing ongoing work at PNNL to better understand the long-term behavior of contaminants in the subsurface.

Task 2. Remediation Research and Technical Support for Savannah River Site

Iodine-129 and uranium stand out as the major risk drivers among radiological acid waste contaminants released at the Savannah River Site's F-Area. Radionuclides, previously disposed of in unlined seepage basins as constituents of acidic aqueous waste, are migrating towards Fourmile Branch and Tims Branch wetlands through natural groundwater flow. Here, they may interact with natural organic materials in the wetland or with humic materials injected for remediation purposes.

There is a pressing need for the Savannah River Site (SRS) to collect results supplementing permit requirements associated with the Area Completion Project (ACP), specifically the Phase 2 strategy evaluating the performance of Phase 1, including areas downgradient of the F-Area inactive process sewer line and at Fourmile Branch. As per the corrective action plan's permitting requirements, ^{129}I concentrations must meet groundwater standards in Fourmile Branch by October 31, 2025, and in the F-Area plume in surface water at the seepline by October 31, 2030. Given the absence of DOE-approved technology for subsurface iodine remediation, understanding its long-term fate in plumes at the Savannah River Site is crucial. Additionally, DOE-EM mandates further study of the fate of co-mingled contaminant plumes due to their complexity (McCabe, D., et al., 2017).

The experiments outlined in this task will contribute to our understanding of the interactions of ^{129}I with organic materials, study the factors controlling the attenuation of ^{129}I in wetlands, and assess the potential for U remediation through the injection of modified humic materials. These findings will provide essential data for meeting the aforementioned permitting requirements and DOE-EM goals.

SRS is undertaking synergistic research, funded by the Department of Energy's Environmental Management Office of Soil and Groundwater Remediation, as part of the Attenuation-Based Remedies for the Subsurface Applied Field Research Initiative (ABRS AFRI). This applied research aims to develop science-based approaches for cleaning and closing sites contaminated with combinations of metals, radionuclides, and other contaminants of concern.

A primary objective of this program is to devise attenuation-based remedies, specifically to investigate and validate the use of humate for subsurface stabilization of metals in contaminated groundwater plumes. SRS successfully conducted a field campaign demonstrating the viability of dissolving and injecting low-cost agricultural humate into the subsurface. The proposal suggests that this method may serve as a viable attenuation-based remedy for uranium and potentially for I-129 as well. Humic acid, with its numerous functional groups, plays a crucial role in ion exchange and acts as a metal complexing ligand with high complexation capacity, influencing the mobility of radionuclides in natural systems.

The fate and transport of uranium and iodine in the subsurface are influenced by various environmental factors, including pH, temperature, ORP, etc. A comprehensive understanding of the environmental conditions affecting these processes is crucial for a more realistic risk assessment. In FIU Performance Year 3, research was conducted to investigate the factors controlling the attenuation of iodine in wetlands. Additionally, ongoing research explored the impact of humic acid on uranium mobility at the Savannah River Site. Various types of humic substances, such as KW-30, were utilized in this research to assess their effect on cocontaminant removal.

The Task 2 component of this end-of-year report provides an overview of subtasks supporting the Area Completion Project to reduce iodine contamination, as well as the Attenuation-Based Remedies for the Subsurface Applied Field Research Initiative.

Task 3: Contaminant Fate and Transport Modeling for the Savannah River Site

This task involves the development and application of integrated hydrology and contaminant transport models for studying the fate of priority pollutants with emphasis on interactions between solute and sediment transport in the stream systems at SRS. The aim is to examine the response of these streams to historical discharges and environmental management remediation actions. The knowledge gained through these studies will provide a means of assessment, evaluation and post-closure long-term monitoring of water quality and environmental conditions following remedial activities. In general, hydrological models are the standard tools used for investigating surface/subsurface flow behavior. They provide uncertainty quantification, risk and decision support for water resource management, and evaluation of water quality, erosion, deposition, and transport. The models being developed by FIU will serve as long-term monitoring tools that provide simulation capabilities to economically assess the fate and transport of heavy metals and radionuclides of concern (e.g., uranium and I-129), that may have direct or indirect impact on the SRS environment. The models will provide information needed for informed decision-making in existing DOE-EM soil and groundwater remediation programs. Results obtained will provide DOE-EM suggestion of key locations for contaminant monitoring. Furthermore, the models can be utilized as forecasting tools to predict suspended sediment loads and the extent of remobilization regimes under different scenarios of extreme storm events and erosion conditions. This research

The Task 3 component of this end-of-year report presents an overview of subtasks that will assist DOE-EM in ensuring the achievement and maintenance of regulatory compliance goals for water quality in the SRS watersheds and in developing cost-effective remediation plans integrated into the SRS Area Completion Project (ACP) thus accelerating progress of the DOE EM environmental restoration mission.

Task 5: Research and Technical Support for WIPP

FIU is engaged in basic research in collaboration with researchers from Los Alamos National Laboratory's Actinide Chemistry and Repository Science (ACRSP) and DOE Carlsbad Field Office (DOE-CBFO) to establish the scientific basis for the long-term disposition of nuclear wastes in the WIPP repository. The solubility of actinides is a key factor influencing the fate and transport of radionuclides in the subsurface environment, particularly in the far field of a nuclear waste disposal site like the Waste Isolation Pilot Plant (WIPP). In addition to the low-probability scenario of groundwater intrusion, the presence of metal-chelating organic ligands, iron oxide minerals

(magnetite), and intrinsic actinide colloids may offer a potential release pathway for the migration of actinides.

This research examines the impact of isosaccharinate (cellulose degradation product) on sorption of actinide onto iron mineral (pyrite, $Fe^{2+}[S_2]^{2-}$) under anaerobic condition and high ionic-strength brine environments representative of the WIPP repository. As a polyhydroxy carboxylic acid similar to gluconate, isosaccharinate (ISA) is an important byproduct of alkaline degradation of cellulose in cement pore waters that is considered a major concern in many performance assessments (PAs) of nuclear waste repositories containing cement materials (Hummel, 2005). This knowledge is important for addressing the low-probability scenario of potential brine inundation and contaminant release due to human intrusions.

The Task 5 component of this end-of-year report provides an overview of subtasks supporting the acquisition of updated sorption data for the interaction of actinides with minerals and organic ligands within the WIPP environment. The goal is to enhance previous risk assessment models characterized by high uncertainty.

Task 6: Hydrology Modeling for Basin 6 of the Nash Draw near the WIPP

Scientists and researchers are concerned about the impact of climate on the karst region surrounding the Waste Isolation Pilot Plant (WIPP) and the long-term vulnerability, integrity and performance of this deep geologic transuranic waste repository due to the influence of characteristic surface features, such as sinkholes, swallets, and karst valleys, on groundwater recharge over time. Long-term changes in climate that are anticipated to occur within the south/southwestern USA are expected to result in more frequent intense precipitation events. It is currently unknown if this will lead to increased groundwater recharge or whether this results in increased surface flow and evapotranspiration. It is unclear whether groundwater recharge would be impacted and how, if impacted, this might affect the dissolution rate of halite within the subsurface. Task 6 was developed to support DOE-EM research and development activities at the Waste Isolation Pilot Plant (WIPP) by developing a high-resolution digital elevation model (DEM) of Basin 6 of the Nash Draw, just west of the repository, to more accurately delineate surface hydrological features and provide a foundation for development of a regional hydrological model using the DOE-developed Advanced Terrestrial Simulator (ATS). A high-resolution DEM will improve the ability of the coupled surface/subsurface flow model to simulate the hydrologic response to a range of storm events, compute the surface water balance and provide more accurate estimates of regional-scale infiltration rates/groundwater recharge. With improved estimates of the spatial and temporal patterns of recharge to force the groundwater model, predictions of halite dissolution and propagation of the shallow dissolution front will be made possible and the potential impact on repository performance quantified.

The Task 6 component of this end of year report presents an overview of subtasks supporting the understanding of the role of heavy precipitation events on groundwater recharge through surface depressions like sinkholes and how this can impact the long-term stability of the WIPP.

Task 7: Engineered Multi-Layer Amendment Technology for Hg Remediation on Oak Ridge Reservation

This task involves the development of a sorbent-based technology for cost-effective remediation of mercury on the Oak Ridge Reservation (ORR). The persistent geochemistry of mercury, its bio accumulative effects, and continuous cycling through the environment complicate efforts to

develop effective technologies for mercury remediation in freshwater stream ecosystems, such as the East Fork Poplar Creek (EFPC) in Oak Ridge, Tennessee.

As a case study, the EFPC ecosystem received large point-source discharges during the 1950s. While upstream mercury discharges to EFPC have declined, mercury releases still persist from point sources within the industrial facility where mercury was used, as well as from diffuse downstream sources such as contaminated bank soils. Recent results suggest that releases from diffuse and historical downstream sources, such as bank soils and sediment, are the key drivers of mercury contamination in the stream ecosystem.

Despite the widespread use of amendments for in-situ sequestration of organic contaminants, large-scale application of mercury sorbents is uncommon due to decreasing effectiveness in the presence of dissolved organic matter (DOM), cost constraints, and fouling problems that can potentially leach constituents and particles into water bodies. Thus, the primary goal of this research is to develop a sustainable, cost-effective solution for mercury cleanup in EFPC.

The Task 7 component of this end of year report presents an overview of the research supporting the DOE's Office of Environmental Management (EM) in addressing its priority mission of improving water quality and ecological health of EFPC.

MAJOR TECHNICAL ACCOMPLISHMENTS

Task 1: Remediation Research and Technical Support for the Hanford Site

Subtask 1.2:

- FIU completed SEM/EDS analysis to evaluate the elemental composition in each of the dried solid samples and provided mapping of elements such as Ca, Fe, Na, Si, Al, and U that allow visualization of elemental associations on the sample surface.
- FIU gave an oral presentation at WM2023 based on the results of Subtask 1.2, *Re-oxidation Behavior of Technetium-99 and Uranium Immobilized by Strong Reductants*, authored by Yelena Katsenovich, Angel Almaguer, Nikolla Qafoku, Jim Szecsody, Hilary Emerson, and Leonel Lagos.
- FIU completed sample collection for the batch experiment and pH, ORP, and O_2 measurements for CPS–amended samples in anaerobic conditions for Phase 1 and aerobic conditions for Phase 2.
- FIU completed reoxidation experiments of samples amended with 0.5% and 5.0 vol% calcium polysulfide (Milestone 2022-P2-M9), which involved a comprehensive two-phase batch-scale study for a total duration of 71 days.
- FIU completed the ICP-MS analysis for U and Tc for the reoxidation experiments of perched and groundwater samples amended with 0.5% and 5.0 vol% calcium polysulfide. FIU also completed anion analysis such as nitrate, nitrite, and sulfate, via an IC instrument.
- An abstract titled *"Re-oxidation Behavior of Technetium-99 and Uranium Immobilized by Zero Valent and Sulfur Modified Iron Reductants"* was submitted for a poster to be presented at the RemPlex Global Summit in Richland, WA in November 2023.

- An abstract titled "The Reoxidation Behavior of Tc(IV) and U(IV) in Perched Water of the Hanford Site Vadose Zone after Treatment with Strong Reductants" authored by Yelena Katsenovich, Hilary Emerson, Jim Szecsody, Nik Qafoku, Leonel Lagos was submitted to WM 2024 and will be presented as an oral presentation.

Subtask 1.3:

- FIU completed batch adsorption experiments with iodine as iodate (IO_3^-) and IO_3^- comingled with uranium (U) and chromium (U) onto Hanford formation sediment with bulk size of ≤ 2 mm in triplicate. The distribution coefficient (Kd) values were determined to assess the adsorption behavior. The results showed that the Kd values decreased in the presence of iodine at a 1:10 U:I molar ratio. Furthermore, in the presence of both chromium and iodine at a 10:1:10 Cr:U:I molar ratio, the decrease in Kd values was even more significant.
- An abstract titled *"Impact of Cr(VI) as a Co-Contaminant on the Sorption and Desorption of U(VI) in Hanford Sediments Under Mildly Alkaline Oxic Conditions"* was submitted for a poster to be presented at the RemPlex Global Summit in Richland, WA in November, 2023.
- FIU completed the column experiments using Br as a tracer and U and Cr as contaminants. FIU obtained transport parameters for columns including the dispersion coefficient, D, and the retardation coefficient, R, which were found using data from our Br tracer test and the CXTFIT code. The adsorption-desorption distribution coefficient, Kd, and R of U in both columns were found by integrating the area under the breakthrough curve.
- FIU presented a poster titled *"Impact of Chromium (VI) as a Co-mingled Contaminant on the Adsorption of Uranium (VI) to Hanford Formation Sediment*" at the 2023 Waste Management Symposia".
- FIU completed a study of the attenuation mechanisms of co-mingled U and Cr in a 1-D column (Milestone 2022-P2-M6). It was clear from stop flow events that U was in non-equilibrium in both columns but was more pronounced when U was co-mingled with Cr. The obtained values matched well to previous physical properties reported in other column experiments using Hanford sediment (Qafoku et al. 2005).
- A manuscript titled "Impact of chromium (VI) as a co-contaminant on the sorption and co-precipitation of uranium (VI) in sediments under mildly alkaline oxic conditions" authored by the DOE Fellow Mariah S. Doughman, Kevin E. O'Shea, Nikolla P. Qafoku, Hilary P. Emerson, James E. Szecsody, Kenneth C. Carroll, and Yelena P. Katsenovich was accepted for publication in the Journal of Environmental Management.

Subtask 1.4:

- FIU finished a long-term static PCT with pH 12 buffer, Ca-amended and grout contacted solutions.
- FIU has completed Milestone 2022-P2-M4, *"Complete long-term static PCT tests at 90°C that include monolithic samples to measure depth of glass alternation layers in Ca-containing and Ca-free coupon samples"*. The long-term experiment was carried out for 42 weeks. In total, 18 polished glass coupons exposed for different periods of time to three

corrosive solutions (pH 12 buffer, Ca-amended and grout-contacted solutions) were collected for SEM/EDS analysis in cross-section. Leachates collected after 8, 16 and 42 weeks of the experiment were analyzed by ICP-OES and ICP-MS methods. Results showed that the grout-contacted solution inhibits glass dissolution for the whole duration of the experiment.

- FIU has completed studying the effect of variable Ca^{2+} concentrations on corrosion behavior of borosilicate glass static PCT at 90ºC. Experiments have been performed in triplicated reactors with different concentrations of Ca^{2+} from 1 mg/L to 120 mg/L at pH 8.6, pH 10 and pH 12. The pH 8.6 corresponds to the pH of grout/sediment-contacted solution. The results of the borosilicate glass leaching at 90°C in the presence of Ca-amended solutions indicate that the addition of calcium in solutions leads to a reduction in the rate of glass dissolution, particularly when the calcium concentration reaches approximately 20 mg/L.
- FIU completed a draft manuscript on the *"Effect of a grout-contacted solution on the dissolution behavior of a borosilicate glass"* (Milestone 2022-P2-M8) for the submission to a peer-reviewed journal. The manuscript was submitted to PNNL collaborators for internal review and information release approval.
- FIU completed BET specific surface area and BJH adsorption cumulative volume of pores for glass powders treated in pH 12, Ca-amended, and grout-contacted solutions over various time periods. The results indicate that the glass powder treated in the pH 12 buffer solution exhibits the highest porosity, followed by the Ca-amended solution, while the powder treated in the grout-contacted solution shows the lowest porosity.
- FIU has completed SEM/EDS analysis of glass powders treated in a Product Consistency Test (PCT) with a Ca-amended solution and conducted ICP-MS analysis of the leachates collected in the static PCT test at 90°C with Ca-amended solutions. The results showed that lowering the pH from 12 to 10 resulted in a decrease in the glass dissolution rate. However, the normalized rate of boron loss at pH 8.6 was significantly higher when compared to both pH 12 and pH 10. FIU plans to redo some experiment at pH 8.6 to confirm these results.

Task 2. Remediation Research and Technical Support for Savannah River Site

Subtask 2.1:

- FIU completed the study on the effect of temperature on the sorption kinetics and maximum sorption of iodide and iodate on soil samples collected at different depth intervals (1-3 ft, 5-6 ft, and 13-14 ft) at 22°C and 8°C.
- FIU completed the investigation on the effect of oxic and anoxic conditions on the sorption kinetics and maximum sorption of iodide and iodate on soil samples at different depth intervals at 22°C.
- FIU performed a control study to observe any release of naturally bound iodine from the soil into the aqueous phase under various conditions.
- FIU completed Milestone 2022-P2-M3 *"Complete batch experiments on the influences of environmental factors on the attenuation and release of Iodine from SRS wetland soils".*

- FIU submitted a draft report on the influence of environmental factors on the attenuation and release of iodine from SRS wetland soils (Deliverable 2022-P2-D2). This study investigated the attenuation of iodide and iodate by wetland soils at various depths under different environmental conditions, such as temperature and redox potential.
- DOE Fellow, Phuong Pham, delivered an oral presentation on the remediation of iodine by organoclays and a Roy G. Post scholarship poster presentation on characterization of SRS wetland soils during the Waste Management Symposia 2023.
- DOE Fellow, Phuong Pham, successfully defended her Ph.D. dissertation and graduated with a Ph.D. degree in chemistry. She subsequently started a Post-Doctoral Associate position at Savannah River National Laboratory (SRNL).
- FIU also initiated isotherm experiments with iodate (IO_3^-) at pH 5.5 with 1.0 g/L organoclays (PM-199 and MRM) with a range of concentrations from 0.05 to 100 mg/L of IO_3^-.

Subtask 2.2:

- FIU revised experimental procedures and discussed them with SRNL. FIU began experiments to study the effect of pH on the uranium removal by KW-30 coated sediments.
- FIU completed the sorption of humic acid on to SRS sediment by combining 200 mg of sediment, 1 mL of 1,000 ppm stock solution of KW-30, and 18.9 mL of DIW to a total volume of ~20mL. After 5 days, the samples were centrifuged for 30 minutes at 2,700 rpm and the supernatant was extracted and analyzed in the UV-Vis to determine the amount of KW-30 remaining in the solution. Using the concentrations obtained from the UV-Vis, FIU calculated the average sorption of humic acid onto SRS sediment. The results showed a relatively consistent sorption of humic acid onto SRS sediment averaging 1,912.8 mg/kg.
- FIU completed batch kinetic experiments to investigate the behavior of sorbed humic (KW-30) substances on uranium. The average sorption for uncoated sediment shows approximately 6 mg/kg being loaded onto the sediment, and for coated sediment samples the sorption averaged at 25 mg/kg. The coated sediment samples showed 4 times greater sorption capacity than uncoated sediment samples.
- FIU formulated a groundwater recipe using data from monitoring wells FOB20 and FOB21. This recipe will be used in subsequent experiments to study the effect of GW on contaminant removal.
- FIU completed an experiment to study the sorption of humic acid with synthetic groundwater. Triplicate samples were prepared with 200 mg of SRS sediment and 20 mL of 50 ppb uranium prepared in synthetic groundwater (SGW) at pH 4. Samples were placed on the shaker at 100 rpm for 7 days and the pH adjusted daily. Results show that the average sorption of humic acid onto the sediment was approximately 3,300 mg/kg, which is higher compared to deionized water.

Task 3: Contaminant Fate and Transport Modeling for the Savannah River Site

Subtask 3.1:

- The MIKE SHE/MIKE 11 model using a grid resolution of 250 meter was completed for Tims Branch and calibrated for the period 1982-1996, where the first 8 years were used for model spin-up and the last 6 years for calibration.
- FIU performed long-term and event-based simulations of suspended sediment transport for Tims Branch and in May, successfully completed the calibration of the MIKE11-AD model for Tims Branch. In June, FIU also completed the optimization/calibration of the Tims Branch (MIKE) hydrology model for long-term simulations (Milestone 2022-P2-M10). The aim of this milestone was to finalize the model setup and define the various hydrological parameters that will allow the model to perform long-term simulations. Furthermore, FIU was able to simulate sediment transport as represented by the suspended solid concentrations for a few extreme precipitation events of 24 hours with a return period of 5 years.

Subtask 3.2:

- FIU completed the development of a watershed-scale hydrological MIKE SHE/MIKE 11 model for the Fourmile Branch watershed at the Savannah River Site. An initial version of the model was created with a 250 m pixel resolution using open-source data in combination within GIS and Python scripts. Initial estimates for the subsurface parameters for lateral groundwater flow were included, representing only the upper two aquifer systems on top of the Gordon confining unit based on literature research. Several flow parameters, such as lateral conductivity, were obtained using documentation provided by DOE collaborators. For the unknown parameters, the values originally estimated for the MIKE SHE/MIKE 11 Tims Branch model developed under Subtask 3.1 were used.
- FIU also completed the generation of the ATS model mesh for the F-Area hillslope. This mesh represents both land surface variability, soil texture variability and variations in the subsurface through different aquifers and aquitards. Furthermore, the domain implicitly makes use of a higher model resolution surrounding the river network, barrier wall as well as seepage basins, as these domains are impacted by small-scale hydrological variations that can impact contaminant transport. These features were explicitly represented in the ATS model mesh and were given separate parameter class numbers.
- FIU completed the development of the hydrological ATS model using Watershed Workflow for the SRS F-Area domain (Milestone 2022-P2-M7). FIU then continued working on the ATS input file to create a script that adds inflow boundary conditions to the F-Area, thus creating flow into the inlets to simulate a stream. This ATS input file addition is an improvement from previously generated files, as usually input of water is dependent on precipitation; however, with these boundary conditions stream flow and precipitation can be added to the model.
- In June, the DOE Fellow working on this subtask, Hannah Aziz, began a 10-week summer internship at Savannah River National Laboratory (SRNL) in Aiken, SC.

Task 5: Research and Technical Support for WIPP

- FIU obtained the physiochemical characteristics of the calcium salt of isosaccharinic acid [$Ca(ISA)_2$], calcium α-D-isosaccharinate, (Thermo Scientific, 98% purity) solid phase(s) employed in batch sorption studies.
- FIU completed batch sorption studies under anaerobic conditions in pyrite-amended 0.1 – 5.0 M NaCl brine spiked with 1 and 100 mg/L of sodium isosaccharinate (NaISA) and 100 µg/L of uranium (U), thorium (Th), and neodymium (Nd) stock solution. Study results showed that addition of 1 mg/L of ISA was inadequate in complexing the added actinide, whereas 100 mg/L ISA amendment enhanced the solubility of actinide in solution. Furthermore, study results showed that the addition of varying dosages of pyrite to ISA-containing brine impacted solution pH, leading to higher solubility enhancement with increasing pyrite dosage.
- FIU completed batch sorption studies under anaerobic conditions in pyrite-amended 0.1 - 1.0 M $MgCl_2$ and 0.1 M $CaCl_2$ brines spiked with 100 mg/L of sodium isosaccharinate (NaISA) and 100 µg/L of uranium (U), thorium (Th), and neodymium (Nd) stock solution. Study results showed that addition of 100 mg/L ISA was adequate in enhancing aqueous actinide solubility of actinide. Furthermore, the addition of varying dosages to ISA-containing brine impacted solution chemistry, leading to solubility enhancement with increasing pyrite dosage. However, addition of pyrite (5 g/L) to the ISA-amended $MgCl_2$ and $CaCl_2$ brines resulted in a decrease in actinide solubility that was attributed to adsorption of actinide onto the pyrite solid phase(s).
- Johnbull Dickson presented results on Task 5 at the ABC Salt Workshop 2023, Santa Fe, NM, June 15-16, 2023. His oral presentation titled *"Gluconate and Magnetite Control on Actinide Transport in WIPP High Ionic-Strength Brines"* was co-authored with Yelena Katsenovich, Leonel Lagos, Juliet Swanson and Donald Reed.

Task 6: Hydrology Modeling for Basin 6 of the Nash Draw near the WIPP

Subtask 6.1:

- Former DOE Fellow, Gisselle Gutierrez-Zuniga, successfully defended her thesis titled *"Development of a High-Resolution Digital Elevation Model of a Pilot Study Area in Basin 6, Located Near the Waste Isolation Pilot Plant (WIPP), New Mexico, USA"*, which was based on Subtask 6.1 that was completed in FIU Performance Year 2. Gisselle graduated with a master's degree in environmental engineering in December 2022 and is now employed as a Civil Analyst in the Surface Water Dept. at Kimley-Horn and Associates, Inc.

Subtask 6.2:

- FIU completed the development of a high-resolution model for Basin 6 using the Advanced Terrestrial Simulator (ATS) model based on a 1-m DEM (Milestone 2022-P2-M5). The software "Watershed Workflow" was successfully installed, and Python scripts were developed to generate a mesh for Basin 6 and the various input files (e.g., national land cover data (NLCD) in XML format) for ATS based on publicly available data. In addition, ATS was successfully installed on FIU's High-Performance Computational (HPC)

computer and test runs were completed using the installed Message Passing Interface (MPI) modules, confirming that ATS simulations can be successfully executed.

- ATS and PFLTORAN simulations were performed for calcite dissolution. Simulations were also run for surface and subsurface columns with the Nash Draw soil properties to see the effects of dispersion, sorption, retardation, radioactive decay, etc. FIU also began conducting an analysis of the meteorological characteristics of southeastern New Mexico in the region where the WIPP site is located, using several data catalogs available with Google Earth Engine Python API, including Vegetation Index (NDVI), Palmer Drought Severity Index (PDSI), Precipitation and Drought, and Climate Change on temperature and precipitation. In June, a spin-up model was developed for Basin 6. Once this spin-up model reaches equilibrium, it will be calibrated using observational data from Subtask 6.3. Model results will be compared with actual data from the pressure transducers that were placed in Basin 6 at the end of May to validate the model, after which a sensitivity analysis can then be performed. The more complex elements such as sinkholes, swallets, heterogenous surface and subsurface features, and man-made site elements (e.g., roads and drainage areas) will then be added after the model has reached a steady state.

Subtask 6.3:

- FIU developed field and laboratory work plans in preparation for work to be executed under this subtask. An FIU team, comprised of a senior research scientist and a DOE Fellow, traveled to New Mexico from May 29 – June 1, 2023 to perform fieldwork in Basin 6 of the Nash Draw just west of the WIPP, which included the deployment of 5 HOBO U20L water level loggers (pressure transducers) and collection of 48 soil samples at various strategic locations within the Basin 6 study area. Fieldwork support was provided by Dr. Anderson Ward from the DOE Carlsbad Field Office as well as Dr. Dennis Powers, a consulting geologist and subject matter specialist on Nash Draw hydrogeology. The water level data loggers will be removed in the Fall and the data downloaded for analysis and incorporation in the Basin 6 ATS hydrology model being developed. The soil samples will be processed at an FIU laboratory and the data will be used for model calibration and validation.

Task 7. Engineered Multi-Layer Amendment Technology for Hg Remediation on Oak Ridge Reservation

- FIU evaluated six sorbents for the mercury removal that were ranked as follows: *eSorb > eBind> sF400> F300 > PBC > Q-Clay*.

- A Toxicity Characteristic Leaching Procedure (TCLP) was completed for four sorbent media: (fsPAC, F300, Si-SH and eSorb) to determine whether a spent solid waste is hazardous or nonhazardous. Test results showed that leaching of mercury from spent eSorb media with TCLP extraction fluid 1 (pH = 4.93) exceeded the TC limit for mercury to be considered safe for disposal in a regulated landfill. However, employing extraction fluid (TCLP-2) to leach eSorb resulted in mercury loss from the media that was below the TC limit. On the other hand, mercury leached from spent Si-SH and fsPAC sorbent media, using both extraction fluids, was significantly below the TC limit, thus allowing for disposal in a landfill due to the nonhazardous nature of the solid waste. The TCLP tests reveal that the leaching of mercury from spent F300 sorbent media exceeded the TC limit for mercury to be considered safe for disposal in a landfill.

- FIU completed a Toxicity Characteristic Leaching Procedure (TCLP) for *Si-SH* and *eSorb* sorbent media. Test results showed that mercury leached from spent *Si-SH* or *eSorb* media into EFPC creek water (pH = 8.5) did not exceed the mandated TC limit, thus allowing for disposal in a landfill due to the nonhazardous nature of the solid waste. The TCLP test completed for the *fsPAC and F300* sorbents showed that EFPC water leached insignificant mercury from both sorbent media loaded with 10 mg/L of Hg^{2+} that was below the mandated TC limit. On the other hand, EFPC water leached significant mercury from *fsPAC* and *F300* sorbents spiked with 50 mg/L of Hg^{2+} that exceeded the mandated TC limit, precluding the disposal of these spent sorbent media in a regulated landfill due to the high potential for mercury release. The results will be verified in the planned column experiment for these sorbent media (*F300 and eSorb*).
- FIU completed batch sorption experiments to investigate the impact of ISA on actinide sorption onto pyrite in WIPP-relevant brines such as NaCl, $MgCl_2$, $CaCl_2$, the U.S. Energy Research and Development Administration Well 6 brine (ERDA-6, low Mg) and Generic Weep Brine (GWB, high Mg) using an actinide concentration of 10^{-7} M.
- FIU completed batch sorption experiments (Milestone 2022-P2-M16) investigating the impact of isosaccharinate (ISA) on actinide sorption onto pyrite under anaerobic conditions.
- A manuscript titled “Engineered Media for Mercury Removal in the Presence of Dissolved Organic Matter” authored by Johnbull Dickson, Caridad Estrada, Yelena Katsenovich, Leonel Lagos, Alexander Johs, Eric Pierce was drafted based on the results of these experiments and is being prepared for submission to a peer-reviewed journal.

TASK 1: REMEDIATION RESEARCH AND TECHNICAL SUPPORT FOR THE HANFORD SITE

Subtask 1.2: Re-oxidation of Redox Sensitive Contaminants Immobilized by Strong Reductants

Subtask 1.2: Introduction

Technetium-99 (^{99}Tc) management is a high-priority activity for the EM complex due to its high aqueous solubility, toxicity, and environmental mobility. Approximately 700 Ci of ^{99}Tc have been released into the Hanford subsurface, and its remediation is challenging due to the variability of waste chemistries and the heterogeneity of the deep vadose zone. A perched water zone beneath the 200-DV-1 Operable Unit at Hanford contains ^{99}Tc as pertechnetate ($Tc^{VII}O_4^-$) that can potentially migrate to the underlying aquifer. Reducing conditions without or with sulfides may temporarily immobilize ^{99}Tc as one or more Tc^{IV} precipitates. Previous research has shown that ^{99}Tc, as pertechnetate that has been reduced to $Tc^{IV}O_2$ or TcSx precipitates, reoxidizes and will eventually remobilize back into the aqueous phase (Lukens, et al. 2005). Additionally, reduced Tc precipitates coated with other low solubility precipitates have been effective in preventing Tc remobilization and may be useful for remediation (Pearce, et al. 2018). Moreover, Tc can be incorporated into low solubility precipitates such as iron oxides (Boglaienko, et al. 2020) or tin oxides (Luksic, et al. 2015), offering potential for ex-situ treatment. Hence, there is a need for additional research under the specific conditions of subsurface remediation for the Hanford Site, as other Tc species may form.

Recent bench-scale evaluations provided insights into the pertechnetate reduction process using strong reductants in the sediment mixture (Lawter, et al. 2018). However, this process was not evaluated for the remobilization of ^{99}Tc under aerobic conditions. The study conducted at FIU between 2019 and 2022 investigated the re-oxidation behavior of ^{99}Tc to mimic field conditions, where the groundwater and perched water zone were slowly re-oxidized to naturally occurring conditions. Laboratory experiments evaluated the re-oxidation behavior of ^{99}Tc initially reduced by strong reductants such as zero-valent iron (ZVI, Hepure Technologies), sulfur-modified iron (SMI-PS Inc), and calcium polysulfide (CPS) in batch-scale experiments under sequential anaerobic conditions followed by aerobic conditions. In FIU Year 3, experimental work was extended to investigate the reoxidation behavior of ^{99}Tc in the presence of collocated uranyl (UO_2^{2+}) and nitrate (NO_3^-) ions.

Sediment samples obtained from the Hanford Site Ringold Formation were sieved, and the ≤ 2 mm size fraction was used in the batch experiments. In FIU Year 3, the batch experiments were conducted in two phases: Phase 1 involved the reduction of ^{99}Tc collocated with NO_3^- and UO_2^{2+} in the presence of strong reductants, 0.5% CPS, or 5.0% CPS, under anaerobic conditions for 4 weeks; and Phase 2 focused on the re-oxidation of reduced ^{99}Tc and other contaminants, NO_3^- and UO_2^{2+}, under aerobic conditions for 5 weeks. Two contacting solutions were used in these experiments: (1) a synthetic perched water (PW) solution amended with 10 µg/L (34 pCi/L) of ^{99}Tc collocated with 150 mg/L of U(VI) and (2) a synthetic groundwater (GW) solution amended with 420 µg/L (122.3 pCi/L) of ^{99}Tc collocated with 124 mg/L NO_3^-.

Subtask 1.2: Objectives

The objective of this subtask is to study the re-oxidation reactions of perched and groundwater contaminants, such as $^{99}Tc(VII)$ as well as NO_3^- and ^{238}U that have been initially reduced by strong reductants such as 0.5% and 5% Calcium Polysulfide (CPS), in batch-scale experiments under anaerobic initial conditions followed by aerobic conditions. This report presents results on Tc(VII) reduction and reoxidation behavior when ^{99}Tc is comingled with UO_2^{2+} in perched water and NO_3^- in groundwater solutions.

Subtask 1.2: Methodology

These batch experiments studied the re-oxidation behavior of reduced forms of technetium [$^{99}Tc^{(IV)}$ oxides and/or sulfides] in the presence of UO_2^{2+} and NO_3^- after treatment with strong reductants, including 0.5 vol% and 5.0 vol% CPS. The batch experiments were conducted in two phases: Phase 1 - Reduction of ^{99}Tc comingled with UO_2^{2+} and NO_3^- in the presence of 0.5 vol% and 5.0 vol% CPS under anaerobic conditions for 4 weeks; and Phase 2 –The re-oxidation behavior of reduced ^{99}Tc comingled with UO_2^{2+} and NO_3^- under aerobic conditions for 40-45 days.

Experimental set up

Ultrapure deionized water (> 18 MΩ-cm, DIW, 5 L) was purged with N_2 for 30 minutes and transferred into the anaerobic chamber (Coy Laboratory) to prepare 1.5 L of each of the two contacting simulant solutions of synthetic perched and groundwater solutions. An anaerobic CAM-12 meter inside the anaerobic chamber monitored oxygen (ppm) and hydrogen (%) levels.

The anaerobic glove box was connected to two cylinders: (i) high purity nitrogen and (ii) nitrogen (95%) mixed with hydrogen (5%). The level of H_2 was kept as ~2% and O_2< 10 ppm. A palladium catalyst in the anaerobic chamber was replaced and regenerated weekly by heating in the oven at 180 ^oC for 4-5 h. The pH adjustment HCl solutions were prepared based on the information presented in Table 1.

Table 1. HCl volume (mL) to prepare 100 mL of pH- adjustment solutions.

MW_{HCl} =36.46 g/mol, density 1.18 g/cm^3, purity- 35-38%		
0.1 M	1 M	2 M
0.835 mL	$V = \frac{36.46 * 100 * 100}{1.18 * 37 * 1000} = 8.35\ mL$	16.7 mL

Sediment collected from the Ringold Formation at the Hanford Site was air dried and then sifted through a 2 mm sieve. 10 g of sediment each was distributed to 22 of the 26 experimental 250 mL bottles. 1.5 L of artificial perched and groundwater was prepared using deionized water purged with nitrogen and then amended with the salts defined in Table 2 before transferring to an anaerobic glovebox. Inside the anaerobic glovebox, the contaminants were measured out and added to the appropriate water sources. Two sediment-free control samples with 100 mL GW and PW synthetic solutions containing the same concentrations of ^{99}Tc, U, and NO_3^- as those used in the experimental samples were prepared inside the glovebox. These sediment-free control samples were treated the same as the experimental samples to determine the initial content of ^{99}Tc, U and NO_3^- in GW and PW solutions. Two reductant-free control samples for GW and PW were created containing contaminants and sediment but no CPS.

Table 2. Salts for Artificial Ground and Perched Water Calculated for 1.5 L

Synthetic Perched Water (PW) Recipe			
Chemical	mmol/L	g/L	Mass to prepare 1.5 L solution, g
$NaHCO_3$	10.708	0.9	1.3494
$KHCO_3$	0.310	0.031	0.0465
(anhydrous) $MgSO_4$	2.703	0.325	0.9993
$CaSO_4\ 2H_2O$ (dite)	0.561	0.097	0.1449
Na_2SO_4	1.744	0.248	0.3716
NaCl	3.3006	0.193	0.2894

Artificial Groundwater (GW) Recipe			
Chemical	mmol/L	g/L	Mass to prepare 1.5 L solution, g
$NaHCO_3$	1.586	0.133	0.1998
$KHCO_3$	0.123	0.012	0.0185
$MgSO_4$	0.366	0.090	0.1353
$MgCl_2\ 6H_2O$	0.247	0.050	0.0753
$CaCl_2\ 2H_2O$	1.071	0.157	0.2361

These solutions were then pH-adjusted by using small quantities of hydrochloric acid (HCl, TraceMetal™ Grade, 0.1 M, 1 M and 2 M) to a pH of 7.8 ± 0.1 and 8.2 ± 0.1 for the artificial GW and PW solutions, respectively. The pH electrode was calibrated using three buffers (pH: 4.01, 7.00, and 10.01) immediately before measuring the pH of the solutions.

The simulant solutions were spiked with contaminants of concern, 150 mg/L U and 10 µg/L ^{99}Tc for the PW and 420 µg/L of ^{99}Tc in addition to 124 mg/L NO_3^- for the GW (Table 3). These concentrations are consistent with previous work conducted at PNNL (Lawter et al., 2018) and experiments conducted by FIU.

Table 3. Amounts of U, NO_3^- and Tc added from stock solutions to 1.5 L of artificial GW or PW solutions

Volume of stock to prepare 1.5 L solution	Tc (stock concentration 414.7 mg/L)	U [uranyl acetate solution (depleted U)], $UO_2(OCOCH_3)_2{\cdot}2H_2O$, stock solution, 2%) *	$NaNO_3$, (124 mg/L of NO_3)
Groundwater (420 µg/L of ^{99}Tc and 124 mg/L nitrate	1.5192 mL		255 mg
Perch water (150 mg/L uranium and 10 µg/L ^{99}Tc)	0.0362 mL	20.05 mL	

*****2% of $UO_2(OCOCH_3)_2{\cdot}2H_2O$ solution (MW= 424.14 g/mol) is 0.047 mol/L. This requires 13.4 mL per L to have 0.15 g/L of U.

******0.01 M $NaNO_3$ (MW= 90.104) requires 0.0901 g of salt dissolved in 100 mL D IW.

Phase 1: Reduction Experiments in the Anaerobic Conditions

After the contaminants were added to the 1.5 L bottles, artificial GW and PW were distributed into the appropriate experimental bottles to obtain a 1:10 solid to liquid ratio. For bottles containing 5.0 vol% CPS, 95 g of water was added to each sample. For bottles containing 0.5 vol% CPS, 99.5 g of water was added. Water weight was recorded using a scale. Figure 1 represents the set of bottles created for the experiment. After the artificial GW and PW were distributed to the appropriate bottles, the calcium polysulfide was injected. For the bottles requiring 5.0 vol% CPS by volume, 5 mL were injected. For the bottles requiring 0.5 vol% CPS, 0.5 mL was injected. Bottles were then shaken for 10 seconds to ensure mixing. After the initial day of distributing water and CPS to the bottles, the bottles were again shaken to ensure mixing. Bottles were shaken about 5 times each weekday.

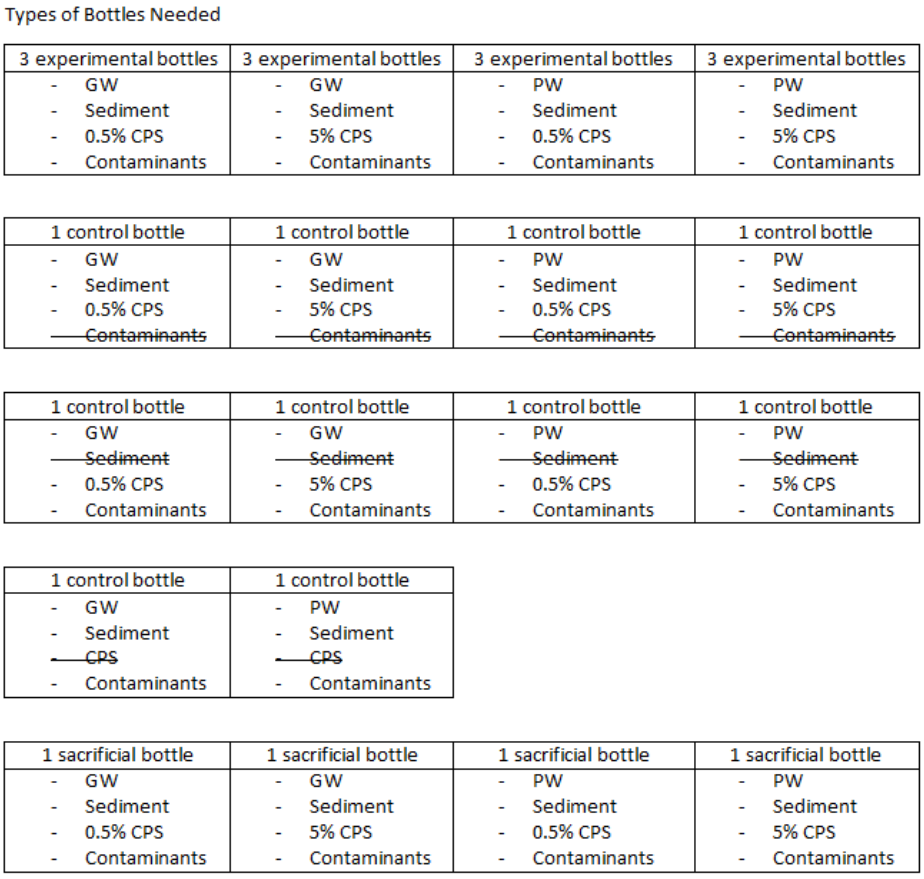

Figure 1. Types of experimental bottles prepared for the Experiment

Table 4 shows the types of experimental, control, and sacrificial samples prepared for the CPS reductant.

Table 4. Types of Bottles Used

No.	Type	Water Type	Sediment?	CPS?	Contaminants?
1	Experimental #1	GW	Sediment	CPS 0.5%	Contaminants
2	Experimental #2	GW	Sediment	CPS 0.5%	Contaminants
3	Experimental #3	GW	Sediment	CPS 0.5%	Contaminants

4	Experimental #1	GW	Sediment	CPS 5%	Contaminants
5	Experimental #2	GW	Sediment	CPS 5%	Contaminants
6	Experimental #3	GW	Sediment	CPS 5%	Contaminants
7	Control	GW	~~**Sediment**~~	CPS 0.5%	Contaminants
8	Control	GW	~~**Sediment**~~	CPS 5%	Contaminants
9	Control	GW	Sediment	~~**CPS**~~	Contaminants
10	Control	GW	Sediment	CPS 0.5%	~~**Contaminants**~~
11	Control	GW	Sediment	CPS 5%	~~**Contaminants**~~
12	Sacrificial	GW	Sediment	CPS 0.5%	Contaminants
13	Sacrificial	GW	Sediment	CPS 5%	Contaminants
14	Experimental #1	PW	Sediment	CPS 0.5%	Contaminants
15	Experimental #2	PW	Sediment	CPS 0.5%	Contaminants
16	Experimental #3	PW	Sediment	CPS 0.5%	Contaminants
17	Experimental #1	PW	Sediment	CPS 5%	Contaminants
18	Experimental #2	PW	Sediment	CPS 5%	Contaminants
19	Experimental #3	PW	Sediment	CPS 5%	Contaminants
20	Control	PW	~~**Sediment**~~	CPS 0.5%	Contaminants
21	Control	PW	~~**Sediment**~~	CPS 5%	Contaminants
22	Control	PW	Sediment	~~**CPS**~~	Contaminants
23	Control	PW	Sediment	CPS 0.5%	~~**Contaminants**~~
24	Control	PW	Sediment	CPS 5%	~~**Contaminants**~~
25	Sacrificial	PW	Sediment	CPS 0.5%	Contaminants
26	Sacrificial	PW	Sediment	CPS 5%	Contaminants

Phase 2: Re-oxidation of redox sensitive contaminants

After the $Tc^{(VII)}$, $U^{(VI)}$ and NO_3^- reduction in Phase 1 for 30 days, experimental bottles, sediment-free controls, reductant-free controls, and contaminant-free controls were removed from the anaerobic glovebox to study the reoxidation behavior of redox-sensitive contaminants under aerobic conditions. The experiment continued under a fume hood in FIU ARC's radiation laboratory. Capped samples were placed on a shaker (110 rpm, ThermoScientific) and kept for 45 days with slow aeration to ensure sufficient oxygen in the aqueous phase throughout Phase 2 experiments and for the slow reoxidation of redox-sensitive contaminants. Twice a week samples were aerated for 30 s. We collected 0.4 mL samples once a week at 1 day, 7 days, 14 days, 21 days, 28 days, 35 days, and 45 days, filtering them through 0.2 µm syringe filters before refrigerating them at 4°C for analysis. Measurements were continued for the solution pH, ORP and DO at each sampling event under aerobic conditions conducted on the bench.

Liquid Analysis (ICP-MS, LSC, IC)

<u>Anion analyses by IC</u>**<u>:</u>**
Ion chromatography (IC, Integrion Dionex) was used to analyze anions, NO^-_3, NO_2^- and SO_4^-. Calibration standards were prepared from a stock solution in DIW using special IC vials. The combined stock solution for NO_3^- and NO_2^- had concentrations of 100 mg/L. The concentration ranges for NO_3^- and NO_2^- calibration standards were 100 – 1,500 µg/L for a 5 mL sample volume.

The analysis utilized the Dionex IonPac AS11 analytical column (2x250 mm) and an Anion Dynamically Regenerated Suppressor (ADRS) (2 mm).

ICP-MS analyses for Tc, U and Fe

^{99}Tc calibration standards ranged from 0.005 µg/L to 50 µg/L through a serial dilution from 1mg/L stock solution was prepared from 4.217 mM (417.483 mg/L) stock solution.

ICP-MS U standards were prepared from 1,000 mg/L commercial uranyl nitrate stock solution purchased from High Purity Standards by the dilution to 1 mg/L stock (0.01 -500 µg/L). The remaining aqueous fraction of contaminant (unitless) was calculated as the ratio of concentration in the solution to the initial concentration.

During the experiment, an issue was encountered when the 5.0 vol% calcium polysulfide created a precipitate with the 2% nitric acid solution used for sample processing in the ICP-MS instrument (Figure 2). This precipitate presented challenges for the ICP-MS analysis. The 5.0 vol% calcium polysulfide creates a precipitate while the 0.5 vol% calcium polysulfide does not create a precipitate. A method was needed to overcome this precipitate interference.

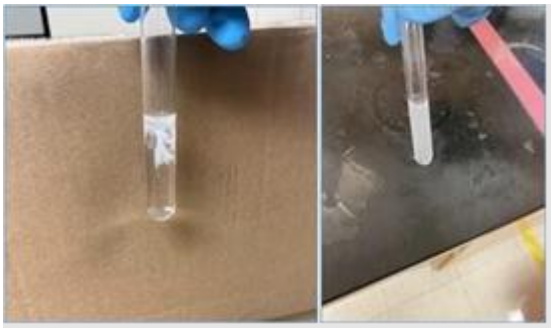

Figure 2. The 5% calcium polysulfide creating a precipitate with the 2% nitric acid solution.

In order to overcome this interference, one of the methods used was the addition of hydrogen peroxide to an aliquot of 5.0 vol% calcium polysulfide sample before mixing it with 2% nitric acid.

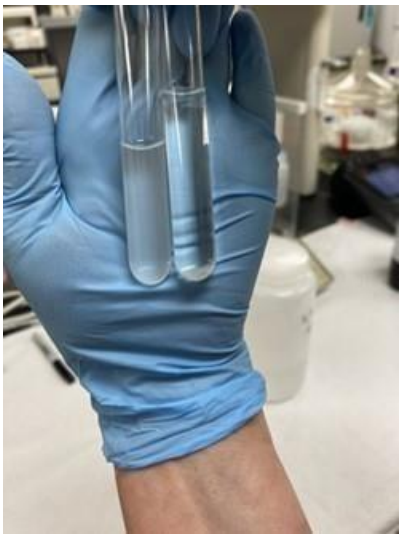

Figure 3. (Left) turbidity observed in the sample after mixing 5% calcium polysulfide with the 2% nitric acid solution; (Right) A clear sample achieved after mixing a 20 µL sample aliquot with 20 µL of H_2O_2 following by mixing with 5 mL 2% HNO_3.

A precipitate was created in sediment-free perched water samples amended with 0.5 vol% and 5.0 vol% calcium polysulfide. This may be the formation of calcium carbonate due to the reaction of carbonate present in perched water with calcium polysulfide. However, CPS 5.0 vol% amended samples still exhibited turbidity issues when mixed with hydrogen peroxide and subsequently with 2% nitric acid. To avoid interference from turbidity, groundwater samples amended with 5.0 vol% CPS were measured using a liquid scintillation counter (LSC). For U analysis, the samples were diluted 200-400 times to minimize cloudiness.

Calculation of rate constants

The oxidation rate constants for Tc^{VII} were calculated using the first-order and second-order rate equations according to Eqns. 1 and 2, respectively (H Scott, 2006). Other kinetic models to calculate reoxidation rate constants will be also considered.

$$ln\left(\frac{[C_t]}{[C_0]}\right) = -K_t \quad (1)$$

$$\frac{1}{[Ct]} - \frac{1}{[C0]} = Kt \quad (2)$$

Where C_t = concentration at the time, t, in mol L^{-1}
C_0 = initial concentration, mol L^{-1}
t =time, min
K = pseudo-first-order rate, min^{-1} for Eq. 1 and pseudo-second-order rate, $M^{-1}min^{-1}$ for Eq. 2.

Subtask 1.2: Results and Discussion

$Tc^{(VII)}$, $U^{(VI)}$, and NO_3^- are redox sensitive contaminants and the reduction of $Tc^{(VII)}$ to $Tc^{(IV)}$, $U^{(VI)}$ to $U^{(IV)}$ and NO_3^- to NO is described by the following equations 1-3 (Bard, 2017; Milazzo et al., 1978).

$$\boldsymbol{TcO_4^-} + 3e^- + 4H^+ \rightarrow \boldsymbol{TcO_2 \cdot xH_2O}(s) + (2-x)H_2O \qquad E^0 = 0.748\ \text{V} \qquad \text{Eq.1}$$

$$\boldsymbol{UO_2^{2+}} + 2e^- + 4H^+ \rightarrow \boldsymbol{UO_2} + H_2O \qquad E^0 = 0.327\ \text{V} \qquad \text{Eq.2}$$

$$\boldsymbol{NO_3^-} + 3e^- + 4H^+ \rightarrow \boldsymbol{NO_g} + 2H_2O \qquad E^0 = 0.96\ \text{V} \qquad \text{Eq.3}$$

Sediment Sieving and Fraction Analysis

Most of the Ringold Formation non-contaminated sediment collected at Hanford was classified as fine sand.

Table 5 depicts the results from the fraction analysis. Fine sediment particles with 500 µm-63 µm size present the largest fraction ~87 %. The clay fraction was the smallest fraction measured by a significant margin.

Table 5. Fraction Analysis of the Background Ringold Formation sediment

Fraction	Soil Weight (g)	Weight Percentage
2000µm-500µm (Sand)	7.52	7.5
500µm-63µm (Sand)	87.15	87.2
63µm-20µm (Silt)	4.06	4.1
<20µm (Clay)	1.22	1.2

Aqueous Removal of ^{99}Tc by CPS reductant

Sample preparation for ICP-MS analysis observed turbidity in the 5.0 vol% CPS-amended samples when mixed with 2% nitric acid. To address this interference, Tc concentrations in GW samples amended with 5% CPS were measured using a liquid scintillation counter (LSC). The results from (Figure 4) revealed that in Phase 1's anaerobic conditions, the Tc concentration in the synthetic GW solution decreased by only 20% from its initial value of 429.36 µg/L. However, under aerobic conditions, the Tc concentration decreased to 0.1, gradually increasing to 0.18 by day 71, indicating Tc reoxidation in the solution. Both sediment-free and sediment samples exhibited similar Tc reoxidation behavior. However, sediment-free samples showed relatively lower Tc reoxidation compared to samples with sediment (Figure 4).

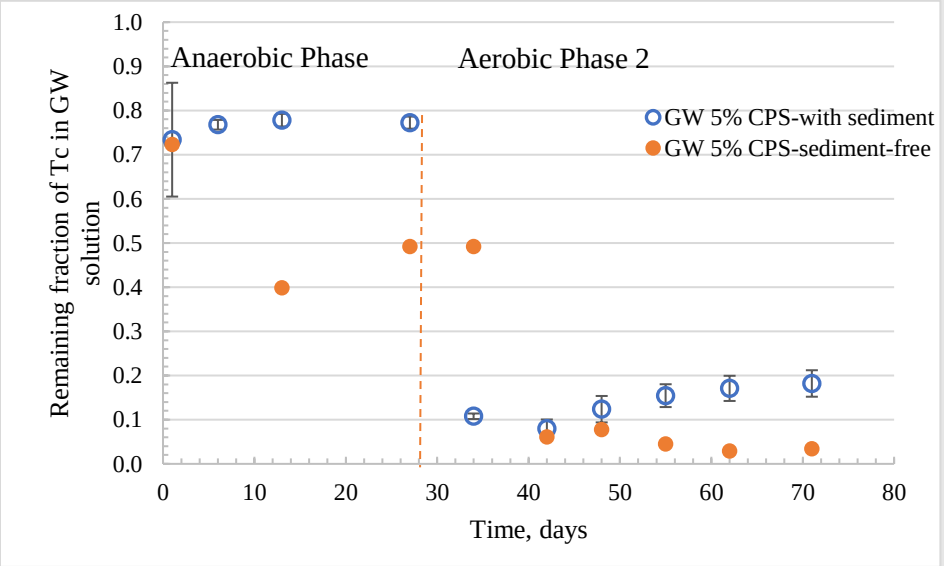

Figure 4. The remaining fraction of Tc in 5.0% CPS–amended GW samples. Note: The remaining aqueous fraction of Tc (Y-axis, unitless) was calculated as the ratio of Tc concentration in the solution to the initial Tc concentration in the control.

Samples in the synthetic GW solution containing 429.36 µg/L of Tc(VI) amended with 0.5vol% CPS showed a substantial decline of almost 99% in Tc concentration under anaerobic conditions (Figure 5). Under aerobic conditions, the concentration of Tc in sediment samples increased from 5-6 µg/L to 33-35 µg/L by day 71. This increase in Tc concentration can be attributed to the reoxidation of Tc in the solution. The presence of oxygen in the aerobic environment facilitates the reoxidation process, leading to the observed higher Tc concentrations compared to the levels achieved in the anaerobic conditions (Figure 5). Under anaerobic conditions, the sediment-free samples exhibited greater removal of Tc, resulting in concentrations of 0.08-0.1 ug/L, compared to the sediment samples where Tc removal was only achieved up to 5-7.0 µg/L. Additionally, the reoxidation of Tc in the sediment free samples was also lower compared to the sediment samples, with concentrations increasing up to 7-9 µg/L by day 71, corresponding to a remaining fraction of 0.02 (Figure 5). In contrast, the sediment samples experienced higher reoxidation, with concentrations reaching 33-35 µg/L when exposed to atmospheric conditions (Figure 5). These

findings highlight the significant impact of sediment on both Tc removal and the subsequent reoxidation process.

This result contrasts with the data obtained for 5.0 vol% CPS, where a higher concentration of CPS of 5.0 vol% only reduced Tc concentrations by approximately 20% from the initial value of 429.36 µg/L (Figure 5). However, when the samples were exposed to aerobic conditions, the Tc concentration dropped to 0.1 remaining fraction. Over time, the remaining fraction slowly increased to 0.18 by day 71, indicating the reoxidation of Tc in the solution. Both sediment-free samples and samples with sediment exhibited similar behavior in terms of Tc reoxidation. However, the reoxidation of Tc was relatively lower in the sediment-free samples compared to the samples with sediment (Figure 5).

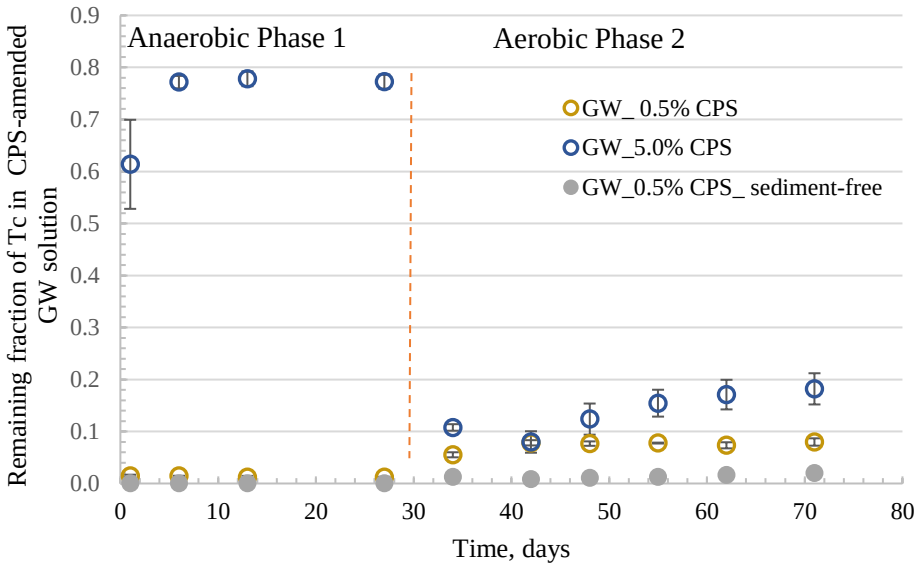

Figure 5. The remaining fraction of Tc in 0.5 vol% and 5.0 vol% CPS–amended GW samples. Note: The remaining aqueous fraction of Tc (Y-axis, unitless) was calculated as the ratio of Tc concentration in the solution to the initial Tc concentration in the control.

In the synthetic PW solution amended with 0.5% CPS, a significant 80% reduction of Tc(VII) was observed from the initial value of 9.2 µg/L under anaerobic conditions. When exposed to aerobic conditions, the remaining fraction of Tc remained relatively stable without significant changes (Figure 6a).

Similarly, approximately 80% of Tc was removed during the experiment in the synthetic PW solution amended with 5.0 vol% CPS, considering the initial Tc concentration of 9.2 ppb. In Phase 2, the remaining fraction of Tc was at a level of 0.13, and no reoxidation of Tc was observed by the end of the experiment on day 71 (Figure 6b). Both sediment-free and sediment-containing samples exhibited similar behavior in terms of Tc reoxidation (Figure 6).

In the synthetic PW, U concentrations showed only a slight reduction of approximately 10-15% under anaerobic conditions. However, upon exposure to aerobic conditions, the U concentration increased to nearly the initial levels for sediment-free samples and to a remaining fraction of 0.85 for sediment samples by the end of the 71-day experiment. This suggests that the presence of

sediment significantly influences the reoxidation and release of U in the PW solution, resulting in higher concentrations compared to sediment-free samples Figure 7.

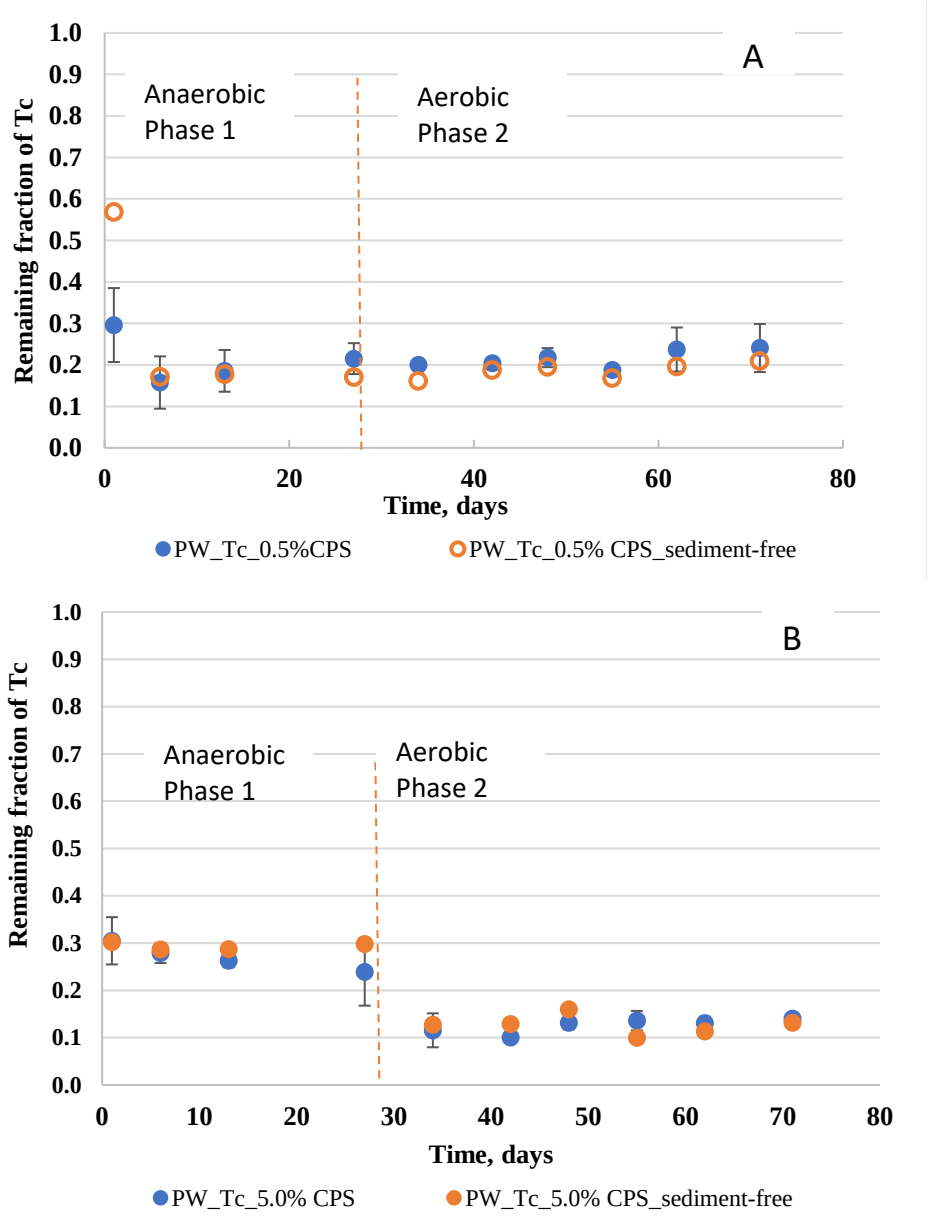

Figure 6. The remaining fraction of Tc in CPS–amended PW samples. A) CPS 0.5 vol%; B) CPS 5.0 vol%. Note: The remaining aqueous fraction of Tc (Y-axis, unitless) was calculated as the ratio of Tc concentration in the solution to the initial Tc concentration in the control.

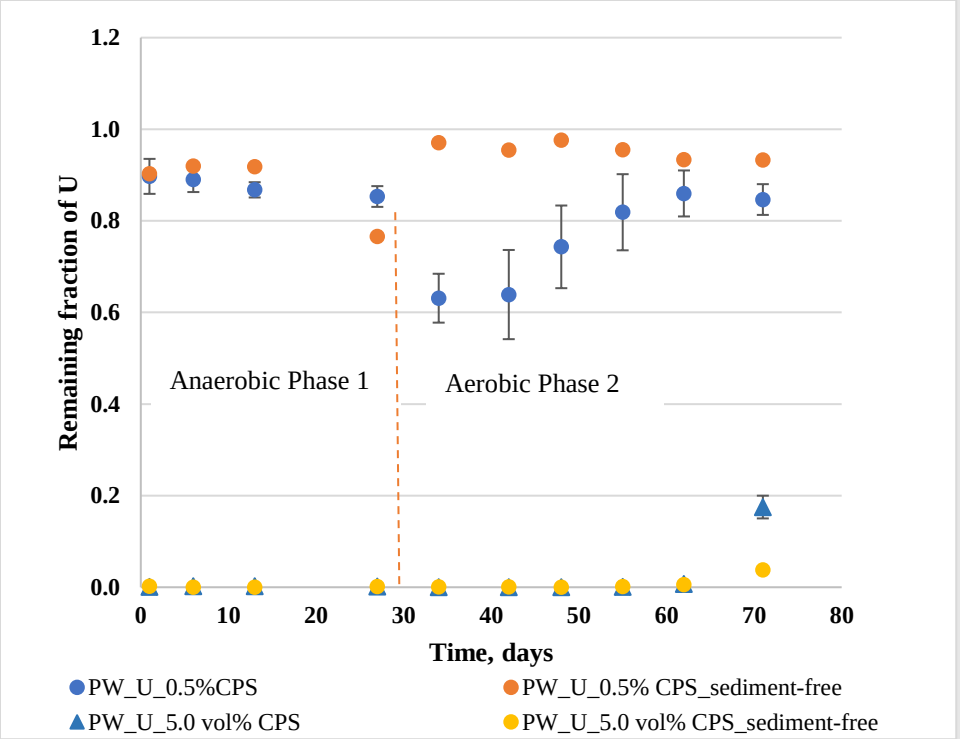

Figure 7. The remaining fraction of U in 0.5 vol% and 5.0 vol% CPS–amended PW samples. Note: The remaining aqueous fraction of U (Y-axis, unitless) was calculated as the ratio of U concentration in the solution to the initial U concentration in the control.

In the 0.5 vol.% CPS-amended samples, the removal of U was relatively low, resulting in a remaining fraction of 0.85±0.03 in the aqueous phase by the end of Phase 2. However, the removal of U was significantly improved in the 5.0 vol.% CPS-amended samples, resulting in a remaining fraction of 0.17±0.03 in the solution. This remaining fraction corresponds to a U concentration of 25,490±3,612 µg/L, which is significantly higher than in 1.0 wt.% ZVI and SMI-treated samples measured in FIU Year 2. As a result, additional optimization would be needed to improve CPS removal of U if field concentrations are this high to meet the required levels or regulatory guidelines.

The rate constants for the reoxidation of Tc(IV) to Tc(VII) and U(IV) to U(VI) with different reductants were fitted to both first-order and second-order linear equations (Katsenovich et al., 2023). While variable R-squared (R^2) values were obtained, the first-order kinetic model provided a better fit to the data (R^2 for Tc = 0.91 to 0.41, R^2 for U= 0.94 to 0.69) regarding the reoxidation rates of Tc(IV) to Tc(VII) and U(IV) to U(VI) (Table 6).

Table 6. First-order rate constants, k_{Tc} and k_U, for reoxidation of Tc(IV) to Tc(VII) and U(IV) to U(VI) for variable reductants in Phase 2 aerobic conditions

Reductants	First-order rate constant k_{Tc} for Tc(IV) reoxidation (hr^{-1}) ± Standard Error	First-order constant k_u for U(IV) reoxidation (hr^{-1}) ± Standard Error
0.5 vol.% CPS_GW	-3.0±0.2, R^2=0.42	
5.0 vol.% CPS_GW	-3.1±0.3, R^2=0.73	
0.5 vol.% CPS_PW	-1.9±0.2, R^2=0.41	-0.8±0.2, R^2=0.77
5.0 vol.% CPS_PW	-2.6±0.3, R^2=0.57	-19.2±2.0, R^2=0.94

The results for the anion analysis by IC to evaluate the amount of NO_3^-, NO_2^-, SO_4^{2-} in GW samples amended with NO_3^- collocated with Tc during treatment with 0.5% and 5.0 vol% CPS are presented in Figure 8 - Figure 10. At both concentrations, CPS was not very effective in removal of nitrate in GW samples from the initial concentration of 104 mg/L. The removal of NO_3^- by the end of anaerobic Phase 1 was almost at the same level as on Day 1. The removal of NO_3^- in GW samples treated with 0.5% CPS was less than 10% and for 5.0% CPS, less than 5% by the end of Phase 2. Sediment-free samples exhibited a similar trend to sediment samples. Data for nitrate concentrations showed no re-oxidation in Phase 2 (Figure 8).

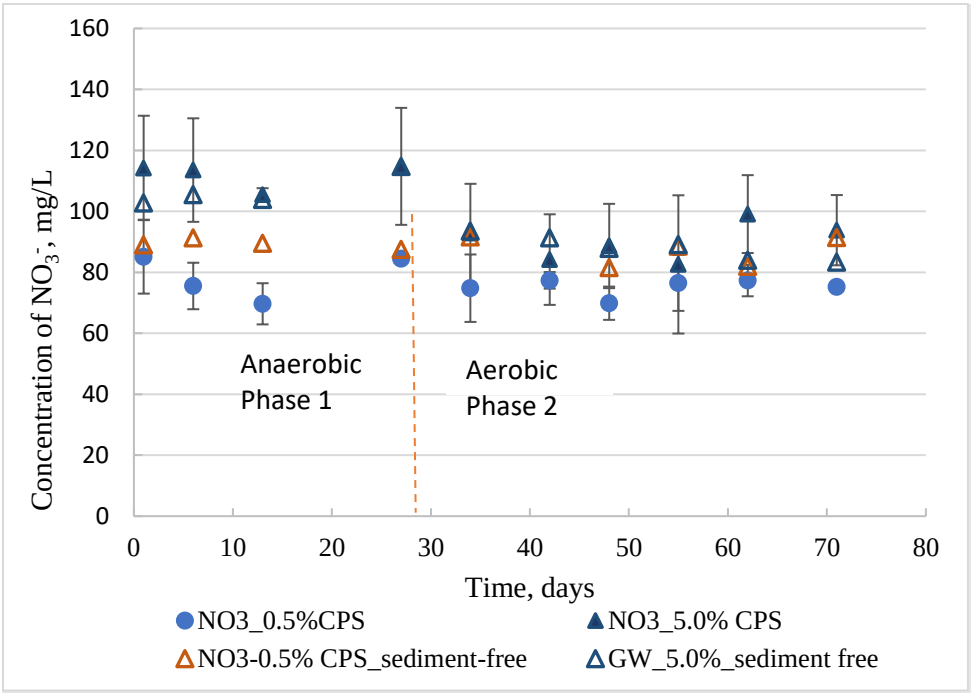

Figure 8. Changes in nitrate concentration in synthetic GW treated with 0.5 vol% and 5.0 vol% CPS.

At the end of Phases 1 and 2, the concentrations of NO_2^- were comparable in samples amended with both CPS concentrations, measuring at the level of 13-17 mg/L for both treatments (Figure 9).

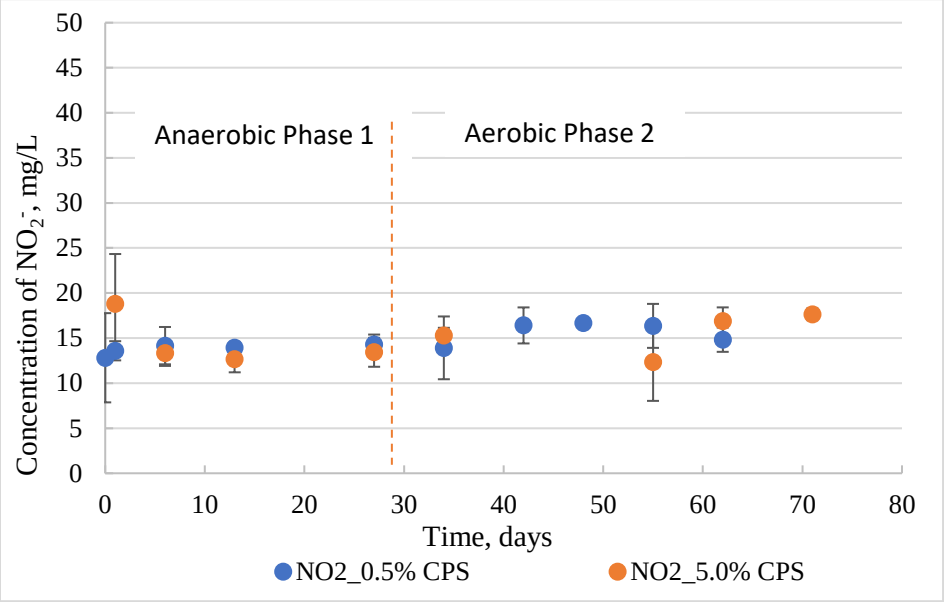

Figure 9.Changes in nitrite concentration in synthetic GW treated with 0.5 vol% and 5.0 vol% CPS.

The sulfate concentration was higher in 5.0 vol%-amended samples compared to 0.5 vol%-amended samples throughout both phases of the experiment (Figure 10). In the 0.5%-treated samples, the concentration of SO_4^{2-} increased in groundwater from an initial concentration of 71.8 mg/L to 340.7±37.9 mg/L by the end of the experiments (Figure 10A). In the 5.0 vol% samples, the concentrations of SO_4^{2-} in Phase 2 ranged from 249 to 276 mg/L. The sulfate concentration in the PW samples was initially at a level of 500-600 mg/L, but it increased to 800 mg/L in the 0.5% CPS-treated samples by day 70 (Figure 10B).

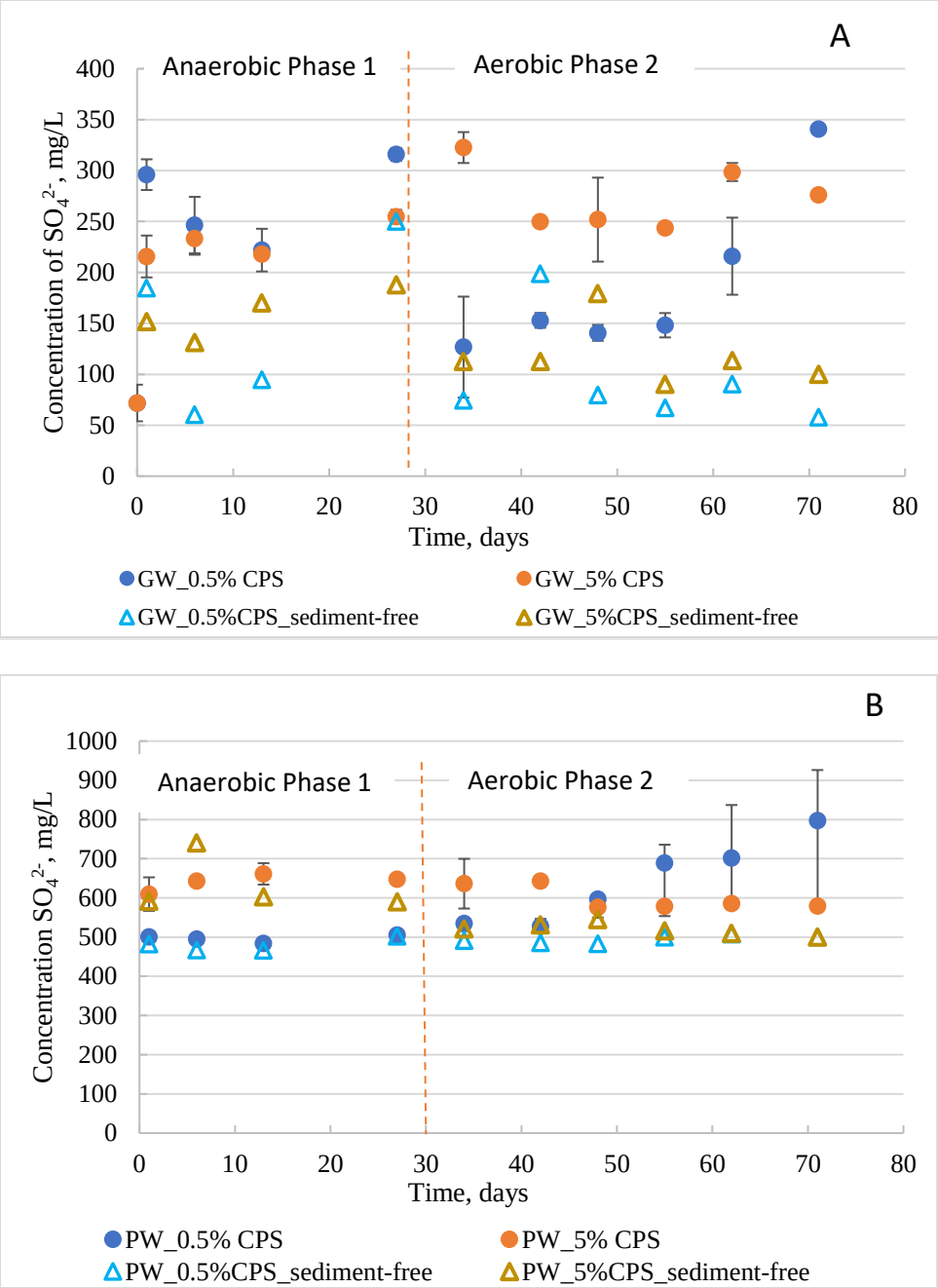

Figure 10. Changes in sulfate concentration. A) in synthetic GW treated with 0.5 vol% and 5.0 vol% CPS; B) in synthetic PW treated with 0.5 vol% and 5.0 vol% CPS PW

Oxidation Reduction Potential (ORP), pH and Dissolved Oxygen (DO)

Readings for pH, oxidation-reduction potential (ORP) and dissolved oxygen (O) measurements continued for the experimental and control samples in both Phase 1 and Phase 2 (Figure 11-Figure 13).

The results indicate an initial increase in pH when the samples were removed from the anaerobic glovebox and exposed to ambient conditions, marking the beginning of Phase 2 of the experiments conducted under aerobic conditions. However, the pH gradually decreased over time

due to the oxidation of calcium polysulfide and a potential increase in sulfate ions in the solution. Confirmation of these findings was obtained through ion chromatography analyses of increasing of sulfate (Figure 10).

The data for oxidation-reduction potential (ORP) correlates with the trend of dissolved oxygen Figure 12 and Figure 13). During Phase 1, ORP measured against an Ag/AgCl reference electrode produced negative results between -300 and -380 mV. However, once the samples were exposed to atmospheric conditions, ORP values increased up to +300 mV by day 70. This trend correlates with low oxygen values, less than 0.1 ppm, during anaerobic Phase 1 that increased to 6-8 mg/L during Phase 2.

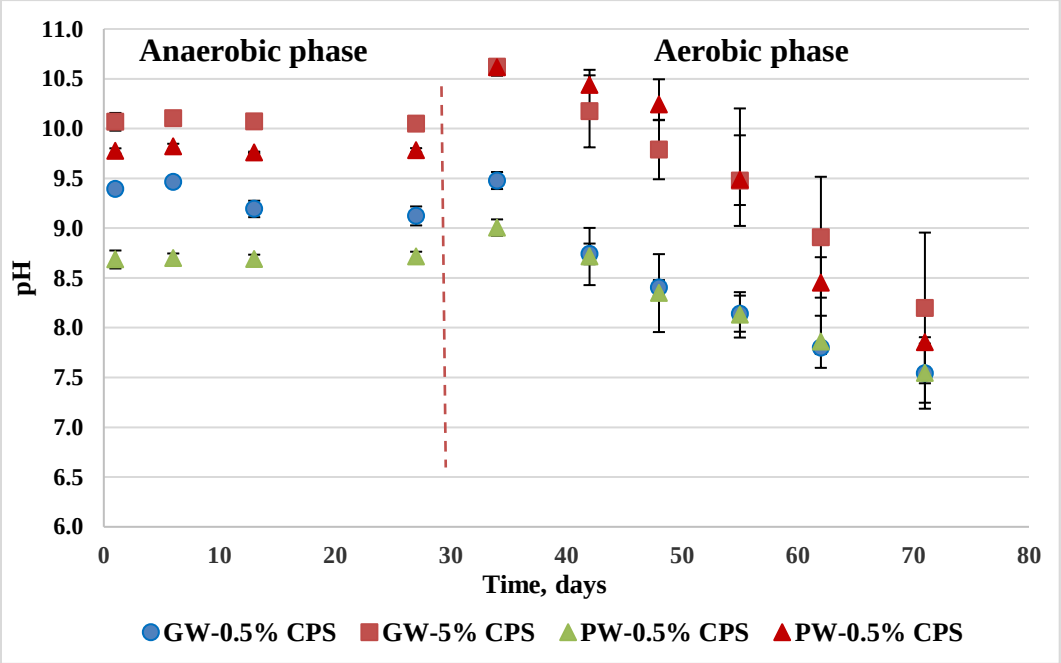

Figure 11. pH changes over time in synthetic GW and PW amended with 0.5% or 5.0% CPS where Phase 1 was conducted in the absence of oxygen and Phase 2 in the presence of oxygen. A dashed line separates Phase 1 and Phase 2 on day 28.

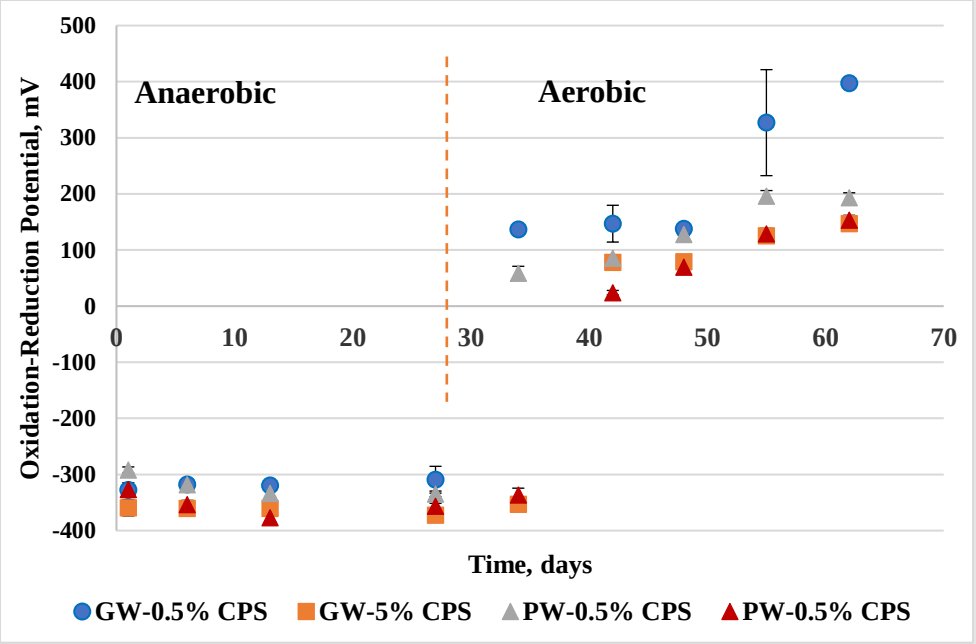

Figure 12. Oxidation-reduction potential (ORP) changes over time in synthetic GW and PW amended with 0.5% or 5.0% CPS where Phase 1 was conducted in the absence of oxygen and Phase 2 in the presence of oxygen. A dash line separates Phase 1 and Phase 2 on day 28.

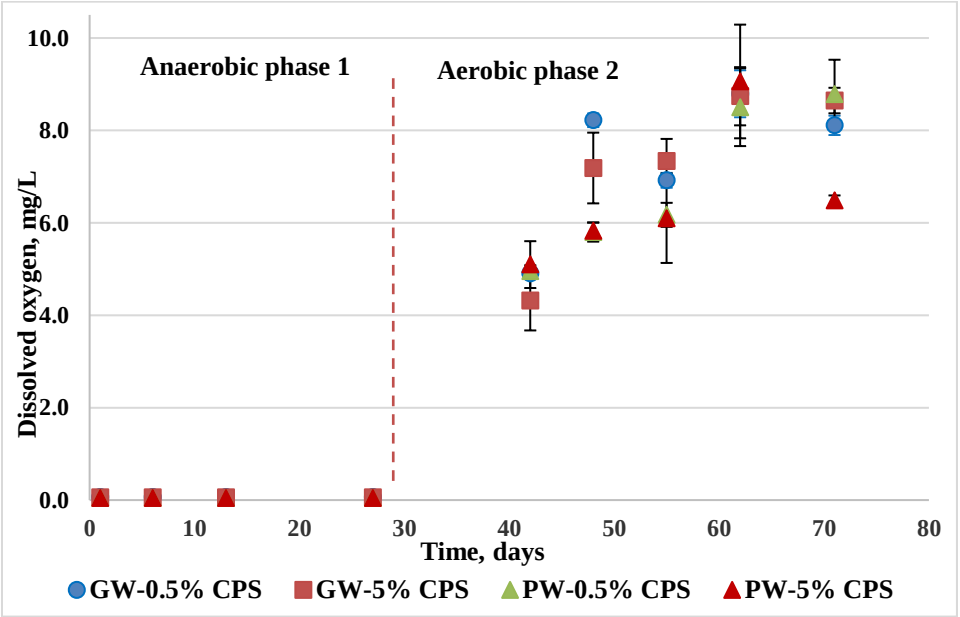

Figure 13. Dissolved oxygen concentration changes over time in synthetic GW and PW amended with 0.5% or 5.0% CPS where Phase 1 was conducted in the absence of oxygen and Phase 2 in the presence of oxygen. A dashed line separates Phase 1 and Phase 2 on Day 28.

Solids characterization

Measurements from the scanning electron microscope (SEM) were used to evaluate the elemental composition in each of the dried solid samples. SEM provides an accurate assessment, which helps

with mineralogical analysis using other methods like X-ray diffraction (XRD). SEM/EDS provided maps of elements such as S, Tc, Fe, Ti, and U, enabling the visualization of elements for comparing their associations on the sample surface. Initially, EDS maps were generated to identify any correlation between Tc and S. Then, several EDS single points were taken from Tc- and S-rich areas. Only one point from the surface of GW samples treated with 0.5 vol% CPS and 5.0% CPS exhibited a low content of Tc, measured at the level of 0.31-0.32% normalized mass (Figure 14, Figure 15). Sulfur normalize mass was measured 7.0% for 0.5 vol% CPS and up to 40% at 5.0 vol% CPS. EDS maps suggest the formation of Tc sulfide in the presence of CPS.

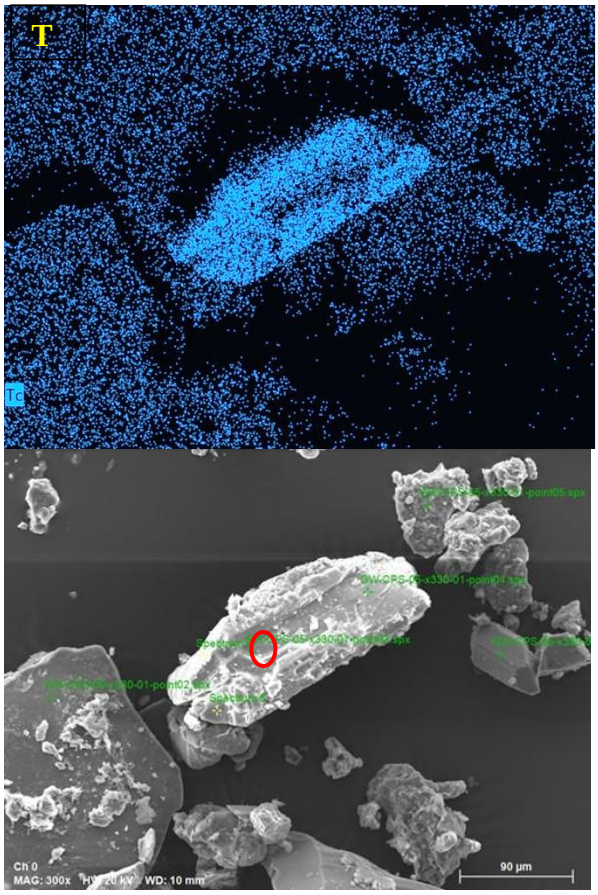

GW-CPS-05-x330-01-point07.spx

Element	At. No.	Netto	Mass [%]	Mass Norm. [%]	Atom [%]	Comp.	Sto. [%]	Sto. Norm. [%]	abs. error [%] (1 sigma)	rel. error [%] (1 sigma)
Oxygen	8	5274	22.66	42.43	62.70		0.00	0.00	0.35	1.53
Magnesium	12	595	0.35	0.65	0.63	MgO	0.57	1.07	0.03	10.09
Aluminium	13	3234	1.48	2.78	2.43	Al2O3	2.80	5.25	0.09	5.98
Silicon	14	25380	8.78	16.44	13.84	SiO2	18.78	35.17	0.40	4.61
Calcium	20	10342	5.63	10.55	6.22	CaO	7.88	14.76	0.24	4.18
Gold	79	2077	0.00	0.00	0.00		0.00	0.00	0.00	0.00
Iron	26	11987	9.43	17.65	7.47	FeO	12.13	22.71	0.34	3.56
Sodium	11	391	0.35	0.65	0.67	Na2O	0.47	0.88	0.04	12.77
Potassium	19	683	0.21	0.39	0.24	K2O	0.25	0.47	0.05	24.19
Sulfur	16	8288	3.73	6.98	5.14	SO3	9.30	17.42	0.16	4.33
Titanium	22	915	0.63	1.18	0.58	TiO2	1.05	1.96	0.04	6.77
Technetium	43	238	0.17	0.32	0.08		0.17	0.32	0.04	24.70
		Sum	53.41	100.00	100.00		53.41	100.00		

Figure 14. EDS maps of GW sample treated with 0.5 vol% CPS.

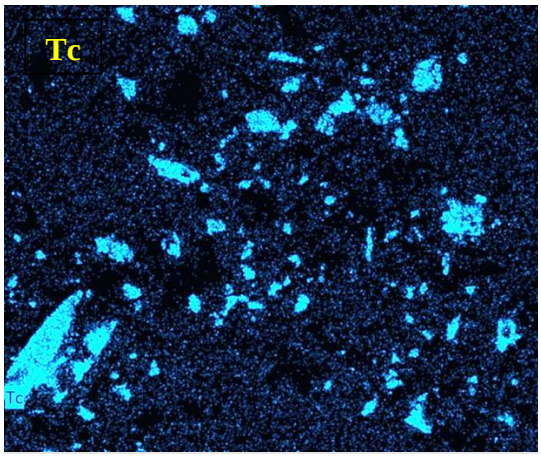

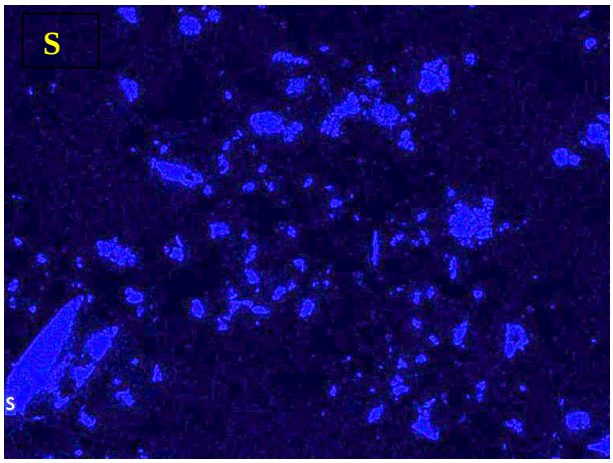

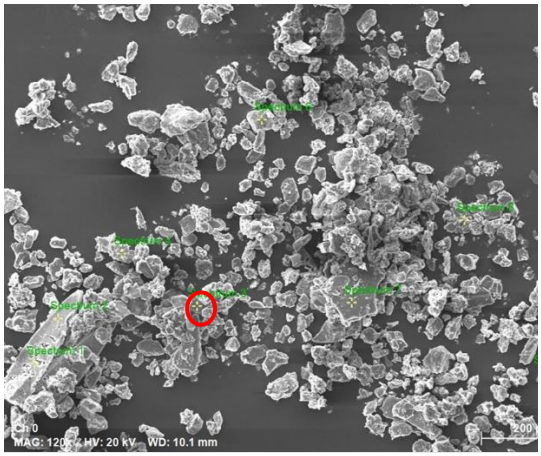

Spectrum 3

Element	At. No.	Netto	Mass [%]	Mass Norm. [%]	Atom [%]	Comp.	Sto. [%]	Sto. Norm. [%]	abs. error [%] (1 sigma)
Oxygen	8	3514	85.44	59.46	74.69		0.00	0.00	1.76
Magnesium	12	214	0.04	0.03	0.02	MgO	0.06	0.04	0.01
Aluminium	13	1050	0.16	0.11	0.08	Al2O3	0.29	0.21	0.02
Silicon	14	9400	1.06	0.74	0.53	SiO2	2.26	1.58	0.04
Calcium	20	535	0.17	0.12	0.06	CaO	0.23	0.16	0.02
Gold	79	1067	0.00	0.00	0.00		0.00	0.00	0.00
Iron	26	1000	0.48	0.34	0.12	FeO	0.62	0.43	0.03
Sodium	11	113	0.03	0.02	0.02	Na2O	0.04	0.03	0.02
Potassium	19	14	0.00	0.00	0.00	K2O	0.00	0.00	0.01
Sulfur	16	383028	56.02	38.98	24.43	SO3	139.87	97.33	1.73
Titanium	22	11	0.00	0.00	0.00	TiO2	0.01	0.00	0.01
Technetium	43	1254	0.31	0.21	0.04		0.31	0.21	0.06
		Sum	143.70	100.00	100.00		143.70	100.00	

Figure 15. EDS maps of GW sample treated with 5.0 vol% CPS.

The same approach was followed for the PW samples. The elemental EDS maps for the PW samples revealed alignment between Tc and S, but this appears to be an overlap in spectra. None of the single points taken from the Tc-rich areas showed the presence of Tc. U maps showed alignment with K, but single points on the surface didn't detect any U presence, suggesting its presence at background levels (Figure 16 and Figure 17).

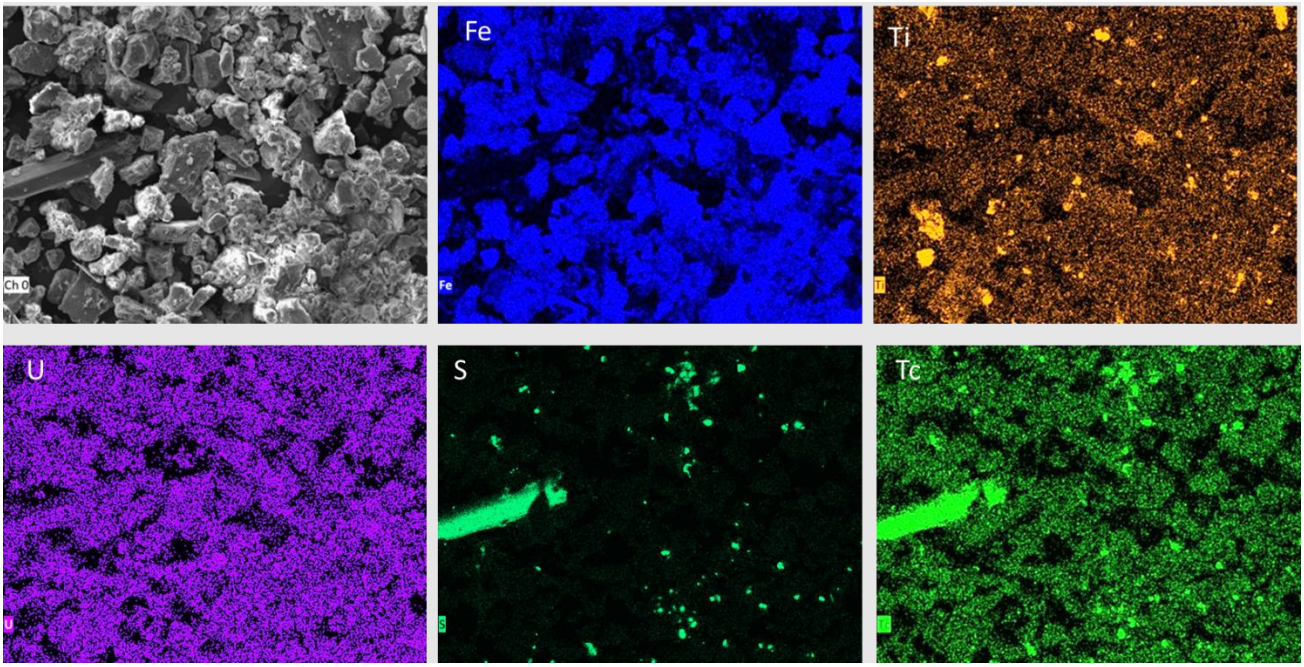

Figure 16. EDS maps of PW sample treated with 0.5 vol% CPS.

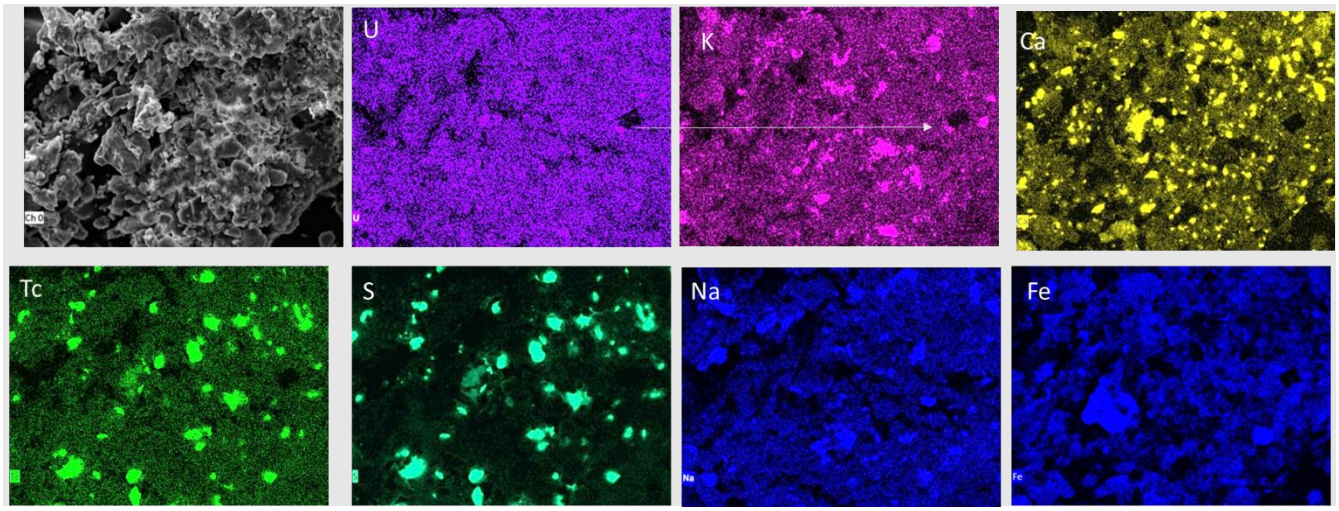

Figure 17. EDS maps of PW sample treated with 5.0 vol% CPS.

The sacrificial samples collected after Phase 1 showed a similar alignment behavior as samples collected after Phase 2. EDS maps collected for GW samples revealed alignment of Tc and S, but none of the single points collected in Tc-rich areas displayed values for the normalized mass of Tc. PW maps depicted alignment of Tc and S, but U was at background levels (Figure 18).

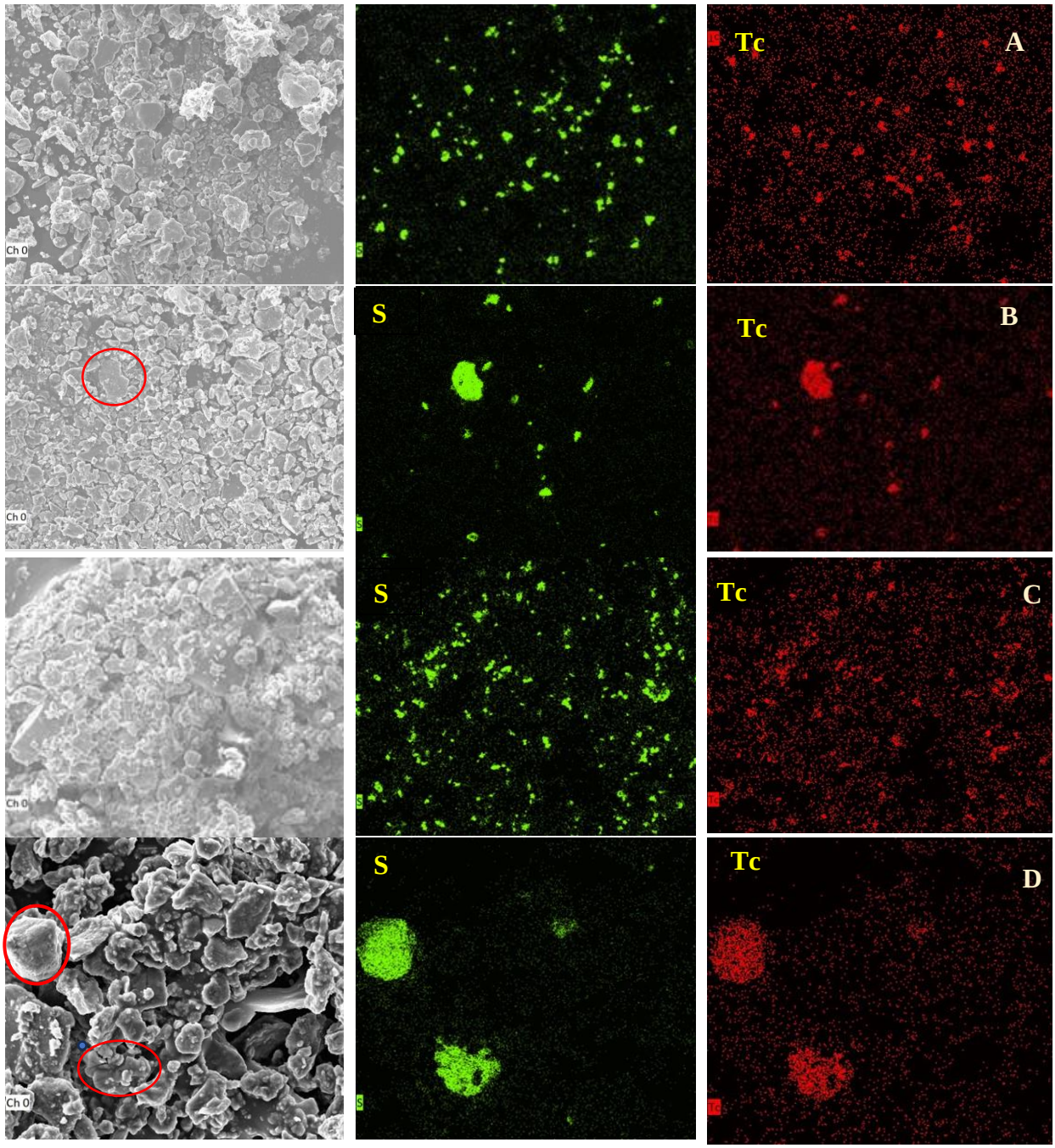

Figure 18. EDS maps of sacrificial GW and PW samples collected after Phase 1; A) GW sample treated with 0.5% CPS, B) GW sample treated with 5.0 vol% CPS, C) PW sample treated with 0.5% CPS, D) PW sample treated with 5.0 vol% CPS. Uranium showed on the background level.

X-Ray diffraction analysis

XRD analysis was conducted in duplicate for each sample. The XRD matching revealed varied solid phases, comprised of quartz, albite, vermiculite, nontronite, and illite. Additionally, samples prepared on synthetic porewater and amended with 0.5% and 5.0% CPS showed a small percentage of Jachymovite, a uranyl-sulfate hydroxide. Lack of homogeneity in the sieved sediment samples

with size fraction < 2 mm caused inconsistent matches for the mineralogy of the obtained X-ray patterns. The percentage of phases varied in GW duplicate samples treated with 0.5vol% CPS, but both contain quartz, albite, vermiculite, nontronite, illite. Samples also contained sulfur due to the CPS oxidation (Figure 19). The XRD results of the duplicate samples are presented in Figures 19-22.

Figure 19. XRD results for duplicate GW samples treated with 0.5% CPS

The GW samples treated with 5.0 vol% CPS exhibited some sulfur presence, attributed to the oxidation of CPS, with no sulfate phases detected (**Figure 20**).

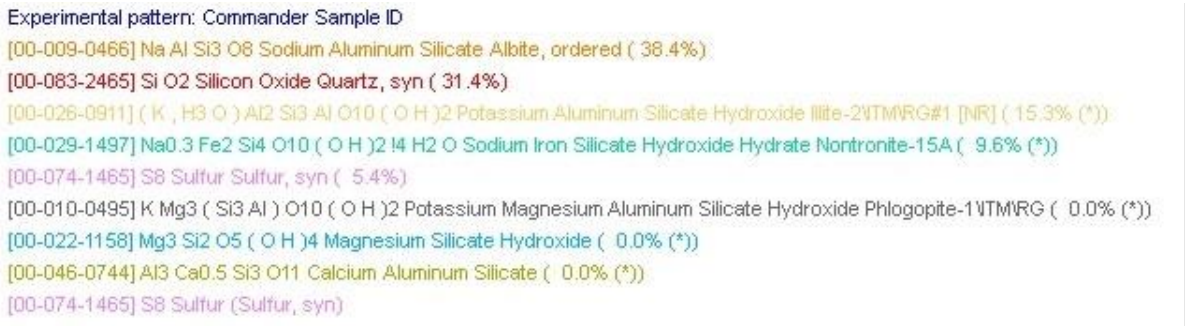

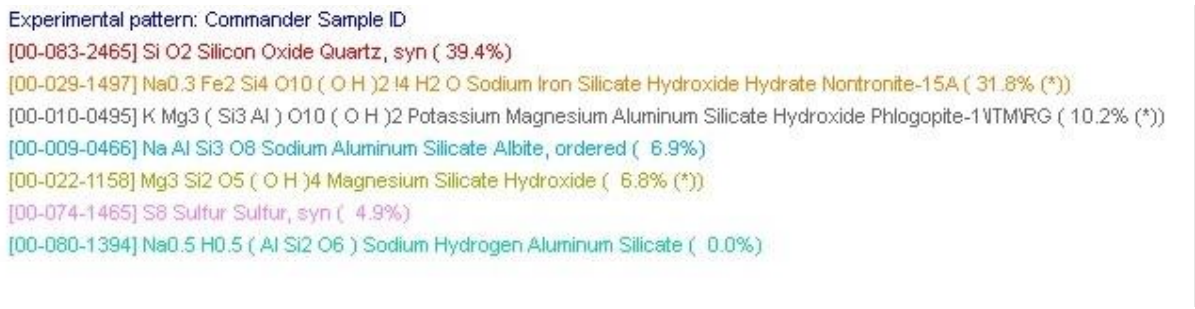

Figure 20. XRD results for duplicate GW samples treated with 5.0 vol% CPS

Figure 21. XRD results for duplicate PW samples treated with 0.5% CPS.

The PW samples treated with 5.0 vol% CPS revealed the presence of Jachymovite (uranyl-sulfate hydroxide) and sulfur (Figure 22).

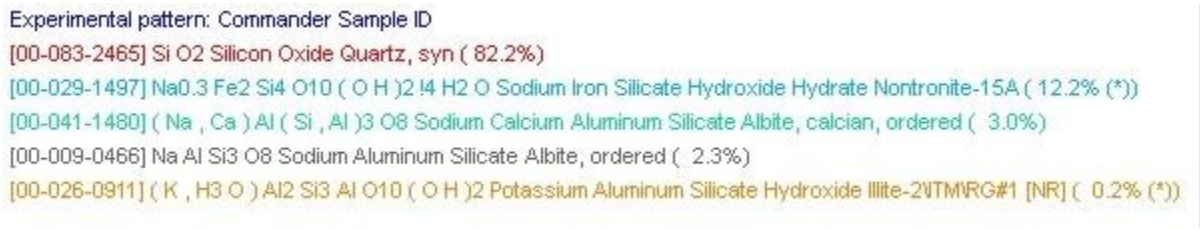

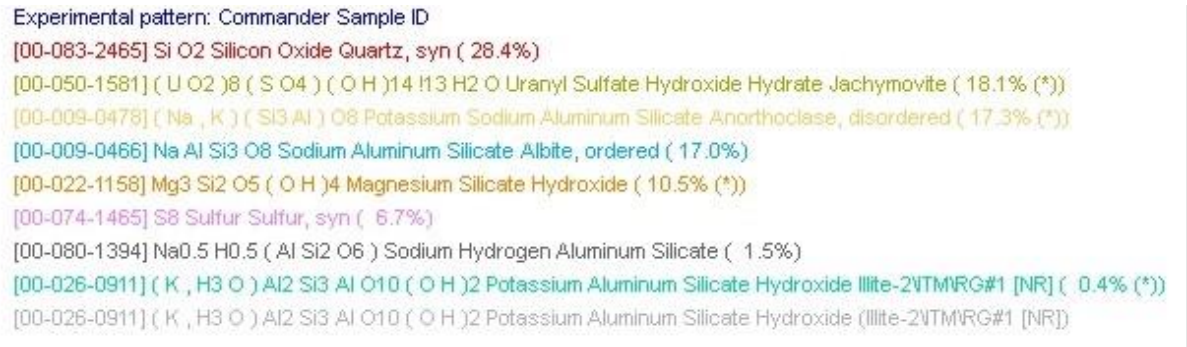

Figure 22. XRD results for duplicate PW samples treated with 5.0 vol% CPS.

Subtask 1.2: Conclusions

These experiments provided insight into the re-oxidation behavior of immobilized ^{99}Tc, ^{238}U, and NO_3^- in GW and PW samples treated with 0.5% and 5.0% CPS. Experimental data revealed a substantial decline of almost 99% in Tc concentration under anaerobic conditions in the presence of 0.5 vol% CPS in GW samples. However, it then increased to 0.08 remaining fraction by day 71 due to reoxidation. These results contrast with the data obtained for 5.0 vol% CPS, where a higher concentration of CPS of (5.0 vol%) only reduced Tc concentrations by approximately 20% from the initial value of 429.36 μ g/L. When the samples were exposed to aerobic conditions, the Tc concentration dropped to 0.1 remaining fraction but then slowly increased to 0.18 by day 71, indicating reoxidation of Tc.

In the PW samples treated with 0.5 vol% of CPS, the removal of U was relatively low, at 0.85 ± 0.03 in the aqueous phase by the end of Phase 2. However, the removal of U was significantly improved in the 5.0 vol.% CPS-amended samples, reaching a remaining fraction of 0.17 ± 0.03 in the solution. This remaining fraction corresponds to a U concentration of $25{,}490 \pm 3{,}612$ µg/L, significantly higher than in 1.0 wt.% ZVI and SMI-treated samples measured in FIU Year 2. Consequently, additional methods to sequester U would be needed to enhance CPS removal of U if field concentrations are this high to meet the required levels or regulatory guidelines.

The concentrations of NO_2^- were comparable in samples amended with both CPS concentrations at the end of Phases 1 and 2. The sulfate concentration was higher in 5.0 vol%-amended samples compared to 0.5 vol%-amended samples throughout both phases of the experiment.

Results obtained through measurements of ORP (mV) in anaerobic conditions supported this data, with average ORP values ranging from -300 to -400 mV; indicating strong reducing conditions. Similarly, the average ORP values in aerobic conditions ranged from +200 to +400 mV, indicating that oxidizing conditions were present throughout.

In Year 3, two abstracts, prepared in collaboration with PNNL, were submitted by FIU to the RemPlex conference (1) titled *"Re-oxidation Behavior of Technetium-99 and Uranium Immobilized by Zero Valent and Sulfur Modified Iron reductants"* and authored by Yelena Katsenovich, Hilary Emerson, Jim Szecsody, Nik Qafoku, Leonel Lagos and (2) *"Re-oxidation Behavior of Technetium-99 and Uranium Immobilized by Strong Reductants"* by Yelena Katsenovich, Angel Almaguer, Nik Qafoku, Jim Szecsody, Hilary Emerson, and Leonel Lagos.

The Remplex presentation was conducted as a poster and WM-2023 abstract was accepted as an oral presentation.

Subtask 1.2: References

Bard, A., 2017, Standard potentials in aqueous solution, Routledge.

Boglaienko, D., Emerson, H. P., Katsenovich, Y. P., and Levitskaia, T. G., 2019, Comparative analysis of ZVI materials for reductive separation of 99Tc (VII) from aqueous waste streams: Journal of hazardous materials, v. 380, p. 120836.

Katsenovich, Y. P., Maria, A. A., Williams, J., Kandel, S., Boglaienko, D., Emerson, H. P., and Levitskaia, T. G., 2023, Reductive removal of pertechnetate and chromate by zero valent iron under variable ionic strength conditions: Journal of Hazardous Materials, v. 445, p. 130546.

Lawter, A. R., Garcia, W. L., Kukkadapu, R. K., Qafoku, O., Bowden, M. E., Saslow, S. A., and Qafoku, N. P., 2018, Technetium and iodine aqueous species immobilization and transformations in the presence of strong reductants and calcite-forming solutions: remedial action implications: Science of the Total Environment, v. 636, p. 588-595.

Milazzo, G., Caroli, S., and Braun, R. D., 1978, Tables of standard electrode potentials: Journal of The Electrochemical Society, v. 125, no. 6, p. 261C.

Pearce, C. I., Cordova, E. A., Garcia, W. L., Saslow, S. A., Cantrell, K. J., Morad, J. W., Qafoku, O., Matyáš, J., Plymale, A. E., and Chatterjee, S., 2020, Evaluation of materials for iodine and technetium immobilization through sorption and redox-driven processes: Science of The Total Environment, v. 716, p. 136167.

Subtask 1.3: Evaluation of Competing Attenuation Processes for Mobile Contaminants in Hanford Sediments

Subtask 1.3: Introduction

Weapons production at the Hanford Site has created large volumes of legacy radioactive and chemical waste. Some contaminants were released to the environment through discharges to liquid disposal sites, cribs and trenches, or accidental leakages from single-shell tanks. Contaminants, including uranium (U), technetium-99 (^{99}Tc), iodine-129 (^{129}I), chromium (Cr), and nitrate (NO_3^-), migrated to the vadose zone creating subsurface plumes at the Hanford 200 Area located in the Central Plateau. These mobile contaminants persist in the subsurface and have potential to enter the groundwater via downward migration through the vadose zone. If allowed to reach the groundwater, contaminants could flow towards the Columbia River, a major water resource in the Pacific Northwest and a path for public exposure. Uranium is in the hexavalent form [U(VI)] primarily existing as tertiary neutral and anionic carbonate complexes ($Ca_2UO_2(CO_3)_3$ aq, $CaUO_2(CO_3)_3^{2-}$ in the natural oxic vadose zone environment at solution pH of ~ 8 (Gorman-Lewis et al. 2009). Technetium-99 is primarily in the form of anionic mobile pertechnetate (TcO_4^-) under oxidizing conditions (Peretyazhko et al. 2012). Chromium is present in the hexavalent form, the most mobile form of chromium, Cr(VI)] as chromate (CrO_4^{2-}) (Zachara et al. 2004). Major aqueous species of I have been distributed as 76% IO_3^-, 22% organo-iodine, and 2% I^- (Xu et al. 2015). Nitrate is stable and mobile in oxygenated environments (Martin 2011).

These co-contaminants in subsurface plumes at the 200 area are currently being remediated with pump and treat technology. Once active remediation is completed, a transition to more passive approaches, such as monitored natural attenuation (MNA) will be investigated. This will allow us to determine if the concentrations of these contaminants are behaving as predicted and if mobility is reduced by natural processes. Effective MNA requires a thorough understanding of the contaminant immobilization processes that keep the contaminants stable and resistant to remobilization during any changes in environmental conditions or groundwater chemistry. Quantifying contaminant attenuation processes via competitive adsorption mechanisms on vadose zone sediment will assess competitive attenuation processes. This effort was supported by conducting a column study with U and U+Cr in artificial groundwater (AGW) and Hanford formation sediment, a batch adsorption study of iodine, and a competition batch adsorption study with I, Cr, and U (both in AGW onto Hanford formation sediment.

Many studies have been conducted to understand the adsorption mechanisms of U(VI) onto a variety of different minerals and even natural sediment. Their findings have indicated that in the pH range of 6-9, the presence of calcium carbonate in sediment (from calcite) reduces U (VI) ability to sorb. This is due to the blockage of reactive sites by Ca^{2+} and the formation of neutral uranyl complexes ($Ca_2UO_2(CO_3)_3^0(aq)$) (Stewart, Mayes, and Fendorf 2010), (Zheng, Tokunaga, and Wan 2003), (Dong et al. 2005), (Fox, Davis, and Zachara 2006). However, there is still a need to incorporate the presence of collocated contaminants into these studies to understand the true adsorption capacity of sediment present at the Hanford Site. These contaminants include Tc-99, iodate, Cr (VI), and NO_3^- which may compete for reactive sites on the same minerals in the vadose zone. There, mineralogy is mainly comprised of quartz and feldspars; the finer-grained sediment includes a variety of phyllosilicates (Um et al. 2010).

This assessment will support the development of site conceptual models with co-located contaminants and identify relevant contaminant fate and transport parameters. Understanding of contaminant sorption behavior is also important for assessing the viability of long-term MNA.

Subtask 1.3: Objectives

This research is focused on competitive adsorption between contaminants of concern onto the Hanford formation vadose zone sediment as an assessment of their mobility and fate.

Uncontaminated sediments were collected at the Tristate Asphalt gravel pit in Pasco, WA. Previous research by Zachara et al. (2007) noted that iron-rich vadose zone sediment contains magnetite ($Fe^{II}Fe_2^{III}O_4$), ilmenite ($FeTiO_3$), Fe(II)/Fe(III) phyllosilicates, Fe(III) oxides (ferrihydrite [$5Fe_2O_3•9H_2O$]), and goethite [α-FeO(OH)]) (Gee et al. 2007). The finer grained sediments might also include the higher weight percentage of clay mineral phases such as illite (a dominant mineral in the clay-size fraction), smectite, biotite and chlorite. Sediment (≤2 mm) was used in all experiments.

The U+Cr competitive sorption capacity of the sediment was studied in column experiments at a ratio of 1:10. Results were compared with data when uranium was present alone. The competitive sorption capacity was further studied with U,I, and Cr competitive batch adsorption experiments. The solid to solution ratio was 1:1 and the ratios between the three contaminants were 1:1:0, 1:10:0, 1:1:10, and 1:10:10.

Subtask 1.3: Methodology

Further details on the methodology can be found in a draft manuscript *"Comparison of batch versus column methods for analysis of the impact of chromium (VI) as a co-contaminant on the sorption of uranium (VI) in sediments under mildly alkaline oxic conditions"* included in Appendix B.

Task 1.3: Results and Discussion

Further details on the experimental results can be found in the draft manuscript titled *"Comparison of batch versus column methods for analysis of the impact of chromium (VI) as a co-contaminant on the sorption of uranium (VI) in sediments under mildly alkaline oxic conditions"* included in Appendix B.

In addition, a manuscript titled *"Impact of chromium (VI) as a co-contaminant on the sorption and co-precipitation of uranium (VI) in sediments under mildly alkaline oxic conditions"* prepared on the results from FIU Year 2 was accepted for publication in the Journal of Environmental Management.

Subtask 1.3: Conclusion

FIU presented experimental results for this subtask during the DOE-FIU Cooperative Agreement Annual Research Review in August 2023. In the month of February, ARC's staff and students also traveled to Phoenix, Arizona for the 2023 Waste Management Symposia. DOE Fellow, Mariah Doughman, presented a poster titled *"Impact of Chromium (VI) as a Co-mingled Contaminant on the Adsorption of Uranium (VI) to Hanford Formation Sediment"* (Figure 23).

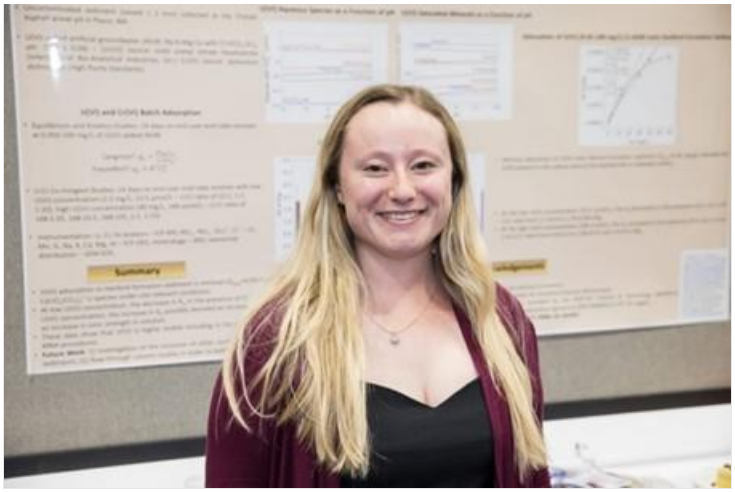

Figure 23. Mariah Doughman in front of poster at Waste Management 2023.

In addition, a manuscript titled *"Impact of chromium (VI) as a co-contaminant on the sorption and co-precipitation of uranium (VI) in sediments under mildly alkaline oxic conditions"* prepared on the results from FIU Year 2 was accepted for publication in the Journal of Environmental Management.

A new draft manuscript *"Comparison of batch versus column methods for analysis of the impact of chromium (VI) as a co-contaminant on the sorption of uranium (VI) in sediments under mildly alkaline oxic conditions"* based on the results of FIU Year 3 is included in Appendix B.

Subtask 1.3: References

Dong, Wenming, William P. Ball, Chongxuan Liu, Zheming Wang, Alan T. Stone, Jing Bai, and John M. Zachara. 2005. "Influence of Calcite and Dissolved Calcium on Uranium(VI) Sorption to a Hanford Subsurface Sediment." *Environmental Science and Technology* 39 (20): 7949–55. https://doi.org/10.1021/es0505088.

Fox, Patricia M., James A. Davis, and John M. Zachara. 2006. "The Effect of Calcium on Aqueous Uranium(VI) Speciation and Adsorption to Ferrihydrite and Quartz." *Geochimica et Cosmochimica Acta* 70 (6): 1379–87. https://doi.org/10.1016/j.gca.2005.11.027.

Gee, G. W., M. Oostrom, M. D. Freshley, M. L. Rockhold, and J. M. Zachara. 2007. "Hanford Site Vadose Zone Studies: An Overview." *Vadose Zone Journal* 6 (4): 899–905. https://doi.org/10.2136/vzj2006.0179.

Gorman-Lewis, Drew, Tatiana Shvareva, Karrie-Ann Kubatko, Peter C Burns, Dawn M Wellman, Bruce Mcnamara, Jennifer E S Szymanowski, Alexandra Navrotsky, and Jeremy B Fein. 2009. "Thermodynamic Properties of Autunite , Uranyl Hydrogen Phosphate , and Uranyl Orthophosphate from Solubility and Calorimetric Measurements." *Environ. Sci. Technol.* 43 (19): 7416–22. https://doi.org/10.1021/es9012933.

Martin, C J. 2011. "Overview of Hanford Hydrogeology and Geochemistry."

Peretyazhko, T S, J M Zachara, R K Kukkadapu, S M Heald, I V Kutnyakov, C T Resch, B W Arey, et al. 2012. "Pertechnetate (TcO4-) Reduction by Reactive Ferrous Iron Forms in Naturally Anoxic, Redox Transition Zone Sediments from the Hanford Site, USA." *Geochimica et Cosmochimica Acta* 92: 48–66. https://doi.org/10.1016/j.gca.2012.05.041.

Stewart, Brandy D., Melanie A. Mayes, and Scott Fendorf. 2010. "Impact of Uranyl - Calcium - Carbonato Complexes on Uranium(VI) Adsorption to Synthetic and Natural Sediments." *Environmental Science and Technology* 44 (3): 928–34. https://doi.org/10.1021/es902194x.

Um, Wooyong, Jonathan P. Icenhower, Christopher F. Brown, R. Jeffery Serne, Zheming Wang, Cleveland J. Dodge, and Arokiasamy J. Francis. 2010. "Characterization of Uranium-Contaminated Sediments from beneath a Nuclear Waste Storage Tank from Hanford, Washington: Implications for Contaminant Transport and Fate." *Geochimica et Cosmochimica Acta* 74 (4): 1363–80. https://doi.org/10.1016/j.gca.2009.11.014.

Xu, Chen, Daniel I. Kaplan, Saijin Zhang, Matthew Athon, Yi Fang Ho, Hsiu Ping Li, Chris M. Yeager, et al. 2015. "Radioiodine Sorption/Desorption and Speciation Transformation by Subsurface Sediments from the Hanford Site." *Journal of Environmental Radioactivity* 139: 43–55. https://doi.org/10.1016/j.jenvrad.2014.09.012.

Zachara, John, Calvin Ainsworth, Gordon Brown, Jeffrey Catalano, James McKinley, Odeta Qafoku, Steven Smith, James Szecsody, Sam Traina, and Jeffrey Warner. 2004. "Chromium Speciation and Mobility in a High Level Nuclear Waste Vadose Zone Plume." *Geochimica et Cosmochimica Acta* 68 (1): 13–30. https://doi.org/10.1016/S0016-7037(03)00417-4.

Zheng, Zuoping, Tetsu K. Tokunaga, and Jiamin Wan. 2003. "Influence of Calcium Carbonate on U(VI) Sorption to Soils." *Environmental Science and Technology* 37 (24): 5603–8. https://doi.org/10.1021/es0304897.

Subtask 1.4: Experimental Support of Lysimeter Testing

Subtask 1.4: Introduction

Vitrification is a well-demonstrated technology for the immobilization of radioactive wastes. This process involves melting waste materials with glass-forming additives to immobilize contaminants in the structure of the final vitreous product. Borosilicate glasses, extensively researched and demonstrated, are the most commonly used class of glasses for radioactive wastes, as they can effectively immobilize larger quantities of actinides (Grambow, 2006; Ojovan and Lee, 2011). While borosilicate glass is a dense material, the apparent dissolution rate, measured by the release of aqueous species into the bulk solution, can result from various processes. The specific process depends on the glass composition and the chemical and physical conditions near the glass surface (Gin et al., 2013). The chemical durability of borosilicate glasses, expressed as a dissolution rate (k, g $m^{-2}day^{-1}$), is a crucial criterion for accepting glass waste forms for geological disposal (Jantzen et al., 2010).

The corrosion of glass is conventionally assessed using ASTM Method C1662-18, *Standard Practice for Measurement of the Glass Dissolution Rate Using the Single Pass Flow-Through (SPFT) Test Method* and the static Product Consistency Test (PCT) (Standard, 2014). The corrosion rate can be calculated utilizing a model based on the transition state theory (TST) equation (Eyring, 1935). Following the dissolution of the glass and interaction with dissolved species in the near field, various secondary phases may precipitate (Cailleteau et al., 2008; Cailleteau et al., 2011). These processes can impact chemical and physical properties at the altered glass surface, leading to the formation of a 'protective' precipitate layer on the glass surface (Icenhower et al., 2004; Pierce et al., 2008) (Standard, 2014), or these phases can act as "sinks" for dissolved species, suppressing the dissolution rate. As the precipitates form, the concentration of controlling species is reduced, and consequently, the corrosion rate may increase.

One configuration at Hanford's Field Lysimeter testing units involves the co-disposal of grout waste forms above glass waste forms. The placement of grout waste forms above the glass is anticipated to significantly influence both the mechanisms and rate of glass corrosion. It is assumed that the alkaline water resulting from contact with the grout waste forms may enhance the dissolution rate of the glass waste forms beneath, and pre-experimental modeling has suggested such behavior. The grout-contacted water, characterized by elevated pH (~12), contains dissolved species from the grout (e.g., Si, Al, Ca, K) that might impact the rate of glass dissolution through common ion effects or precipitation reactions. If the composition of the pore water contacting the glass is predominantly influenced by the grout, the formation of calcium-silicate-hydrates is anticipated due to the strong affinity between calcium and silica gels in alkaline media (Armelao et al., 2000).

A field lysimeter test is currently ongoing at the Hanford site in which glass and cementitious waste forms are placed within disposal backfill near the planned disposal facility (Bacon et al., 2018).

In FIU Year 3, research efforts have been dedicated to examining the impact of calcium ions within solutions of varying pH levels on the corrosion behavior of borosilicate glass and finilyze a static long-term PCT experiment with three solutions: a pH 12 buffer, Ca^{2+} (130 ppm) in a pH 12 buffer, and grout-contacted solutions.

Subtask 1.4: Objectives

The objective of this study is to assess the influence of temperature, pH, and dissolved components on the dissolution rate of borosilicate glass in the presence of grout-contacted solution. This investigation aims to determine whether the dissolution behavior of the glass is primarily controlled by a pH-mediated effect induced by the sediment or by the chemical composition of the grout-contacted groundwater.

Subtask 1.4: Methodology

Further details on the methodology can be found in the draft manuscript titled *"Tracking the effect of Ca on the dissolution of Re and B from the borosilicate glass"* included in Appendix C

Subtask 1.4: Results and Discussion

Further details on the experimental results can be found in the draft manuscript titled "Tracking the effect of Ca on the dissolution of Re and B from the borosilicate glass" included in Appendix C".

Subtask 1.4: Conclusion

The outcomes of these experiments will offer valuable insights to inform the design of future Field Lysimeter Testing Units (FTLF) dedicated to exploring the dissolution of waste forms at the Hanford Site Integrated Disposal Facility (IDF). Further details on methodology and results of experiments can be found in a draft manuscript included in Appendix C.

The achievement of this task also includes a manuscript titled "The corrosion behavior of borosilicate glass in the presence of cementitious waste forms" and authored by Yelena Katsenovich, Vadym Drozd, Shambhu Kandel, Leonel Lagos, R. Matthew Asmussen" prepared on the results of the FIU Year 2. The draft is currently on the revision after PNNL review.

Subtask 1.4: References

Armelao, L., Bassan, A., Bertoncello, R., Biscontin, G., Daolio, S. and Glisenti, A., 2000. Silica glass interaction with calcium hydroxide: a surface chemistry approach. Journal of Cultural heritage, 1(4): 375-384.

Bacon, D.H., Meyer, P.D., Neeway, J.J., Fang, Y., Asmussen, R.M. and Strickland, C.E., 2018. Field-Scale Lysimeter Studies of Low-Activity Waste Form Degradation, Pacific Northwest National Lab.(PNNL), Richland, WA (United States).

Cailleteau, C., Angeli, F., Devreux, F., Gin, S., Jestin, J., Jollivet, P. and Spalla, O., 2008. Insight into silicate-glass corrosion mechanisms. Nature materials, 7(12): 978-983.

Cailleteau, C., Devreux, F.o., Spalla, O., Angeli, F. and Gin, S., 2011. Why do certain glasses with a high dissolution rate undergo a low degree of corrosion? The Journal of Physical Chemistry C, 115(13): 5846-5855.

Eyring, H., 1935. The activated complex in chemical reactions. The Journal of Chemical Physics, 3(2): 107-115.

Gin, S., Abdelouas, A., Criscenti, L.J., Ebert, W.L., Ferrand, K., Geisler, T., Harrison, M.T., Inagaki, Y., Mitsui, S. and Mueller, K.T., 2013. An international initiative on long-term behavior of high-level nuclear waste glass. Materials Today, 16(6): 243-248.

Grambow, B., 2006. Nuclear waste glasses-How durable? Elements, 2(6): 357-364.

Icenhower, J.P., Samson, S., Lüttge, A. and McGrail, B.P., 2004. Towards a consistent rate law: glass corrosion kinetics near saturation. Geological Society, London, Special Publications, 236(1): 579-594.

Jantzen, C.M., Brown, K.G. and Pickett, J.B., 2010. Durable glass for thousands of years. International Journal of Applied Glass Science, 1(1): 38-62.

Ojovan, M.I. and Lee, W.E., 2011. Glassy wasteforms for nuclear waste immobilization. Metallurgical and Materials Transactions A, 42(4): 837-851.

Pierce, E.M., Rodriguez, E.A., Calligan, L.J., Shaw, W.J. and McGrail, B.P., 2008. An experimental study of the dissolution rates of simulated aluminoborosilicate waste glasses as a function of pH and temperature under dilute conditions. Applied Geochemistry, 23(9): 2559-2573.

Standard, A., 2014. C1285-14, Standard Test Methods for Determining Chemical Durability of Nuclear, Hazardous, and Mixed Waste Glasses and Multiphase Glass Ceramics: The Product Consistency Test (PCT). ASTM International, West conshohocken, PA.

TASK 2: REMEDIATION RESEARCH AND TECHNICAL SUPPORT FOR THE SAVANNAH RIVER SITE

Subtask 2.1: Environmental Factors Controlling the Attenuation and Release of Contaminants in the Wetland Sediments at Savannah River Site

Subtask 2.1: Introduction

The F-Area Seepage Basins located within the Savannah River Site (SRS) are approximately 6.5 acres in size and comprise three unlined basins. Low-level radioactive effluent from the reprocessing of radioactive fuel at the F-Area Separation Facility was disposed of in these basins. The waste solution contained diluted nitric acid, radionuclides such as cesium-137, strontium-90, uranium-238, technetium-99, and iodine-129, as well as non-radioactive metals [1]. A large amount of ^{129}I and other radionuclides migrated to the vadose zone and contaminated the groundwater, where it was transported to the wetland associated with a local stream, Fourmile Branch [2-4]. At the F-Area, several remediation techniques were used, including pump-and-treat and funnel-and-gate with base and silver chloride injection. The natural attenuation of contaminants in the organic-rich soils of the Fourmile Branch wetland is also important in the remediation of the F-Area Seepage Basins' groundwater.

In the past, the wetland at the F-Area has been an important sink for ^{129}I and other contaminants, but changes in biogeochemical conditions could cause the release of these contaminants into the surrounding areas [3, 5-10]. Recently, elevated levels of radioiodine were detected in the groundwater of the Fourmile Branch wetland, mostly as ^{129}I with multiple anionic species (i.e., I^-, IO_3^-, and organo-iodide) [11]. Previous field sampling events have indicated that ^{129}I is being accumulated in the topsoil at the wetland [3, 12]. The availability of iodine species is primarily dictated by its speciation, with I^- being the dominant species near the basin while IO_3^- and organo-iodine are the major species near the wetland [13]. Adsorption onto mineral surfaces, natural organic matter, and colloids is the primary geochemical process affecting iodine species, which is controlled by the redox potential and solution pH [7]. The geochemical environment in wetlands is complex due to the abundance of organic matter, vegetation, rainwater, seasonal temperatures, and the cycles of sediment saturation and unsaturation. Both naturally occurring ^{127}I and the contaminant ^{129}I, have been shown to strongly bind to natural organic matter [9-10, 14-15], whereas interactions with inorganic minerals are relatively weak. Hence, a better understanding of the environmental conditions that affect these processes is critical to a more realistic risk assessment.

The goal of this study is to elucidate the attenuation and release mechanisms of ^{129}I occurring at the wetland. Detailed solid characterization of the soil samples was carried out before the treatment of iodine species. A sequential extraction of the wetland soils was conducted to understand the iodine bound to different fractions of the soil profile at different depth intervals. The uptake of iodide and iodate by wetland soils at various depths and under various environmental conditions was investigated.

Subtask 2.1: Objectives

The research objective of this study is to better understand the dominant attenuation mechanisms for ^{129}I in the wetlands, how strong is the attenuation, and what conditions would reverse it. The potential findings of this study will improve the understanding of the effect of environmental factors on the adsorption and release of iodine species and determine if organoclays are feasible amendments for in-situ remediation of iodine species in the SRS wetland environments. The study will also determine conditions for optimal iodide, iodate, and organo-iodine removal from the aqueous phase.

Subtask 2.1: Methodology

Chemicals:

The iodide standard (I^-, 1000 µg/mL) and rhenium (Re, 1000 µg/mL) were purchased from SPEX CertiPrep. The VeriSpecTM iodate standard (IO_3^-, 1000 ppm) and VeriSpec® Tellurium concentration were obtained from Rica Chemical. Tetramethylammonium hydroxide (TMAH, 25%) and sodium chloride (NaCl) were obtained from Fisher Scientific. Ammonium acetate (NH_4OAc) and hydroxylamine hydrochloride $(NH_3OH)_2 \cdot HCl$ were purchased from Alfa Aesar. Millipore water (MilliQ water, resistivity ~18.2 $M\Omega \cdot cm^{-1}$ at 22 °C) was used for samples and standards preparation unless indicated.

In this study, riparian wetland soils were collected in January 2021 at an uncontaminated area along the Fourmile Branch stream, a tributary of Savannah River located within the Savannah River Site that has not been affected by site operations. The study area is in the upper Coastal Plain of South Carolina, where the sediments are composed of stratified quartz sand, clay, calcareous sediments, and conglomerates [16]. The water table at Fourmile Branch watershed fluctuates between 30 cm above and below the soil surface, keeping the soil profile saturated throughout the year [17]. Vertical soil profile sampling was performed using a Geoprobe (model 6620DT) for deeper samples (≥ 1.5 meters) and a hand auger for shallower samples (≤ 0.9 meter). The soils were dried in an oven at 30°C for 2 weeks until the weight of the dried sample was stabilized and sieved using a 2 mm sieve.

Effects of Environmental Factors on the Attenuation of Iodine:

To understand the factors controlling the attenuation and release mechanisms of iodine, the effects of dissolved organic content, temperature, oxidation and reduction potential on the adsorption/desorption of iodide and iodate on wetland soils were investigated. Based on the results from the sediment depth profile study conducted by the Savannah River National Laboratory [12], the following depth intervals were chosen for the batch experiments: 0.3 - 0.9, 1.5 - 1.8, and 4.0 - 4.3 m, representing the organic layer (high organic carbon content), transition layer (intermediate organic carbon content), and the aquifer layer (low organic carbon content) as shown in Table 7 the soil parameters data at different depth intervals were obtained from Gonzalez-Raymat et al., 2021 [12].

Table 7. Soil parameters at three different depth intervals [12]

Soil depth interval (m)	pH	Total Organic Carbon (mg/kg)	Aluminum (mg/kg)	Iron (mg/kg)	Manganese (mg/kg)	Sulfur (mg/kg)

0.3 - 0.9	4.79±0.10	25,300 -119,000	5,310 - 7,130	1340 - 8940	20.3 - 126	170 - 297
1.5 - 1.8	5.05	41,700	4,310	215	3.49	356
4.0 - 4.3	5.49	350	2,920	180	4.21	27

The general procedure for the batch experiments is described as the following: triplicate background soils (25.0 g/L) were equilibrated with 0.01 M NaCl solution for a week. The pH of samples was adjusted to 5.5 ± 0.2 by adding 0.1 M NaOH or HCl during the contact time. Then, the samples were spiked with 10 mg/L stock solution of either iodide or iodate to achieve the final concentration of 100 µg/L of the analyte. A control study was also performed to monitor the effect of temperature, organic matter, and redox conditions on the wetland soil as well as release of natural iodine incorporated in the soil (if any) during the experiment. Finally, the samples were shaken at 100 rpm for 7 days and aliquots were collected at predetermined time intervals and centrifuged at 12,000 rpm for 6 min to separate the solid phase from the aqueous phase. The supernatants were transferred into new vials and analyzed by ICP-MS for total iodine in the aqueous solutions.

The seasonal temperature of the surface water at the Fourmile Branch wetland fluctuates between 5 and 25ºC. The effect of temperature study was conducted by measuring the adsorption and desorption of either I^- or IO_3^- at different temperatures, 8ºC and 22 ± 1.0ºC, in a temperature controlled environmental chamber, which represented the warm temperature climate prevailing in the Fourmile Branch wetland. The temperatures of 8°C and ~22°C represent the average temperature of surface water during the winter and summer months, respectively. The soil samples were exposed to the proposed temperatures for 7 days before the kinetic studies were initiated. Then I^- or IO_3^- was spiked into the solution following the described procedure above.

The effect of redox condition study was carried out by performing the anoxic condition experiment in the anaerobic glovebox. The anaerobic chamber (Figure 24) was set up and purged with mixed gas (5% H_2 + 95% N_2) multiple times to remove oxygen in the chamber, in conjunction with a palladium catalyst to create an anaerobic environment to study the effects of oxidation-reduction potential on the sorption and release of iodine from the wetland soil. First, the I^- and IO_3^- stock solutions (10 mg/L), 0.01 M NaCl, 0.1 M NaOH, or 0.1 M HCl, and DI water solutions were purged with nitrogen gas for 60 min at a low flow rate to remove dissolved oxygen in the solutions. Next, the weighed soil samples and working solutions were moved to an anaerobic glovebox. The soil samples and the working solutions were uncapped and exposed to the anoxic environment for at least 3 days at 22 ± 1.0ºC before 0.01 M NaCl solution was added into the soil samples following the general protocol described above for the effect of redox condition experiment.

Figure 24. FIU's anaerobic chamber for conducting anaerobic experiments.

Subtask 2.1: Results and Discussion

Effects of Temperature

At 22 ± 1.0°C in an oxic environment, an apparent instantaneous uptake of iodide from solution occurred for all soil layers in less than 1 h (Figure 25a), followed by a time-dependent sorption. The sorption of iodide onto the surface of 0.3 – 0.9 and 1.5 – 1.8 m soil samples gradually increased over a 7–day sorption time ($q_{t,7d}$ = 1.726 ± 0.183 and 1.665 ± 0.142 mg/kg, respectively). The slow and quasi-steady-state pattern of iodide uptake was also observed previously for other soils sampled from the F-Area at different locations (OC, 8.4 wt %) [18] and FSI18 (OC, 24.1 wt %) [14], which were then assigned to abiotic and biotic reactions depending on the pH conditions. Meanwhile, the iodide sorption onto 4.0 – 4.3 m sample was stabilized over the next 7 days. Because of the low amount of organic matter in the aquifer soil sample, as shown Figure 25, saturation of available sorption sites on the surface resulted in sorption capacity stabilization. Whitehead [19] and Couture and Seitz [20] reported that no iodide sorption onto kaolinite mineral was observed in their studies. Kaplan *et al.*, demonstrated that goethite and quartz minerals exhibit little to no iodide sorption [21]. Fox *et al.*, observed that under an oxic environment, iodide was oxidized to I_2 and IO_3^- after being injected in the soil [22]. There are several potential iodide oxidants such as dissolved O_2, NO_3^-, and Mn/Fe oxides present in the soil. Due to an elevated concentration of nitrate in the Fourmile Branch soil [23], NO_3^- could potentially oxidize I^- to form I_2. Another possible pathway for the uptake of iodide by soils is iodide oxidation by Mn oxides and FeOOH, which is favorable in the circumneutral pH range [24]. As shown by Reiller *et al.*, the binding of iodine to organic matter was related to redox transformation of iodide by humic substances to reactive iodine species [25]. These reactive iodine species then bind to organic matter via electrophilic substitution, which primarily takes place on the aromatic ring of humic components within the soil [25-26]. Under our experimental conditions (pH = 5.5 ± 0.2), microbial enzymatically catalyzed iodination of soil organic matter is another potential pathway for iodide uptake by soils

[14]. Furthermore, the nitrogen-containing substituents of soil organic matter are protonated under acidic conditions, which can adsorb iodide via an electrostatic interaction.

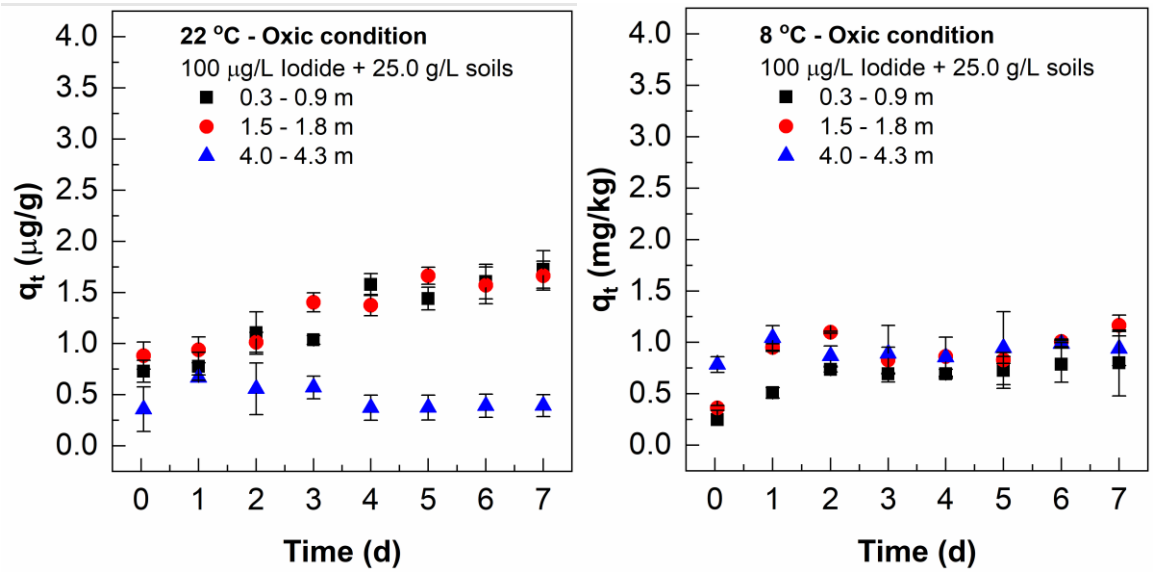

Figure 25. Uptake of iodide on wetland soil at (a) 22 ± 1°C and (b) 8 °C at different layers: 0.3 – 0.9, 1.5 – 1.8, and 4.0 – 4.3 m.

At 8°C, iodide initially adsorbed onto all soil samples within 24 hours and the sorption was slower and stabilized over the next 7 days (Figure 25b). Although, freezing conditions are known to induce the formation of volatile elemental iodine from iodide solutions [15], volatilization of iodine from solution is considered unlikely since the range of iodine loss rate constants was very small ($< 10^{-9}$ s) in previous reports [15, 27-28]. The differences in uptake of iodide between 8 and 22 ± 1.0°C could be attributable to an increase in the kinetic energy of the molecules and an increase in enzymatic activity affecting iodide incorporation into organic matter in the top and intermediate soil samples. Similar to our result, Lusa *et al.*, showed iodide sorption exhibited dependence on the temperature when compared to the sorption of iodide to peat at 4 and 20°C [29]. On the contrary, Söderlund *et al.*, [30] and Fukui *et al.*, [31] found no systematic relationship between temperature and iodide sorption on soils, which can be caused by the low organic carbon content in soils in their studies (< 1 % and 2.3 %).

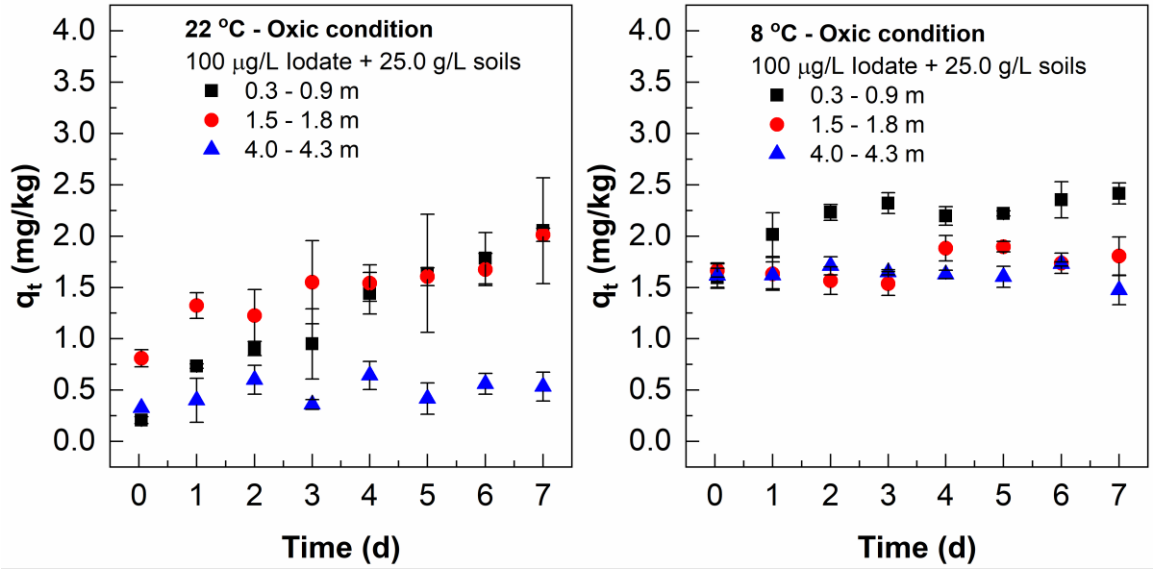

Figure 26. Uptake of iodate on wetland soil at (a) 22 ± 1 °C and (b) 8 °C at different layers: 0.3 – 0.9, 1.5 – 1.8, and 4.0 – 4.3 m.

Uptake of iodate by the soil at different depths also followed a similar quasi-steady-state pattern and was not significantly higher than iodide at 22°C (Figure 26**Figure 26**a). The rapid initial loss of iodate may be due to a combination of volatilization, electrostatic and chemisorption on inorganic soil fractions, and rapid immobilization by reduction at reactive sites in organic matter such as hydroquinone [32]. In the subsoil layer (4.0 – 4.3 m), iodate uptake was slightly higher than that of iodide at room temperature ($q_{t,7d}$ = 0.533 ± 0.140 and 0.392 ± 0.107 mg/kg for iodate and iodide sorption at 22°C, respectively). Previous studies have shown that iodate adsorbed more readily onto mineral surfaces than iodide [20]. In the absence of organic matter, iodate preferentially binds to iron and aluminum oxides at pH < 6 [33]. As discussed by Kaplan *et al.*, IO_3^- favors hard – hard interactions with the hard acid binding sites on the mineral surfaces due to the harder base nature of IO_3^- compared to the soft nature of I^- [21], whereas I^- readily diffuses into intragranular spaces in the soil particles in addition to ion-exchange on the surfaces, which is a more irreversible process [31]. Natural organic matter can induce iodate reduction to electrophilic species such as hypoiodous acid (HIO) or I_2 before incorporation into the organic structure of natural organic matter [32]. Shetaya *et al.*, selected 9 different soils with a range of pH values, Fe/Mn oxide content, and organic matter for incubation with $^{129}I^-$ or $^{129}IO_3^-$ at 10 and 20°C [34]. They reported that conversion of added $^{129}IO_3^-$ to Org-^{129}I was significantly slower than conversion of $^{129}I^-$ to Org-^{129}I. According to previous research, humic acid can reduce IO_3^- and oxidize I^- in soils [35]. As mentioned above, unless Fe(III) and Mn(IV) oxides catalyze the oxidation of I^- [24], the reduction of IO_3^- to I^- is much faster than the oxidation of I^- to IO_3^- by organic matter [36]. The largest initial iodate uptake was observed in all soils at 8°C. Similar to our result, Fukui *et al.*, observed iodate sorption was higher at the low temperature when compared the solid–liquid distribution coefficient values at 15, 32, and 55°C [31], however, no explanation was given. Satoh and Imai found that the dissolution of iodate was not correlated to the temperature as the dissolution rate was similar at high, medium, and low temperature [37].

Effect of Redox Potential

Oxic and anoxic batch sorption experiments were conducted in parallel using I^- and IO_3^- concentrations of 100 μg/L, pH ≈ 5.5, background ionic strength of 0.01 M NaCl, and 25 g/L of

the wetland sediments at different depths. The q_t values of I^- uptake on 0.3 – 0.9 m and 1.5 – 1.8 m soil samples in anoxic conditions were significantly less than those completed under oxic conditions ($q_{t,7d}$ = 0.740 ± 0.143, 0.817 ± 0.097, 1.626 ± 0.183, and 1.665 ± 0.142 mg/kg for top and intermediate layers in anoxic and oxic conditions, respectively). Similar to our results, Sheppard and Hawkins reported a decrease in sorption of ^{125}I onto peat in an anoxic environment [38]. Bird and Schwartz observed that there was little ^{125}I sorption onto lake sediments under an anoxic environment [39]. Ashworth and Shaw also found that iodine sorption was significantly reduced in their column studies under an anoxic environment [40]. The reduced sorption of iodine onto organic-rich soils under an anoxic environment may be linked to both the microbial activity and the chemical reactions involving I^-. In the anoxic environment, I^- is chemically stable, and there is little microbial activity so the majority of I^- remains soluble. Keppler *et al.*, discovered that halide ions can be alkylated when organic matter is oxidized by an electron acceptor such as Fe(III) in the soils [41]. Because of faster Fe(III) reduction at lower pH, the formation of alkyl halides was significantly higher than those formed at the higher pH condition [42]. Under our experimental conditions, the loss of iodide from the aqueous solution in all soil samples could be assigned to the abiotic halogenation of organic compounds.

Metal (oxy)hydroxides are often bound to soil organic matter through functional groups, such as phenolate and carboxylate groups [43]. Under reducing conditions, iodate can undergo abiotic reduction to its lower valence, highly soluble form, I^- in Mn(IV) and Fe(III) reducing conditions [44]. As mentioned above, iodate can be converted to HIO and I_2 by natural organic matter before adsorbing onto natural organic matter [32]. Iodate can also be reduced biotically with several IO_3^--reducing microorganisms that have been reported, which include Shewanella putrefaciens [45], Shewanella oneidensis, Desulfovibrio desulfuricans [46], and Pseudomonas sp. strain SCT [47].

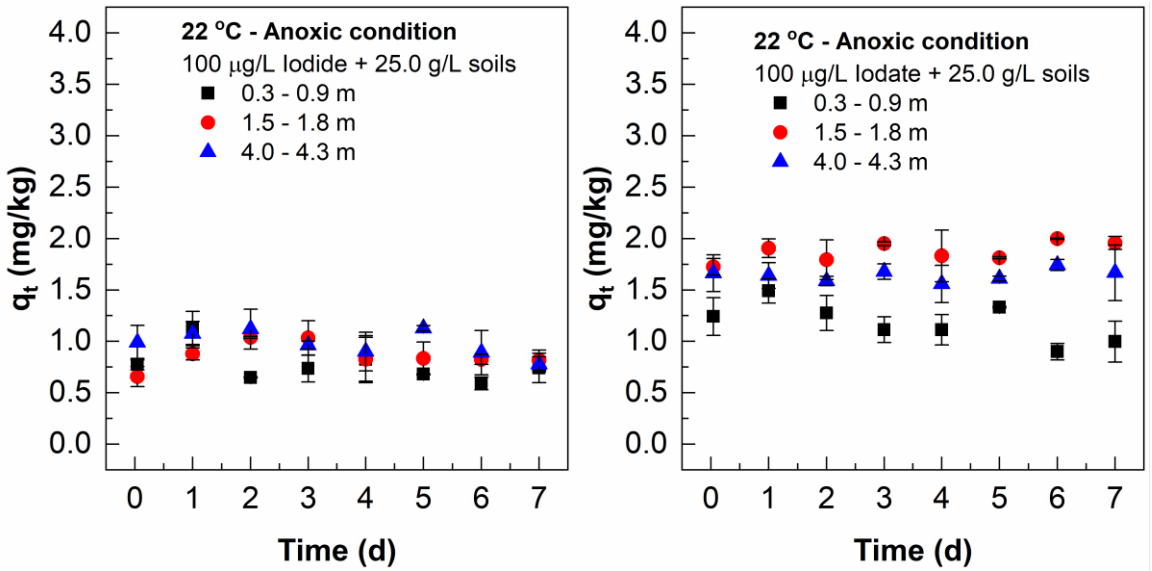

Figure 27. Uptake of iodide (a) and iodate (b) on wetland soils at 22 ± 1 °C under the anoxic conditions at different layers: 0.3 – 0.9, 1.5 – 1.8, and 4.0 – 4.3 m.

A control study was performed to observe any release of naturally bound iodine in the soils into the aqueous phase under various conditions. Under an anoxic environment, the naturally bound iodine was released into the aqueous environment from the organic-rich topsoil sample (Figure 28). Under anoxic conditions, halogenated aliphatic and aromatic pollutants commonly undergo reductive dehalogenation [48-49]. The biotic dehalogenation of halogenated organic compounds has

been studied extensively with various anaerobic bacteria including the genera Desulfitobacterium [50-51] and Dehalococcoides [52]. Redeker *et al.*, detected partially deiodinated products of diatrizoate in anoxic batch experiments with sediment collected from a polishing pond and groundwater [53]. The abiotic dehalogenation catalyzed by free corrinoids have been studied for iodinated compounds [54]. Under a reducing environment, the organic matter in the organic-rich soil would be more likely to undergo abiotic and biotic reductive dehalogenation, releasing inorganic I^- into the aqueous phase.

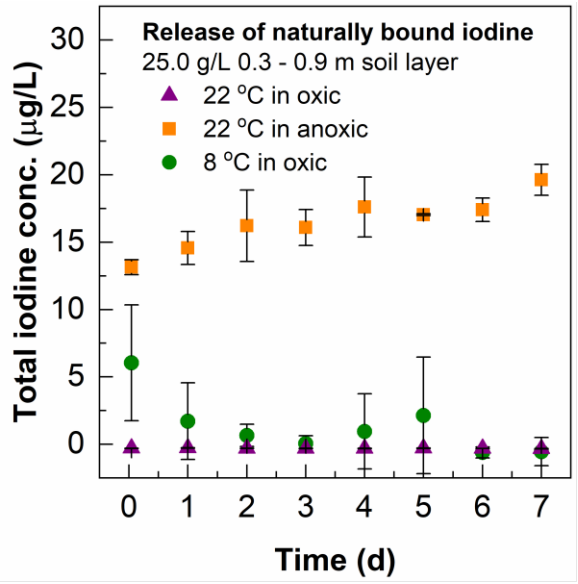

Figure 28. Release of naturally bound iodine from 0.3 – 0.9 m soil layer at 22ºC oxic, anoxic, and 8ºC oxic conditions.

The uptake of iodide onto the soils was extended to 3-4 weeks for anoxic and oxic conditions, respectively. At 22 ± 1.0 °C in an oxic environment, an apparent instantaneous uptake of iodide from solution occurred for all soil layers in less than 1 h, followed by a time-dependent sorption (Figure 29). While, in an anoxic condition, uptake of iodide was observed for the first hour and then stabilized. In the anoxic environment, I^- is chemically stable, and there is little microbial activity so that the majority of I^- remains as a soluble species.

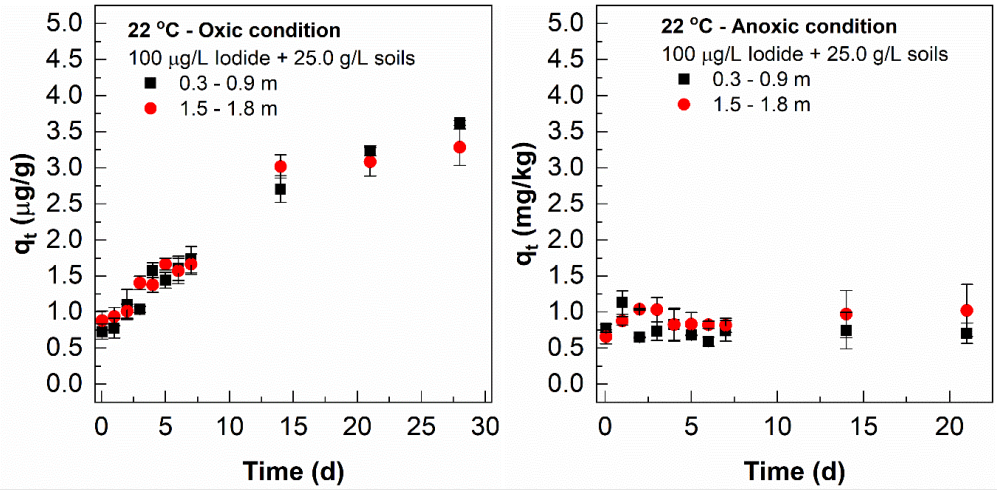

Figure 29. Uptake of iodide by wetland soils (a) oxic and (b) anoxic conditions.

The uptake of iodate onto the soils was extended to 3-4 weeks for anoxic and oxic conditions, respectively (Figure 30.). At 22 ± 1.0 °C in an oxic environment, an apparent instantaneous uptake of iodate from solution occurred for all soil layers in less than 1 h, followed by a time-dependent sorption. While, in an anoxic condition, a fast uptake of iodate was observed for the first hour and then stabilized over 3 weeks. Under reducing conditions, iodate can undergo abiotic reduction to its lower valent, highly soluble form, I^-, in Mn(IV) and Fe(III) reducing conditions. Iodate can be converted to hypoiodous acid (HIO) and I_2 by natural organic matter before adsorbing onto natural organic matter. It has been reported that iodate can also be reduced biotically by several IO_3^--reducing microorganisms, which include Shewanella putrefaciens, Shewanella oneidensis, Desulfovibrio desulfuricans, and Pseudomonas sp. strain SCT.

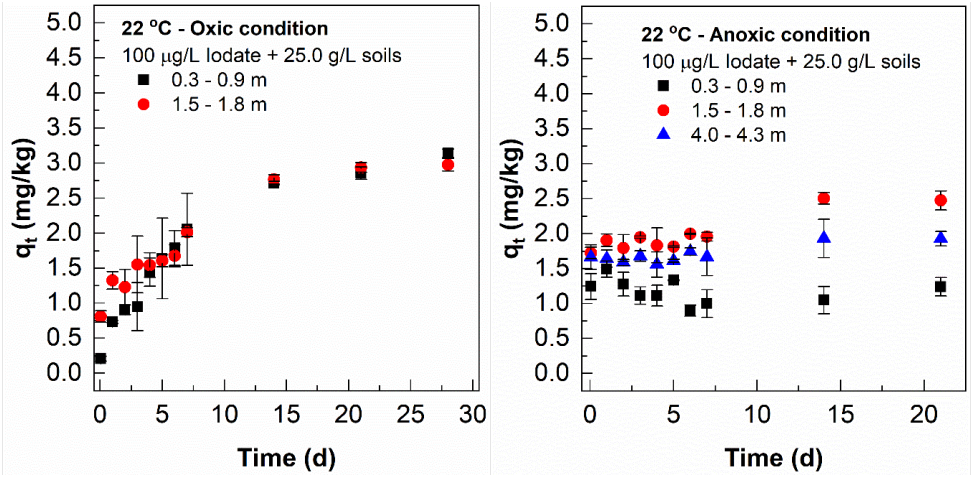

Figure 30. Uptake of iodate by wetland soils (a) oxic and (b) anoxic conditions.

Subtask 2.2: Conclusions

In the current study, the uptake of iodide and iodate by wetland soils at various depths was studied under various environmental conditions including temperature and redox potential. The uptake was slightly faster with IO_3^- compared to systems spiked with I^- due to the better sorption of iodate to the mineral surfaces within the soil matrix. The organic matter and microbes present in the soil show a significant influence on the uptake of iodide and iodate. The iodide uptake was significantly lower at 8°C than at 22°C, indicating that temperature has an effect on iodide uptake, which could be explained by a decrease in kinetic energy and enzymatic activity at 8°C. The uptake of iodate by organic-poor soil at 8°C was much higher than at 22°C. This was most likely due to a decrease in the enzymatic reduction of iodate to reactive iodine species, which maintains free iodate in the aqueous phase to bind to mineral surfaces in the soil.

The reduced uptake of iodine onto organic-rich soils under an anoxic environment may be linked to both the microbial activity and the chemical reactions involving I^-. In the anoxic environment, I^- is chemically stable, and there is little microbial activity so the majority of I^- remains as a soluble species. Under reducing conditions, iodate can undergo abiotic and biotic reduction to reactive iodine species by natural organic matter and microbes before adsorbing onto the organic structure of natural organic matter. A control study was conducted with soils at different depths and the release of iodine was observed for the organic-rich soil sample. Under anoxic conditions, halogenated aliphatic and aromatic pollutants commonly undergo reductive dehalogenation.

Subtask 2.2: Other Activities

DOE Fellow Phuong Pham prepared a poster for the annual DOE Fellows Poster Exhibition which will be held on November 7, 2022 at the FIU Engineering Center. The poster is based on her current DOE-related research at ARC.

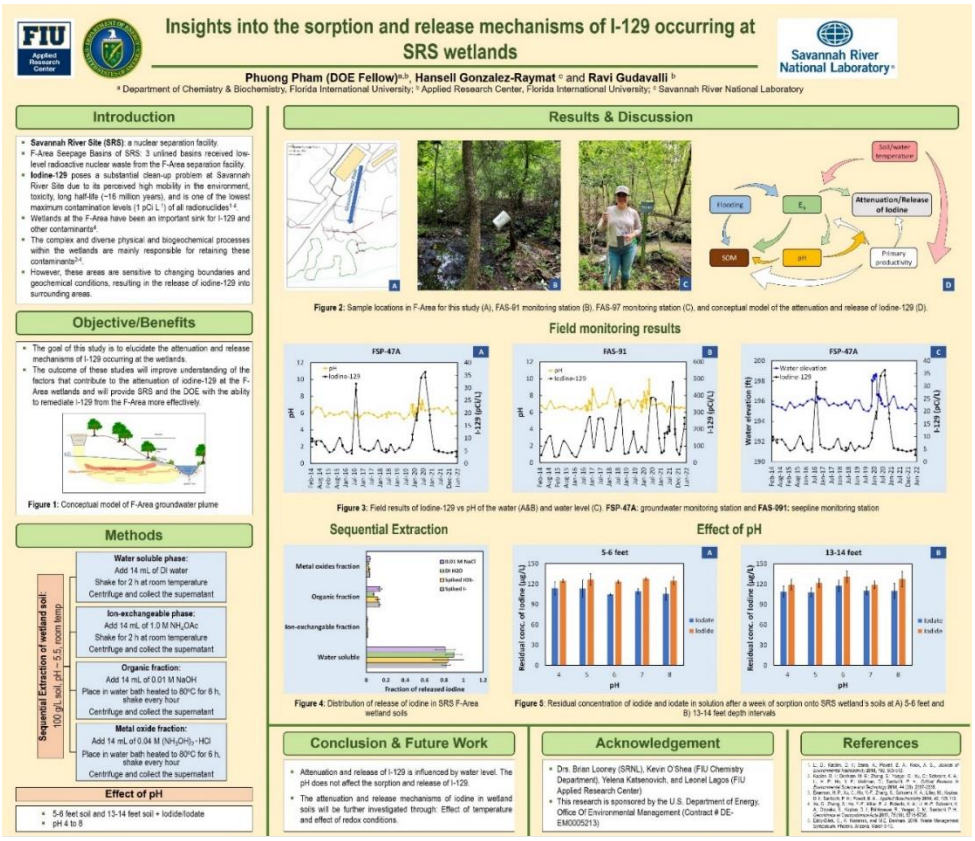

Figure 31. Poster prepared by DOE Fellow Phuong Pham for the 2022 DOE Fellows Poster Exhibition.

FIU completed Milestone 2022-P2-M3 *"Complete batch experiments on the influences of environmental factors on the attenuation and release of Iodine from SRS wetland soils"*. The uptakes of iodide and iodate by wetland soils at various depths under different environmental conditions such as temperature and redox potential were investigated. The initial uptake of I^- was slightly slower than that of IO_3^-, indicating that iodate readily adsorbs onto the positively charged metal-oxide surface and nitrogen-containing constituents of soil organic matter. The iodide uptake was significantly lower at 8°C than at 22°C, indicating that temperature has an effect on iodide uptake. The uptake of iodate by organic-poor soil at 8°C was much higher than that at 22°C, which was likely due to a decrease in the enzymatic reduction of iodate to reactive iodine species, which allows free iodate in the aqueous phase to bind to mineral surfaces in the soil. The reduced sorption of iodine onto organic-rich soils under an anoxic environment may be linked to both the microbial activity and the chemical reactions involving I^-. Under reducing conditions, iodate can undergo abiotic and biotic reduction to reactive iodine species by natural organic matter and microbes before adsorbing onto the organic structure of natural organic matter. A control study was conducted with soils at different depths, a release of total iodine was observed for organic-rich soil samples. Under anoxic conditions, halogenated aliphatic and aromatic pollutants commonly undergo reductive dehalogenations.

DOE Fellow, Phuong Pham, presented an oral presentation on the remediation of iodine by organoclays and a Roy G. Post scholarship poster presentation on characterization of SRS wetland soils during the Waste Management Symposia 2023 (WM2023).

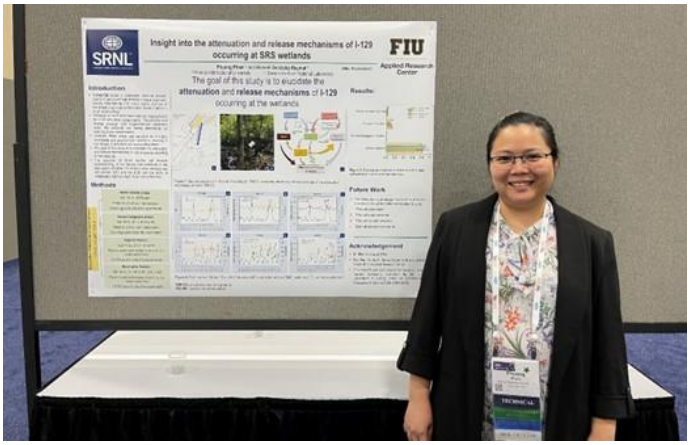

Figure 32. DOE Fellow Phuong Pham presenting poster during WM2023.

DOE Fellows Phuong Pham successfully defended her dissertation on March 21st. Upon completion of her Ph.D. program she joined SRNL as a Postdoctoral Associate.

Figure 33. DOE Fellow, Phuong Pham, at her Ph.D. defense.

Subtask 2.1: References

1. Corbo, P.; Killian, T. H.; Kolb, N. L.; Marine, I. W. F-Area Seepage Basins: Environmental information document; United States, 1986; p Medium: X; Size: Pages: 245.
2. Zhang, S.; Ho, Y.-F.; Creeley, D.; Roberts, K. A.; Xu, C.; Li, H.-P.; Schwehr, K. A.; Kaplan, D. I.; Yeager, C. M.; Santschi, P. H., Temporal Variation of Iodine Concentration and Speciation (127I and 129I) in Wetland Groundwater from the Savannah River Site, USA. Environmental Science & Technology 2014, 48 (19), 11218-11226.
3. Kaplan, D. I.; Zhang, S.; Roberts, K. A.; Schwehr, K.; Xu, C.; Creeley, D.; Ho, Y.-F.; Li, H.-P.; Yeager, C. M.; Santschi, P. H., Radioiodine concentrated in a wetland. Journal of Environmental Radioactivity 2014, 131, 57-61.
4. Kaplan, D. I.; Denham, M. E.; Zhang, S.; Yeager, C.; Xu, C.; Schwehr, K. A.; Li, H. P.; Ho, Y. F.; Wellman, D.; Santschi, P. H., Radioiodine Biogeochemistry and Prevalence in Groundwater. Critical Reviews in Environmental Science and Technology 2014, 44 (20), 2287-2335.
5. Neeway, J. J.; Kaplan, D. I.; Bagwell, C. E.; Rockhold, M. L.; Szecsody, J. E.; Truex, M. J.; Qafoku, N. P., A review of the behavior of radioiodine in the subsurface at two DOE sites. Science of The Total Environment 2019, 691, 466-475.
6. Santschi, P. H.; Xu, C.; Zhang, S.; Schwehr, K. A.; Grandbois, R.; Kaplan, D. I.; Yeager, C. M., Iodine and plutonium association with natural organic matter: A review of recent advances. Applied Geochemistry 2017, 85, 121-127.
7. Emerson, H. P.; Xu, C.; Ho, Y.-F.; Zhang, S.; Schwehr, K. A.; Lilley, M.; Kaplan, D. I.; Santschi, P. H.; Powell, B. A., Geochemical controls of iodine uptake and transport in Savannah River Site subsurface sediments. Applied Geochemistry 2014, 45, 105-113.
8. Chang, H.-s.; Xu, C.; Schwehr, K. A.; Zhang, S.; Kaplan, D. I.; Seaman, J. C.; Yeager, C.; Santschi, P. H., Model of radioiodine speciation and partitioning in organic-rich and organic-poor soils from the Savannah River Site. Journal of Environmental Chemical Engineering 2014, 2 (3), 1321-1330.
9. Zhang, S.; Du, J.; Xu, C.; Schwehr, K. A.; Ho, Y. F.; Li, H. P.; Roberts, K. A.; Kaplan, D. I.; Brinkmeyer, R.; Yeager, C. M.; Chang, H.-s.; Santschi, P. H., Concentration-Dependent Mobility, Retardation, and Speciation of Iodine in Surface Sediment from the Savannah River Site. Environmental Science & Technology 2011, 45 (13), 5543-5549.
10. Xu, C.; Zhang, S.; Ho, Y.-F.; Miller, E. J.; Roberts, K. A.; Li, H.-P.; Schwehr, K. A.; Otosaka, S.; Kaplan, D. I.; Brinkmeyer, R.; Yeager, C. M.; Santschi, P. H., Is soil natural organic matter a sink or source for mobile radioiodine (129I) at the Savannah River Site? Geochimica et Cosmochimica Acta 2011, 75 (19), 5716-5735.
11. Kaplan, D. I.; Nichols, R.; Xu, C.; Lin, P.; Yeager, C.; Santschi, P. H., Large seasonal fluctuations of groundwater radioiodine speciation and concentrations in a riparian wetland in South Carolina. Science of The Total Environment 2022, 816, 151548.
12. Gonzalez-Raymat, H., J. Kidd, and M.E. Denham Baseline Study Report of the Vertical Distribution of Contaminants within the F-Area Wetlands; Savannah River National Laboratory: Aiken, SC, 2021.

13. Otosaka, S.; Schwehr, K. A.; Kaplan, D. I.; Roberts, K. A.; Zhang, S.; Xu, C.; Li, H.-P.; Ho, Y.-F.; Brinkmeyer, R.; Yeager, C. M.; Santschi, P. H., Factors controlling mobility of 127I and 129I species in an acidic groundwater plume at the Savannah River Site. Science of The Total Environment 2011, 409 (19), 3857-3865.

14. Xu, C.; Miller, E. J.; Zhang, S.; Li, H.-P.; Ho, Y.-F.; Schwehr, K. A.; Kaplan, D. I.; Otosaka, S.; Roberts, K. A.; Brinkmeyer, R.; Yeager, C. M.; Santschi, P. H., Sequestration and Remobilization of Radioiodine (129I) by Soil Organic Matter and Possible Consequences of the Remedial Action at Savannah River Site. Environmental Science & Technology 2011, 45 (23), 9975-9983.

15. Bostock, A. C.; Shaw, G.; Bell, J. N. B., The volatilisation and sorption of 129I in coniferous forest, grassland and frozen soils. Journal of Environmental Radioactivity 2003, 70 (1), 29-42.

16. Wyatt, D. E.; Harris, M. K., Overview of the history and geology of the Savannah River Site. Environmental Geosciences 2004, 11 (4), 181-190.

17. Dosskey, M. G.; Bertsch, P. M., Forest Sources and Pathways of Organic Matter Transport to a Blackwater Stream: A Hydrologic Approach. Biogeochemistry 1994, 24 (1), 1-19.

18. Schwehr, K. A.; Santschi, P. H.; Kaplan, D. I.; Yeager, C. M.; Brinkmeyer, R., Organo-Iodine Formation in Soils and Aquifer Sediments at Ambient Concentrations. Environmental Science & Technology 2009, 43 (19), 7258-7264.

19. Whitehead, D. C., The sorption of iodide by soil components. Journal of the Science of Food and Agriculture 1974, 25 (1), 73-79.

20. Couture, R. A.; Seitz, M. G., Sorption of anions of iodine by iron oxides and kaolinite. Nuclear and Chemical Waste Management 1983, 4 (4), 301-306.

21. Kaplan, D. I.; Serne, R. J.; Parker, K. E.; Kutnyakov, I. V., Iodide Sorption to Subsurface Sediments and Illitic Minerals. Environmental Science & Technology 2000, 34 (3), 399-405.

22. Fox, P. M.; Kent, D. B.; Davis, J. A., Redox Transformations and Transport of Cesium and Iodine (−1, 0, +5) in Oxidizing and Reducing Zones of a Sand and Gravel Aquifer. Environmental Science & Technology 2010, 44 (6), 1940-1946.

23. Killian, T.; Kolb, N.; Corbo, P.; Marine, I., Environmental information document F-area seepage basins. EI du Pont de Nemours and Company, Savannah River Laboratory, Aiken, SC 1987.

24. Allard, S.; von Gunten, U.; Sahli, E.; Nicolau, R.; Gallard, H., Oxidation of iodide and iodine on birnessite (δ-MnO2) in the pH range 4–8. Water Research 2009, 43 (14), 3417-3426.

25. Reiller, P.; Mercier-Bion, F.; Gimenez, N.; Barré, N.; Miserque, F., Iodination of humic acid samples from different origins. Radiochimica Acta 2006, 94 (9-11), 739-745.

26. Choung, S.; Um, W.; Kim, M.; Kim, M.-G., Uptake Mechanism for Iodine Species to Black Carbon. Environmental Science & Technology 2013, 47 (18), 10349-10355.

27. Sheppard, M. I.; Thibault, D. H.; Smith, P. A.; Hawkins, J. L., Volatilization: a soil degassing coefficient for iodine. Journal of Environmental Radioactivity 1994, 25 (3), 189-203.

28. Sheppard, S. C.; Sheppard, M. I.; Tait, J. C.; Sanipelli, B. L., Revision and meta-analysis of

selected biosphere parameter values for chlorine, iodine, neptunium, radium, radon and uranium. Journal of Environmental Radioactivity 2006, 89 (2), 115-137.

29. Lusa, M.; Bomberg, M.; Aromaa, H.; Knuutinen, J.; Lehto, J., Sorption of radioiodide in an acidic, nutrient-poor boreal bog: insights into the microbial impact. Journal of Environmental Radioactivity 2015, 143, 110-122.
30. Söderlund, M.; Virkanen, J.; Aromaa, H.; Gracheva, N.; Lehto, J., Sorption and speciation of iodine in boreal forest soil. Journal of Radioanalytical and Nuclear Chemistry 2017, 311 (1), 549-564.
31. Fukui, M.; Fujikawa, Y.; Satta, N., Factors affecting interaction of radioiodide and iodate species with soil. Journal of Environmental Radioactivity 1996, 31 (2), 199-216.
32. Steinberg, S. M.; Kimble, G. M.; Schmett, G. T.; Emerson, D. W.; Turner, M. F.; Rudin, M., Abiotic reaction of iodate with sphagnum peat and other natural organic matter. Journal of Radioanalytical and Nuclear Chemistry 2008, 277 (1), 185-191.
33. Whitehead, D. C., The Influence Of Organic Matter, Chalk, And Sesquioxides On The Solubility Of Iodide, Elemental Iodine, And Iodate Incubated With Soil. Journal Of Soil Science 1974, 25 (4), 461-470.
34. Shetaya, W. H.; Young, S. D.; Watts, M. J.; Ander, E. L.; Bailey, E. H., Iodine dynamics in soils. Geochimica et Cosmochimica Acta 2012, 77, 457-473.
35. Yamaguchi, N.; Nakano, M.; Takamatsu, R.; Tanida, H., Inorganic iodine incorporation into soil organic matter: evidence from iodine K-edge X-ray absorption near-edge structure. Journal of Environmental Radioactivity 2010, 101 (6), 451-457.
36. Schlegel, M. L.; Reiller, P.; Mercier-Bion, F.; Barré, N.; Moulin, V., Molecular environment of iodine in naturally iodinated humic substances: Insight from X-ray absorption spectroscopy. Geochimica et Cosmochimica Acta 2006, 70 (22), 5536-5551.
37. Satoh, Y.; Imai, S., Evaluation of dissolution flux of iodine from brackish lake sediments under different temperature and oxygenic conditions. Science of The Total Environment 2020, 707, 135920.
38. Sheppard, M. I.; Hawkins, J. L., Iodine and microbial interactions in an organic soil. Journal of Environmental Radioactivity 1995, 29 (2), 91-109.
39. Bird, G. A.; Schwartz, W., Distribution coefficients, Kds, for iodide in Canadian Shield Lake sediments under oxic and anoxic conditions. Journal of Environmental Radioactivity 1997, 35 (3), 261-279.
40. Ashworth, D. J.; Shaw, G., Effects of moisture content and redox potential on in situ Kd values for radioiodine in soil. Science of The Total Environment 2006, 359 (1), 244-254.
41. Keppler, F.; Eiden, R.; Niedan, V.; Pracht, J.; Schöler, H. F., Halocarbons produced by natural oxidation processes during degradation of organic matter. Nature 2000, 403 (6767), 298-301.
42. Keppler, F.; Borchers, R.; Elsner, P.; Fahimi, I.; Pracht, J.; Schöler, H. F., Formation of volatile iodinated alkanes in soil: results from laboratory studies. Chemosphere 2003, 52 (2), 477-483.
43. Gu, B.; Schmitt, J.; Chen, Z.; Liang, L.; McCarthy, J. F., Adsorption and desorption of natural

organic matter on iron oxide: mechanisms and models. Environmental Science & Technology 1994, 28 (1), 38-46.

44. Lam, P.; Kuypers, M. M. M., Microbial Nitrogen Cycling Processes in Oxygen Minimum Zones. Annual Review of Marine Science 2011, 3 (1), 317-345.
45. Farrenkopf, A. M.; Dollhopf, M. E.; Chadhain, S. N.; Luther, G. W.; Nealson, K. H., Reduction of iodate in seawater during Arabian Sea shipboard incubations and in laboratory cultures of the marine bacterium Shewanella putrefaciens strain MR-4. Marine Chemistry 1997, 57 (3), 347-354.
46. Councell, T. B.; Landa, E. R.; Lovley, D. R., Microbial Reduction of Iodate. Water, Air, and Soil Pollution 1997, 100 (1), 99-106.
47. Amachi, S.; Kawaguchi, N.; Muramatsu, Y.; Tsuchiya, S.; Watanabe, Y.; Shinoyama, H.; Fujii, T., Dissimilatory Iodate Reduction by Marine Pseudomonas sp. Strain SCT. Applied and Environmental Microbiology 2007, 73 (18), 5725-5730.
48. Mohn, W. W.; Tiedje, J. M., Microbial reductive dehalogenation. Microbiological Reviews 1992, 56 (3), 482-507.
49. Sims, J. L.; Suflita, J. M.; Russell, H. H. Reductive dehalogenation of organic contaminants in soils and ground-water. ground water issue; United States, 1991; p Medium: X; Size: Pages: (15 p).
50. Lecouturier, D.; Godon, J. J.; Lebeault, J. M., Phylogenetic analysis of an anaerobic microbial consortium deiodinating 5-amino-2,4,6-triiodoisophthalic acid. Applied Microbiology and Biotechnology 2003, 62 (4), 400-406.
51. Breitenstein, A.; Saano, A.; Salkinoja-Salonen, M.; Andreesen, J. R.; Lechner, U., Analysis of a 2,4,6-trichlorophenol-dehalogenating enrichment culture and isolation of the dehalogenating member Desulfitobacterium frappieri strain TCP-A. Archives of Microbiology 2001, 175 (2), 133-142.
52. Löffler, F. E.; Ritalahti, K. M.; Zinder, S. H., Dehalococcoides and Reductive Dechlorination of Chlorinated Solvents. In Bioaugmentation for Groundwater Remediation, Stroo, H. F.; Leeson, A.; Ward, C. H., Eds. Springer New York: New York, NY, 2013; pp 39-88.
53. Redeker, M.; Wick, A.; Meermann, B.; Ternes, T. A., Removal of the Iodinated X-ray Contrast Medium Diatrizoate by Anaerobic Transformation. Environmental Science & Technology 2014, 48 (17), 10145-10154.
54. El-Athman, F.; Adrian, L.; Jekel, M.; Putschew, A., Abiotic reductive deiodination of iodinated organic compounds and X-ray contrast media catalyzed by free corrinoids. Chemosphere 2019, 221, 212-218.

Subtask 2.2: Humic Acid Batch Sorption Experiments with SRS Soil

Subtask 2.2: Introduction

The Savannah River Site (SRS), located in South Carolina, was a pivotal nuclear facility during the Cold War, from 1953 to 1988, producing nuclear weapons and nuclear energy programs, involving the manufacturing of materials such as plutonium and tritium for nuclear weaponry

(Evans, et. al., 1992). These operations generated radioactive waste and environmental contamination, which continue to pose complex challenges requiring ongoing remediation efforts and environmental management at the site. The F-Area Seepage Basins received approximately 1.8 billion gallons of low level acidic waste solutions that contained nitrate, metals, and several radionuclides. At that time, it was believed that most of the radionuclides present in the waste solution would bind to the soil, precluding the migration of the radionuclides. Throughout the years, radionuclides, including Uranium isotopes, strontium-90, and Iodine-129, have gradually permeated from the vadose zone into the saturated zone. As these contaminants infiltrated the groundwater, they found their way through the Fourmile Branch. The uranium contamination further intensified the situation by its properties that increase the pH of the groundwater, which poses an additional challenge. The groundwater remains acidic with uranium concentrations surpassing the Environmental Protection Agency (EPA) maximum contaminant levels (Dong et. al., 2012). Efforts such as pump-and-treat systems were deployed in an attempt to mitigate the contamination. However, these approaches were costly and generated additional radioactive waste. In 2004, the pump-and treat system was replaced by a funnel and gate system in order to create a treatment zone via injection of a solution mixture composed of two components, sodium hydroxide and carbonate. The injections were done directly into the gates of the F-Area groundwater to raise pH levels. The purpose of the treatment zone was to reverse the acidic nature of the contaminated sediments, thereby producing a more negative net charge on the surface of sediment particles and enhancing the adsorption of cationic contaminants. This amplified the adsorption of cationic contaminants on the sediment and resulted in the decrease of Sr-90 and U-238 concentrations but had no effect on the treatment of iodine. To maintain the pH neutral within the treatment zone, systemic injections were required. Carbonate forms strong complexes with uranium and could remobilize uranium that was already adsorbed within the treatment zone (Gudavalli et. al., 2013).

Humic substances (HS) are major components of soil organic matter, which are polyfunctional organic macromolecules that are formed from the decomposition of biomass or dead organic matter (Trevisan, et. al., 2010). Humic substances can be divided into three main fractions: humin, which is insoluble at all pHs; humic acid (HA), soluble at pHs greater than 3.5; and fulvic acids, which are soluble at all pHs (Choppin et. al., 1992). Humic acid is an important ion exchange and metal complexing ligand with a high complexation capacity, allowing it to chemically bind to metals and influence their migration behavior (Davis et. al., 2002). Previous studies suggest that the sorption of U(VI) in the presence of humic acid is a complex process (Perminova et. al., 2002). Ivanov et al (2012) studied U(VI) sorption onto bentonite with and without humic acid and proved enhanced uranium sorption at pHs lower than 3.8, while it was reduced at pHs above 3.8. In another study, U(VI) sorption proved to be influenced by pH, the U(VI) concentration, humic acid, and inorganic carbon species (Krepelova et al., 2007).

Chemically modified humate materials, commercially known as KW-30, is being tested for its use in remediation techniques to reduce the mobility of uranium, strontium and iodine in the subsurface at SRS.

Subtask 2.2: Objectives

The objective of this research is to investigate the effect of sorbed modified humic acid (KW-30) on the sequestration of commingled contaminants, specifically uranium, strontium, and iodine, within the Savannah River Site (SRS) F-Area. This investigation takes place under varying site-specific conditions, aiming to identify a feasible remediation technology for deployment. The

study not only assesses the potential for in-situ contaminant remediation at SRS Fourmile Branch using humic acid but also suggests its future applicability to other sites with distinct conditions.

Subtask 2.2: Methodology

Materials:

This study utilized sediment samples that were collected from the F-Area at SRS (FAW1 70-90 ft) and sieved through a 2mm sieve. The fraction ≤ 2 mm was used in the experiments. This sediment was chosen due to its comparability to the soil composition in the uranium-contaminated aquifer layer. For U(VI), a commercial 1,000 ppm uranyl stock solution in 2% nitric acid was used. A humate stock solutions (KW-30) consisting of 1,000 mg in 1,000 mL of deionized water (DIW) was prepared for use in the experiments. Strontium (Sr(II)) stock solution was prepared at 1000 ppm using salt manufacturer. Iodide and Iodate solutions were prepared using 1000ppm stock solutions, with a commercial Iodide standard (I^-, 1000 ug/mL) obtained from SPEC CeroPrep, and an Iodate standard (IO_3^-, 1000 mg/L) obtained from VeriSpec. To maintain ionic strength, 0.2M Sodium Perchlorate was used, and the sample's pH was adjusted using 0.1M HCl/NaOH. Synthetic groundwater was prepared using the SRS monitoring wells FOB20 and FOB21 elemental data and recreated in laboratory.

Experimental Procedures:

Humate Sorption

Sorption experiments were prepared using 200 mg of dried SRS sediment combined with 50 ppm modified humic acid (KW-30) in 20 mL deionized water in triplicates. The samples were adjusted to pH 4.0 daily using 0.1 M HCl/NaOH during the sorption period. The samples were placed on a platform shaker at 100 rpm for 7 days to reach equilibrium. After sorption period, the samples were centrifuged at 2700 rpm for 30 minutes and the supernatant was removed and analyzed via UV-Vis spectrophotometer. The same procedure was performed using synthetic groundwater instead of DIW for the synthetic groundwater experiments.

Contaminant Sorption

To humate-coated sediment, 0.6 mL of 10 mg/L strontium (Sr(II)) stock solution was added for a total concentration of 300 μg/L in 20 ml. Similar to the strontium sample preparation, a set of triplicate batch reactors was created using 200 mg of SRS humate-coated sediment, by combining with DIW and 14 mL of 1000 μg/L uranium stock solution in 20 ml. Finally, another two sets of triplicate samples were prepared with 200 mg of SRS humate-coated sediment and DIW mixed with 0.3 mL of 10 mg/L iodide (I^-) and iodate (IO_3^-), for a total concentration of 150 μg/L. Each respective sample was adjusted to pH 4.0 using 0.1 M HCl and 0.1 M NaOH during the sorption period. The samples were placed on a platform shaker at 100 rpm for the entirety of the sorption process. A volume of 200 μL of supernatant was carefully removed from each of the unfiltered samples and stored for analysis on the ICP-MS.

Two experiments were conducted to study the sorption of uranium and strontium onto sediment coated with and without KW-30 with synthetic groundwater (SGW). Three samples of each contaminant were prepared in triplicates: control samples (no sediment), uncoated sediment samples (no KW-30), and coated sediment samples (with KW-30) using the combination seen in Table 8. A volume of 1 ml of sodium perchlorate solution was added to maintain ionic strength. An initial uranium concentration of 700 ppb and initial strontium concentration of 300 ppb was

introduced into respective vials. The pH of the samples was monitored and adjusted to pH 4 using 0.1M HCl/NaOH. Samples were placed on a platform shaker at 100 rpm for two weeks and pH was monitored and adjusted periodically. Subsequently, 200 µl aliquots were collected and analyzed via ICP-MS.

Table 8. Recipe for Each Sample

Contaminant	Samples	$NaClO_4$ (mL)	1000 ppb U (mL)	SGW (mL)	Sediment (mg)
Uranium	Control	1	14	4.5	0
	Uncoated	1	14	4.5	200
	Coated	1	14	4.5	200
Strontium	Control	1	6	12.5	0
	Uncoated	1	6	12.5	200
	Coated	1	6	12.5	200

Subtask 2.2: Results and Discussion

Synthetic Groundwater Receipe (SGW)

SRS groundwater recipe was formulated by utilizing the groundwater data obtained from wells FOB20 and FOB21. Elemental concentrations were converted from mg/L to mmol/L as shown in Table 9.

Table 9. Concentrations of Elements from Wells FOB20 and FOB21

Element	FOB 21 (mg/L)	FOB 20 (mg/L)	Molar Mass (g/mol)	Average (mmol/L)	Min Value (mmol/L)	10% less of Min	Max Value (mmol/L)	10% more Max
Potassium	**1.33**	**0.625**	39.1	0.025	0.016	0.015	0.034	0.037
Sulfate	**1.15**	**11.6**	96.09	0.066	0.012	0.011	0.121	0.133
Magnesium	**8.35**	**1.86**	24.03	0.212	0.077	0.070	0.347	0.382
Calcium	**34.3**	**1.8**	40.08	0.450	0.045	0.041	0.856	0.941
Chloride	**18.5**	**15.2**	35.45	0.475	0.429	0.390	0.522	0.574
Nitrate	**104**	**41.7**	62.01	1.175	0.672	0.611	1.677	1.845
Sodium	**74.9**	**49.6**	22.99	2.708	2.157	1.961	3.258	3.584

Three scenarios were formulated to optimize the groundwater recipe. The objective was to balance the concentration of each ion to make synthetic groundwater match site conditions by use of common salts such as $CaCl_2$, $NaSO_4$, $MgCl_2$, NaCl, KCl, and $NaNO_3$ mixed with DIW.

- The first scenario used the average concentration between the two wells, which proved unfeasible due to the imbalance of ions for each salt not corresponding to the needed concentrations (Table 10).
- The second scenario was made by using the minimum, maximum and average of the two wells as seen in Table 11. The issue with this scenario was that sodium concentrations needed to increase while chloride concentrations needed to decrease.

- The third scenario used the values 10% above the maximum values and 10% below the minimum values between the two wells, as can be seen in Table 12. It was observed from the third scenario that the balance of the salts and the necessary concentrations were more suitable than Scenario 2. Scenario 3 has all ions resulting in average and ±10% of maximum and minimum values to stay within site conditions.

Table 10. Scenario 1 of Groundwater Recipe with Average Concentrations

Salt	Molecular wt. g/mol	Ca^{2+}	Mg^{2+}	K^{+}	Na^{+}	SO_4^{2-}	NO_3^{-}	Cl^{-}
$CaCl_2$	110.98	0.450						0.901
$NaSO_4$	142.04				0.066	0.066		
$MgCl_2$	95.211		0.212					0.425
NaCl	58.44				0.000			0.000
KCl	74.55			0.025				0.025
$NaNO_3$	84.99				1.175		1.175	
	Total	0.450	0.212	0.025	1.241	0.066	1.175	1.351

Table 11. Scenario 2 of Groundwater Recipe with Maximum and Minimum Concentrations

Salt	Molecular wt. g/mol	Ca^{2+}	Mg^{2+}	K^{+}	Na^{+}	SO_4^{2-}	NO_3^{-}	Cl^{-}
$CaCl_2$	110.98							
$NaSO_4$	142.04				0.076	0.076		
$MgCl_2$	95.211		0.212					0.425
NaCl	58.44				0.072			0.072
KCl	74.55			0.025				0.025
$NaNO_3$	84.99				1.677		1.677	
$CaSO_4$		0.045				0.045		
	Total	0.045	0.212	0.025	1.825	0.121	1.677	0.522

Table 12. Scenario 3 of Groundwater Recipe using ±10% of Maximum and Minimum Values

Salt	Molecular wt. g/mol	Ca^{2+}	Mg^{2+}	K^{+}	Na^{+}	SO_4^{2-}	NO_3^{-}	Cl^{-}
$CaCl_2$*2H_20	147.02	0.041						0.082
$NaSO_4$	142.04				0.266	0.133		
$MgCl_2$	95.211		0.077					0.155
NaCl	58.44				0.313			0.313
KCl	74.5513			0.025				0.025
$NaNO_3$	84.9947				1.845		1.845	
	Total	0.041	0.077	0.025	2.423	0.133	1.845	0.574

Synthetic groundwater recipe was formulated replicating SRS F-Area wells (FOB20 and FOB21) conditions. Synthetic groundwater was prepared by combining salts with deionized water at 1000 times concentration in one liter. The amount of salt needed for each element can be found in Table 13, where the amount of each salt needed was calculated by multiplying the molecular weight

(mg/mmol) by the concentration (mol/L) found from the previous procedure in the groundwater recipe.

Table 13. Calculations for the amount of each salt needed in one liter of DIW

Salts	Molecular Weight (mg/mmol)	Concentration (mmol/L)	Concentration (mol/L)	Concentration Calculations [x1000] (mg/L)	g/L
$CaCl_2*2H_20$	147.02	0.04	40.83	6002.45	6.00
$NaSO_4$	142.04	0.13	132.79	18861.80	18.86
$MgCl_2$	95.21	0.08	77.40	7369.64	7.37
NaCl	58.44	0.31	312.59	18267.56	18.27
KCl	74.55	0.03	25.00	1863.78	1.86
$NaNO_3$	84.99	1.84	1844.86	156803.64	156.80

Sorption of KW-30 and contaminants

The results showed that the average sorption of humic acid onto the sediment with synthetic groundwater was around 3300 mg/kg, as seen in Figure 34. In comparison to the experiment condcuted with deionized water where the average sorption was 2000 mg/kg as seen in Figure 35, synthetic groundwater resulted in a higher sorption than with deionized water. Possible reasons for a higher sorption with synthetic groundwater in comparison to DIW could be that there are more reactions occurring in the sample given the introduction of more ions in the synthetic groundwater. As shown in Figure 36, sorption of humic acid is much higher in the presence of SGW compared to DIW.

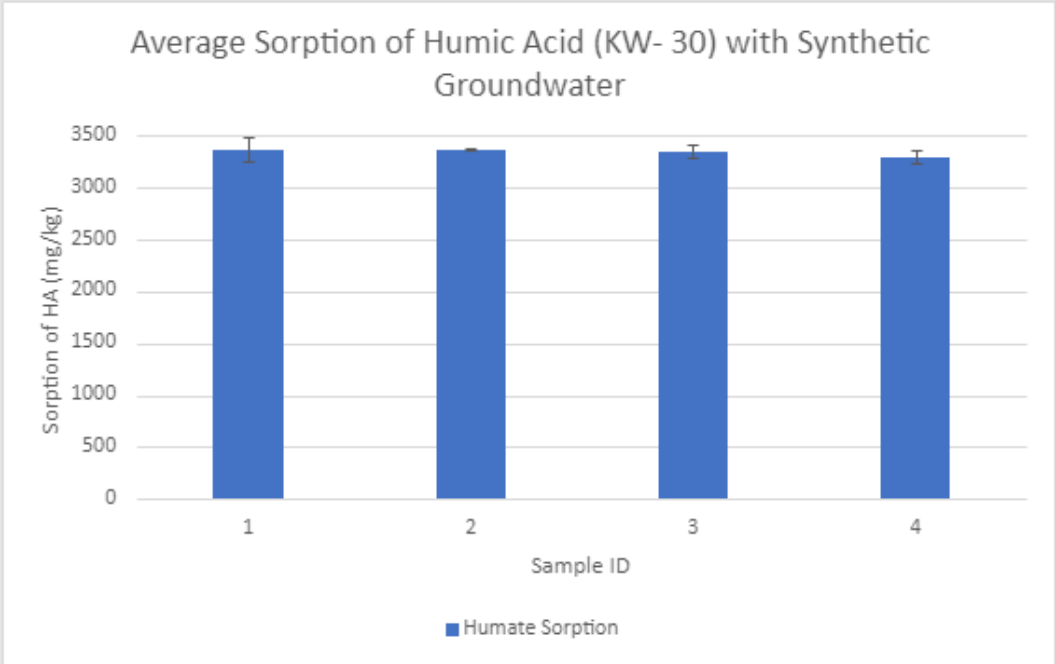

Figure 34. Average sorption of modified humic acid (KW-30) with synthetic groundwater.

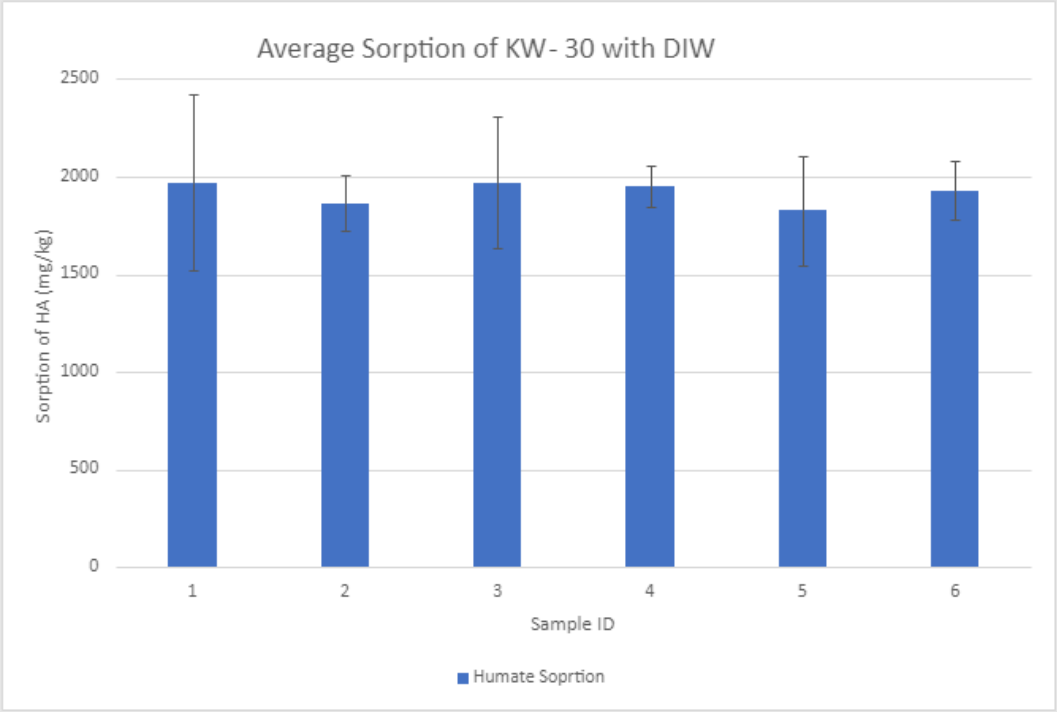

Figure 35. Average sorption of modified humic acid (KW-30) with deionized water.

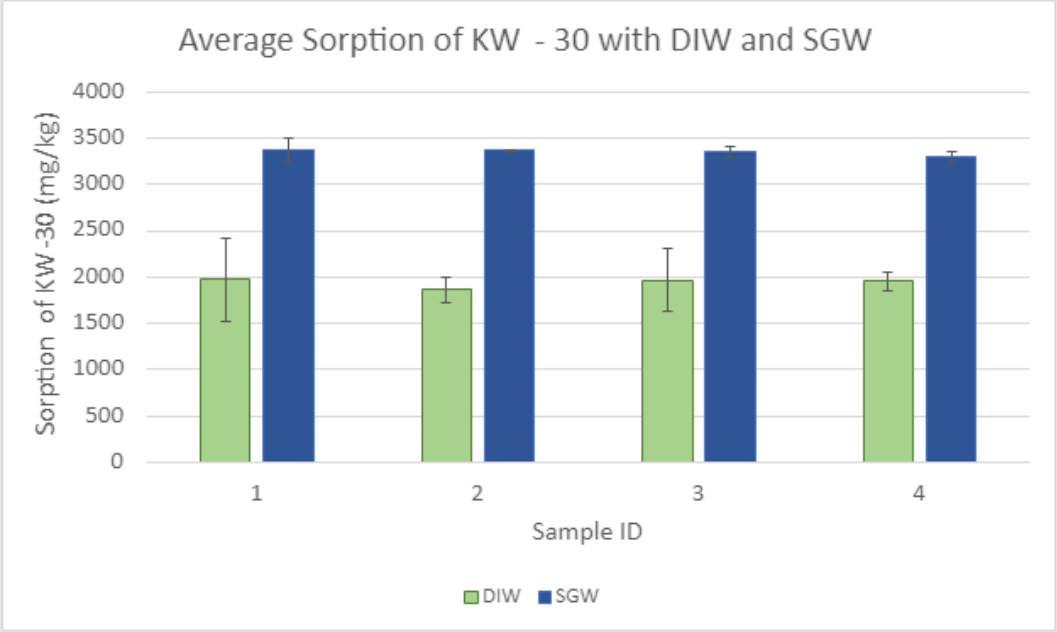

Figure 36. Average sorption of modified humic acid (KW-30) with deionized water and synthetic groundwater.

The percent removal of contaminants was calculated by using the equation $\frac{(Ci - Cf)}{Ci} \times 100$. After two weeks for samples with SGW, the strontium samples' aqueous concentrations did not change and remined at 300 ppb in all samples tested. Uranium removal for control (sediment free), uncoated sediment and coated sediment samples is shown in Figure 37. Control samples were found to have approximately 8% uranium removal at Day 1 and remained constant throughout the experiment. Uncoated samples had approximately 20% uranium removal initially and increased to

about 30% by Day 4. At the end of the experiment, uranium removal reached 35%. Samples coated with humic acid (KW-30) had 30% removal initially and by Day 2 reached approximately 80% and remained in the same range throughout the experiment.

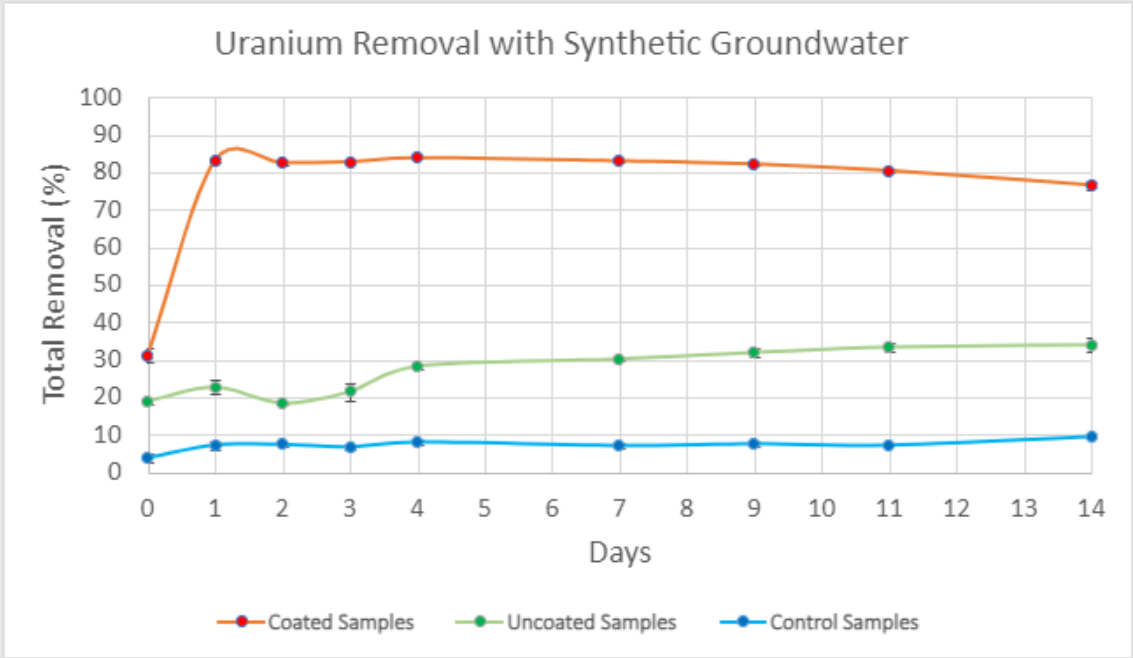

Figure 37. Uranium kinetics with synthetic groundwater.

Figure 38 shows the uranium removal in the presence of DIW. Control samples showed an average removal of 15%, uncoated samples averaged 7% removal, and coated samples at 27%. Coated samples with SGW showed 3 times more removal of about 85% compared to coated samples with DIW which had an average removal of 27%. This increase in uranium removal can be attributed to the amount of humate sorbed in each experiment.

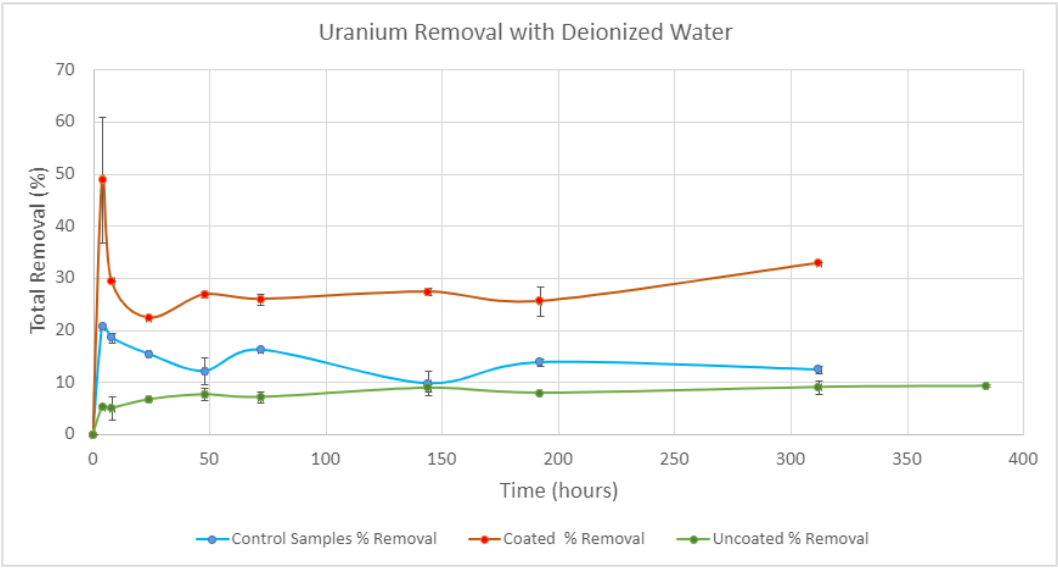

Figure 38. Uranium kinetics with deionized water.

Subtask 2.2: Conclusions

Modified humic acid (KW-30) has no effect on strontium sorption at pH 4. In the presence of synthetic groundwater (SGW), uranium removal increased compared to sorption with deionized water (DIW). Coated and uncoated samples have about 3 times more sorption in the presence of SGW compared to DIW. The ions present in SGW do influence the sorption of uranium, while neither KW-30 nor SGW has any affect on strontium removal.

Subtask 2.2: References

Choppin, G.R., 1992. The role of natural organics in radionuclide migration in natural aquifer systems. *Radiochim. Acta* 58/59, 113.

Davis. J.A., Adsorption of natural dissolved organic matter at the oxide/water interface, 1982, 2002. Geochim. Cosmochim. Acta 46, 2381-2393.

Dong, W., Tokuanga, T. K., Davis, J. A., Wan, J., (2012). Uranium(VI) Adsorption and Surface Complexation Modeling onto Background Sediments from the F-Area Savannah River Site. Environ. Sci. Technol. 46, 1565-1571.

Evans, A.G., Bauer, L.R., Haselow, J.S., Hayes, D.W., Martin, H.L., McDowell, W.L., Pickett, J.B., 1992. Uranium in the Savannah River Site environment. Westinghouse Savannah River Co., Aiken, SC (United States), p. 95.

Gonzalez-Raymat, H., Anagnostopoulos, V.; Denham, M.; Cai, Y.; Katsenovich, Y. P., Unrefined humic substances as a potential low-cost amendment for the management of acidic groundwater contamination. Journal of Environmental Management 2018, 212, 210-218.

Gudavalli, R., Katsenovich, Y., Wellman, D., Idarraga, M., Lagos, L., Tansel, B., 2013. Comparison of the kinetic rate law parameters for the dissolution of natural and synthetic autunite in the presence of aqueous bicarbonate ions

Hay, M. B., Myneni, S. C. B., Structural environments of carboxyl groups in natural organic molecules from terrestrial systems. Part 1: Infrared spectroscopy. Geochimica et Cosmochimica Acta 2007, 71 (14), 3518-3532.

Ivanov, P., Griffiths, T., Bryan, N.D., Bozhikov, G. and S. Dmitriev, 2012. The effect of humic acid on uranyl sorption onto bentonite at trace uranium levels. *J. Environ. Monit.,* 14, 2968 - 2975.

Jiang, W., Cai, Q., Xu, W., Yang, M., Cai, Y., Dionysiou, D. D., O'Shea, K. E., Cr (VI) adsorption and reduction by humic acid coated on magnetite. Environmental science & technology 2014, 48 (14), 8078-8085.

Kimmig, S. R., C. Thompson, S. Baum and C. F. Brown (2021). "Evaluation of iodine speciation and 129I/127I ratios at low concentrations in environmental samples using IC-ICP-MS." Journal of Radioanalytical and Nuclear Chemistry 327(2): 929-937.

Köhler, F., B. Riebe, A. C. Scheinost, C. König, A. Hölzer and C. Walther (2019). "Sorption of iodine in soils: insight from selective sequential extractions and X-ray absorption spectroscopy." Environmental Science and Pollution Research 26(23): 23850-23860.

Krepelova. A., 2007. Influence of Humic Acid on the Sorption of Uranium(VI) and Americium(III) onto Kaolinite (Dissertation).

Largitte, L. and R. Pasquier (2016). "A review of the kinetics adsorption models and their application to the adsorption of lead by an activated carbon." Chemical Engineering Research and Design 109: 495-504.

Perminova, I.V, Hatfield, K., Hertkorn, N., 2002. Use of humic substances to remediate polluted environments: from theory to practice. In the proceedings of the NATO Advance Research Workshop, Springer, P.O Box 17, 3300 AA Dordrech, The Netherland.

Trevisan, Sara, et al. “Humic Substances Biological Activity at the Plant-Soil Interface.” *Plant Signaling & Behavior*, vol. 5, no. 6, 2010, pp. 635–643., doi:10.4161/psb.5.6.11211.

Wang, W. and J. Wang (2018). "Comparative evaluation of sorption kinetics and isotherms of pyrene onto microplastics." Chemosphere 193: 567-573.

Zhou, T., S. Huang, D. Niu, L. Su, G. Zhen and Y. Zhao (2018). "Efficient Separation of Water-Soluble Humic Acid Using (3-Aminopropyl)triethoxysilane (APTES) for Carbon Resource Recovery from Wastewater." ACS Sustainable Chemistry & Engineering 6(5): 5981-5989.

TASK 3: CONTAMINANT FATE AND TRANSPORT MODELING FOR THE SAVANNAH RIVER SITE

This task involves the development and application of integrated hydrological, hydraulic and contaminant transport models for studying the fate of priority pollutants in the stream systems at SRS. For Year 3, Subtask 3.1 has been focused on finalizing the event-based contaminant transport model for Tims Branch watershed. This model was developed in previous years to enable simulation of the impact of extreme storm events on the hydrological response and the transport of uranium in Tims Branch watershed. The aim is to examine the response of this stream to historical discharge events and environmental management remediation actions and to provide a means of assessment, evaluation and post-closure long-term monitoring of water quality and environmental conditions following remedial activities. For Subtask 3.2, FIU continued its investigation on the F-Area wetland hydrology within Fourmile Branch watershed using a detailed model that focuses on the F-Area seep line interaction. FIU also worked on calibrating the watershed-scale hydrological model developed in Year 2 using historical observations. The focus of this work is two-fold, first improve our understanding of the interaction between the groundwater flow downslope of F-Area with the seepage face and riparian zone adjacent to the braided river network, making use of model and in-situ observations; and second, attempt to understand the flow and sediment transport variability across Fourmile Branch watershed as this will impact the migration of F-Area contaminants downstream. Long-term changes in climate are anticipated to lead to more frequent intense precipitation events and prolonged periods of drought, which can impact hydrological conditions as well as the fate and transport of contaminants. For both subtasks the impact of these long-term changes will be evaluated using the models developed.

The knowledge gained through these studies will provide a means of assessment, evaluation and post-closure long-term monitoring of water quality and environmental conditions following remedial activities. The models provide information needed for informed decision-making in existing DOE-EM soil and groundwater remediation programs. Results obtained will provide DOE-EM suggestion of key locations for contaminant monitoring. Furthermore, the models can be utilized as forecasting tools to predict suspended sediment loads and the extent of remobilization regimes under different scenarios of extreme storm events and erosion conditions. This research will assist in developing cost-effective remediation plans integrated into the SRS Area Completion Project (ACP) and accelerate progress of the DOE EM environmental restoration mission.

Subtask 3.1: Calibration of the Tims Branch Watershed Model and Scenario Analysis

Subtask 3.1: Introduction

Subtask 3.1 specifically focuses on Tims Branch watershed and aims to examine the response of this stream to historical discharge events and environmental management remediation actions and to provide a means of assessment, evaluation and post-closure long-term monitoring of water quality and environmental conditions following remedial activities. In Year 3 this work has focused on generating long-term as well as event-based flow and sediment transport simulations for Tims Branch watershed.

Tims Branch watershed is situated within DOE's Savannah River Site (SRS). Tims Branch has been affected by contaminated runoff and wastewater discharge from nuclear facilities in the A/M-Area over the past century. This has resulted in uranium (U), nickel (Ni), mercury (Hg), chromium (Cr), and other heavy metal and radionuclide contamination (Evans et al., 1992; Pickett, 1990).

The majority of these sediment-bound heavy metals and radionuclides were deposited in the main channel bed along the A-14 tributary, Beaver Pond 2 and the former farm pond Steed Pond. A number of dams and spillways, including one at the outlet of Steed Pond, allowed for settling and limited the transport of sediment-bound heavy metals downstream (Evans et al., 1992). As a result, Steed Pond has been estimated to have received 43,500 kg of depleted U, with 94% of this U remaining in association with streambed and surrounding wetland sediments (Kaplan et al. 2020; 2023). After the spillway collapsed in 1984 sediment particles were able to migrate more freely downstream (Hayes, 1986; Evans et al., 1992). These sediments have been shown to remobilize especially during intense storm events, resulting in up to a three orders of magnitude increase in U transport in contrast to baseflow conditions (Batson et al., 1996; Batson, 1994).

Recently, Kaplan et al. (2023) used spectral analysis from gamma and X-ray spectra to identify currently existing locations along the main tributary with elevated levels in uranium. Besides the abovementioned original deposit locations within Tims Branch, elevated uranium values were also observed within Beaver Pond 3, about 1,000 m downstream of Steed Pond and Railroad Pond, close to the outlet. It is currently unknown whether and how the originally deposited particles migrated downslope due to channel bed erosion during intense flow events. To gain an improved understanding of this, the current report presents an in-depth modeling approach.

FIU has developed a MIKE SHE/MIKE 11 integrated hydrology and contaminant transport model to simulate the impact of extreme storm events on the hydrological response and the transport of uranium in the Tims Branch watershed, and to assess the anticipated role of climate change on flow and contaminant transport in Tims Branch. Tims Branch represents an important applied science opportunity due to significant past research by Savannah River National Laboratory (SRNL) and Savannah River Ecology Laboratory (SREL). Tims Branch has served as an ideal test bed for the development of a modeling approach to examine the response of a braided stream system at SRS to historical and future discharge events, for simulation of heavy metal transport, and assessment of environmental management remediation actions. The current version of the model simulates surface water flow (velocity, depth, and discharge), sediment and uranium fluxes throughout Tims Branch during extreme precipitation events ranging from 5-year to 500-year return periods, with storm durations ranging from 6-hour to 96-hour. In addition, in FIU Year 3, longer-term simulations were performed to assess the long-term impact of storm events and base flow conditions on the fate and transport of major contaminants of concern.

Subtask 3.1: Objectives

The goal of this subtask is to examine the response of the Tims Branch stream network to historical discharge events and environmental management remediation actions and to provide a means of assessment, evaluation and post-closure long-term monitoring of water quality and environmental conditions following remedial activities. More specifically, the aim is to understand how stable these existing deposits of uranium are in the channel bed and assess the susceptibility of channel bed sediment particles to erosion and deposition. This report presents a multi-year evaluation on how variations in weather impact the hydrological response of Tims Branch watershed. As explained above, several locations along the main branch of the Tims Branch channel network are

contaminated with heavy metal particles. The long-term evaluation of erosion and deposition presented here will enable us to speculate and hypothesize on the fate and transport of these contaminated particles. Climate change is anticipated to result in more frequent extreme precipitation leading to intensified flood conditions. Therefore, a second objective of this work is to understand how extreme weather events impact the Tims Branch flow response as well as erosion and deposition.

Subtask 3.1: Methodology

Hydrological and Sediment Transport Modeling

In Years 1-3 of the FIU-DOE Cooperative Agreement, FIU developed a hydrological model for Tims Branch watershed using MIKE SHE/MIKE 11 software. This model is able to simulate the hydrological response of the unsaturated and saturated zone as well as the hydraulic response of the channel network. As an example, this model was run for the year 1993 and compared to observations in Figure 39. This year is of particular interest due to the availability of in situ observations of uranium concentration at specified locations in Tims Branch. Overall, the model does a good job of simulating the hydrological response, although baseflow conditions are slightly underestimated. Since the focus of this work is to understand the hydrological response from intense flood events, this underestimation is not of particular concern. To enable the MIKE model to also perform simulations of suspended solid transport, the MIKE 11 Advection Dispersion (AD) routine was used. This routine assumes that erosion occurs once local flow velocities are above a critical velocity level (v_{crit}), and deposition takes place when the velocity is below the deposition velocity. To calibrate the parameters of this model routine, observational data from Hayes (1986) were used. For the winter period 1984/1985 this dataset contains daily flow rates and suspended solid concentrations as measured close to the outlet. Various MIKE 11-AD model parameters were calibrated using these observations of which the optimal results are presented in Figure 40. The blue markers show the observational data for the winter of 1984/1985, and the red markers the MIKE 11-AD simulations for the year 1993. For a given discharge, it can be observed that the updated MIKE 11-AD does a reasonable job simulating suspended solid concentration, especially for discharges above 0.4 m^3/s. For lower discharges the model has more difficulty representing observed values. It is believed that this is due to the assumption of a single velocity threshold that the model uses, above which sediment is released in the water column.

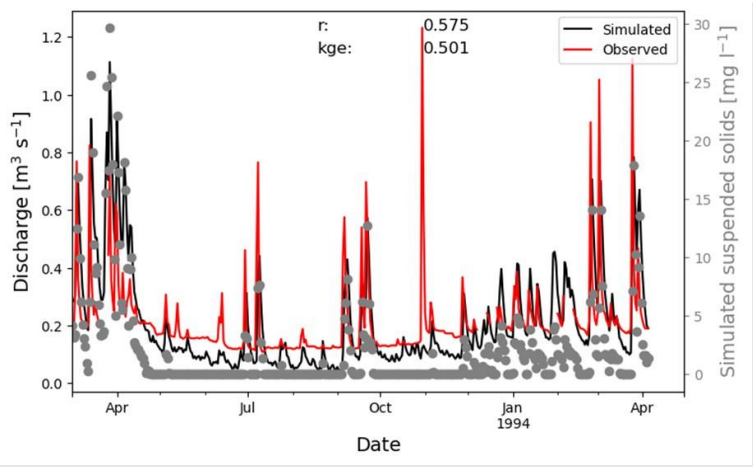

Figure 39. Observed and simulated discharge for the year 1993 as well as the simulated suspended solid concentrations using MIKE 11-AD at the outlet of Tims Branch.

Using these optimally calibrated MIKE 11-AD parameter values, in Figure 39, for the year 1993. the simulated suspended solids concentration within the water column is shown. It can be observed from this figure that MIKE 11-AD simulates increased amounts of suspended solids with increasing discharge. Furthermore, for flow rates below 0.1 m^3/s the suspended solids concentrations are (near) zero for extended periods of time.

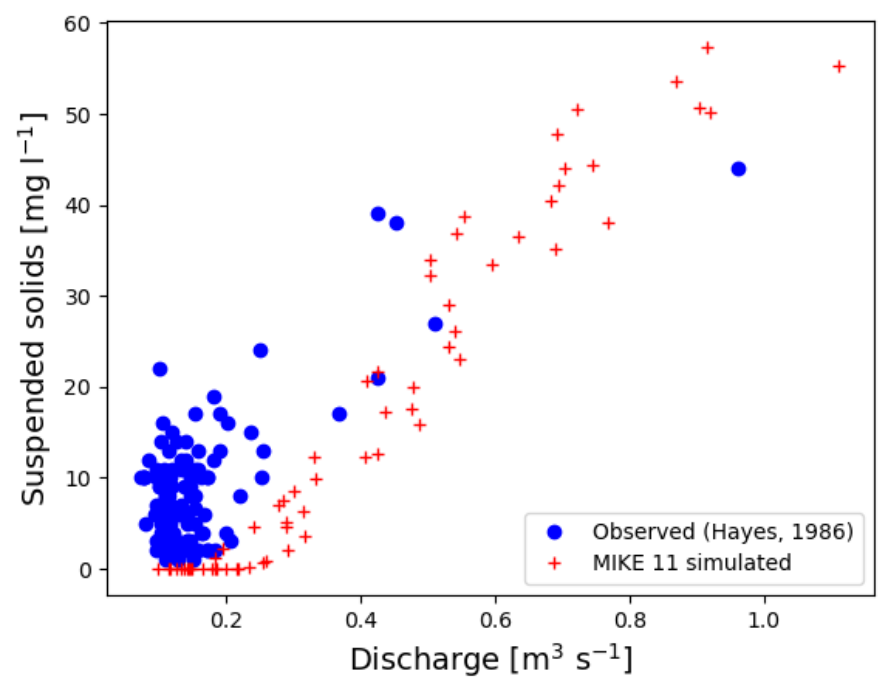

Figure 40. Comparison between the observed and simulated relationship between discharge and suspended solids concentrations at the Tims Branch outlet.

This calibrated MIKE SHE/MIKE 11 model, including the calibrated MIKE 11-AD routing, will be used to produce long-term simulations of flow and sediment transport within Tims Branch. More specifically, in this report the results for the period 1986 until 1992 are presented. Precipitation and temperature data for this period were obtained previously from national datasets as well as from in situ observations taken within Tims Branch.

Identifying the Role of Climate Change

Long-term changes in climate are anticipated to lead to more frequent and intense precipitation events. These events are expected to result in more increased flow events, which can lead to increased erosion of heavy metal-contaminated channel bed particles. Precipitation data for the 21st century for different climate scenarios can be derived from global or regional climate model simulations. However, running these multi-decadal simulations for various scenarios within MIKE SHE/MIKE 11 is a very cumbersome process. Therefore, instead of running these lengthy time series, for this report it was decided to focus on individual extreme precipitation events. More specifically, for Tims Branch watershed information about the intensity of precipitation events for various durations and return periods was used. As climate change is expected to result in more frequent extreme events, it is anticipated that in the future the return period of the extreme events will become smaller as they are observed more frequently.

Precipitation event information was generated for 5, 10, 25, 100 and 500-year return periods and 6, 12, 24 and 96-hour storm events. The hypothetical precipitation data of these events was

downloaded from the NOAA website. Besides providing event-based totals for each return period and duration (see figure below), for each duration the data also contains information on the hypothetical intra-event precipitation intensity variability. This is done by splitting up each duration into four quarters, representing the period during which the majority of precipitation was observed (Figure 42). For each quarter a representative intensity series was generated.

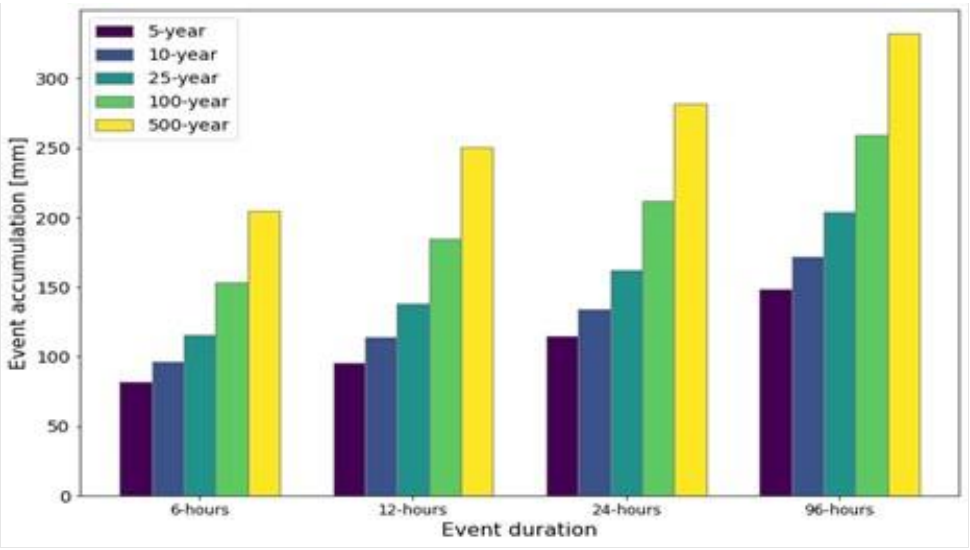

Figure 41. Total event accumulation for Tims Branch for an intense precipitation event of a given event duration and return period.

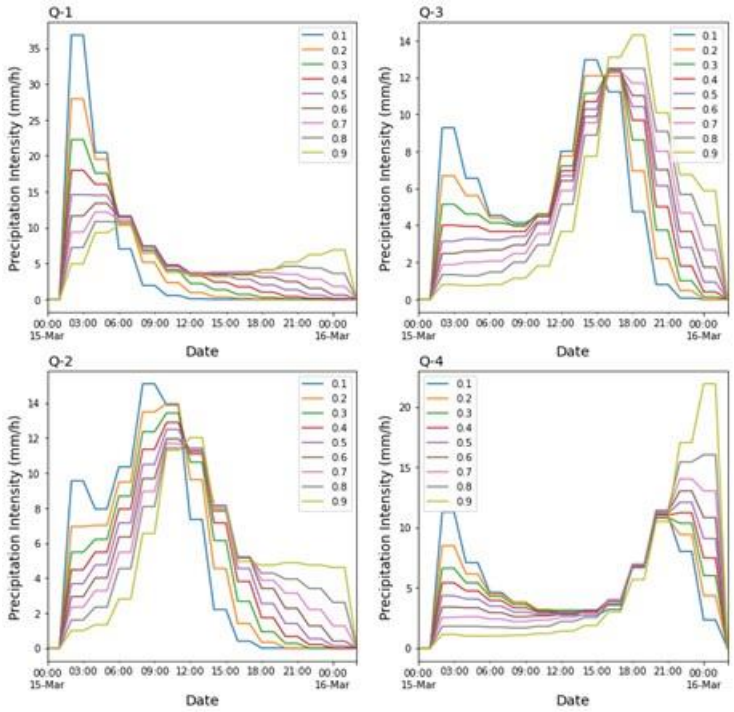

Figure 42. Example of the intra-event precipitation intensity variability for a 24-hour event corresponding to a 10-year return period. The four quarters shown in each panel (Q1-Q4) correspond to the period where the majority of precipitation is observed.

Given the intense computational demands of the MIKE SHE/MIKE 11 model, it was decided not to use all these precipitation series as input to the model. Instead, for each quartile the 0.1 and 0.9 probability events were used, which correspond to the maximum and minimum values for a given timestep. The MIKE SHE/MIKE 11 model was subsequently forced with these precipitation series to simulate the discharge response of Tims Branch. For a 24-hour precipitation event for a 10-year return period, Figure 43 shows the simulated discharge for each of the quartiles for the 2 forcing series. Although the response is similar, some variability in the simulated discharge response can be observed.

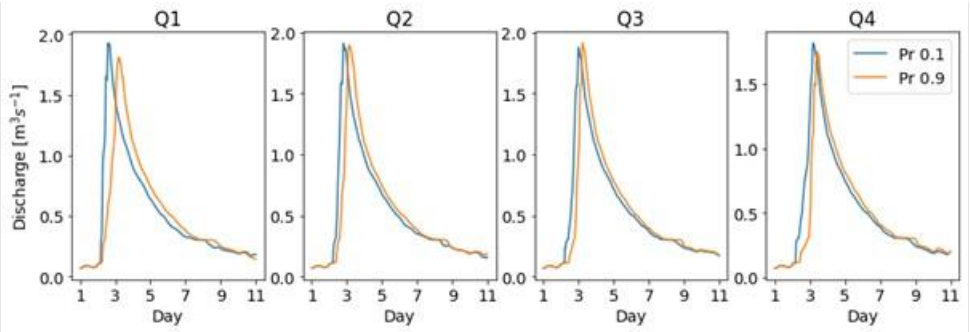

Figure 43. Discharge response as simulated by MIKE SHE/MIKE 11 for a 24-hour event with a 10-year return period. Each panel corresponds to a given quartile, with the two lines corresponding to an event probability of 0.1 and 0.9.

These precipitation series were used to force the MIKE SHE/MIKE 11 model including sediment transport. The calibrated MIKE 11-AD model was subsequently used to simulate the amount of sediment transport occurring with Tims Branch during extreme precipitation events.

Subtask 3.1: Results and Discussion

Hydrological and Sediment Transport Modeling

The long-term simulations presented here focus on the period 1986-1991, containing both wet (1987, 1991) and dry years (1988-1990). Figure 44 shows the simulated discharge and suspended solid concentrations for the period 1986-1991. Discharges are generally higher in winter due to reduced amount of evapotranspiration, though also during the summer, heavy precipitation events lead to short intense flow periods.

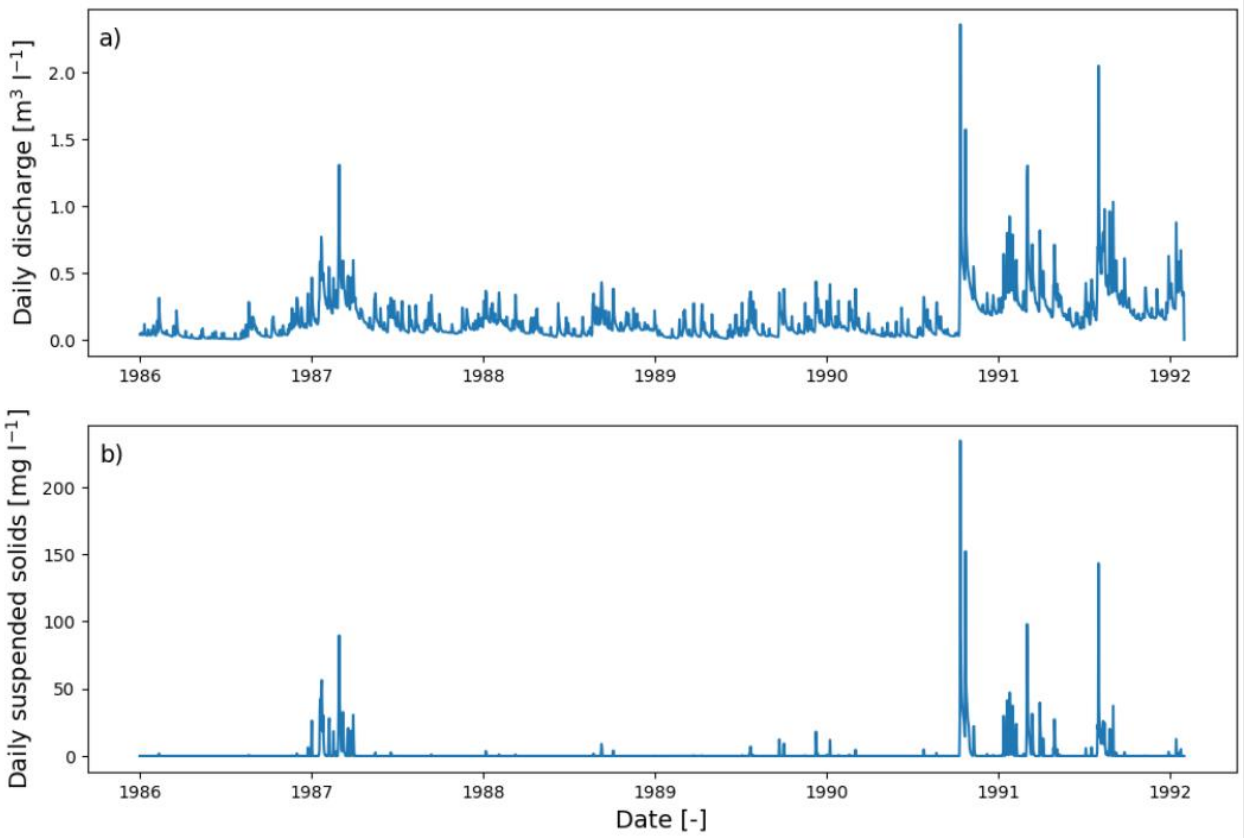

Figure 44. Top panel shows the MIKE SHE/MIKE 11 simulated discharge near the outlet of Tims Branch for the period 1986-1991. Bottom panel shows the simulated suspended solid concentration using the MIKE 11-AD module for the same location.

During these elevated flow periods, increased flow velocities increase erosion leading to higher simulated suspended solid concentrations. This can be observed in the bottom panel of Figure 44, where the simulated daily average suspended solid concentrations close to the outlet are shown. Throughout the year, simulated concentrations are small or close to zero. However, once discharges become substantial (>0.2 $m^3 s^{-1}$, see Figure 40), concentrations increase. The large flow events are simulated for November 1990 and September 1991. During these periods the maximum daily average suspended solid concentration at the outlet exceeds 100 mg l^{-1}.

To gain an improved understanding about simulated variations in erosion and deposition throughout the basin, Figure 45 shows the total channel bed level change for individual years. During dry years in 1986 and 1988, overall changes are small. However, for the dry year of 1989 some considerable erosion and deposition occurs. It is anticipated that this is caused by a few intense flow events observed during this overall dry year. As such, these individual events have a considerable amount of impact on observed suspended solid concentrations. For the wetter years of 1987, 1990 and 1991, erosion is simulated for a large number of locations along the main branch. However, at the northern end of Beaver Pond 3 as well as closer to the outlet near Railroad Pond, deposition of suspended solid particles is observed. These locations were shown by Kaplan et al. (2023) to contain elevated levels of uranium, even though the original deposition occurred up to Steed Pond. As such, uranium-contaminated particles, which were originally deposited upstream of Steed Pond, were able to migrate downstream and deposit at these locations.

What can also be observed from Figure 45, is that besides the lower end of Steed Pond with the branch upstream, hardly any bed level changes are detected. As such, at the locations, during both wet and dry years, flow velocities are too low to result in considerable erosion of contaminated channel bed particles.

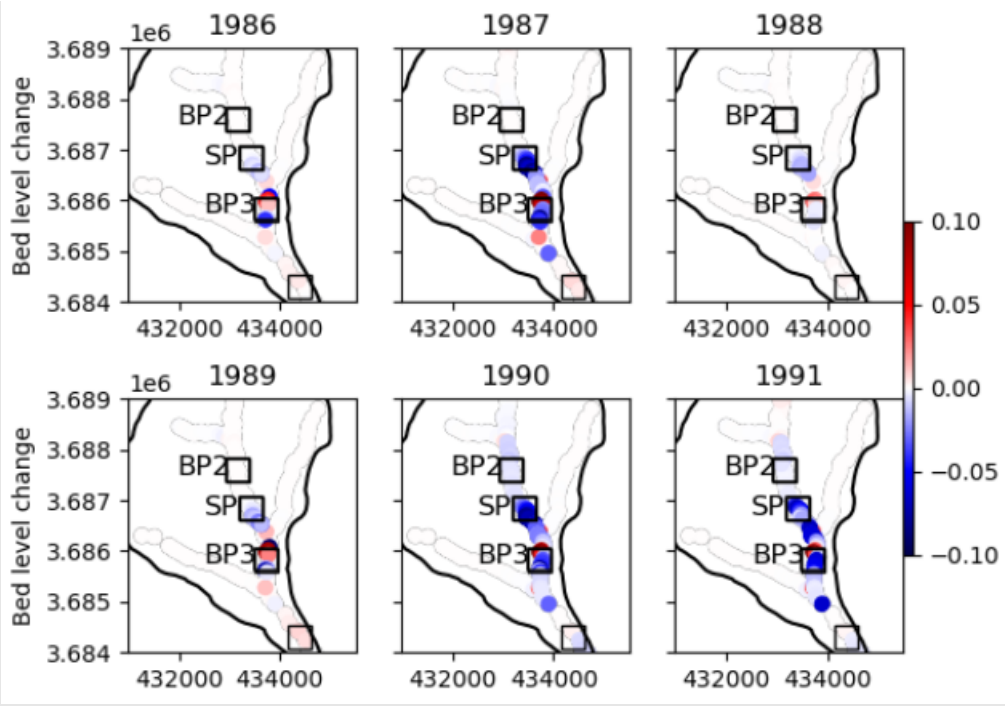

Figure 45. Erosion and deposition response for various locations within Tim Branch for various years. Also shown in the panels are the Beaver Pond 2 (BP2), Steed Pond (SP), Beaver Pond 3 (BP3) and Railroad Pond, which are known locations containing uranium contamination.

Identifying the role of climate change

The simulated variability in discharge for all return periods for a 24-hour event using MIKE SHE/MIKE 11 is presented in the figure below. To highlight the variability, on the side and on top, an error bar is shown indicating the maximum and minimum values. Although variations can be observed, for return periods up to 100-years, variability is small. However, for a 500-year return period, considerable uncertainty in the simulated discharge response can be observed. As these variations are anticipated to result in uncertainty in flow velocities, which impact erosion and sedimentation of suspended solids, it is anticipated that these intra-event precipitation variabilities will impact the transport of heavy metals.

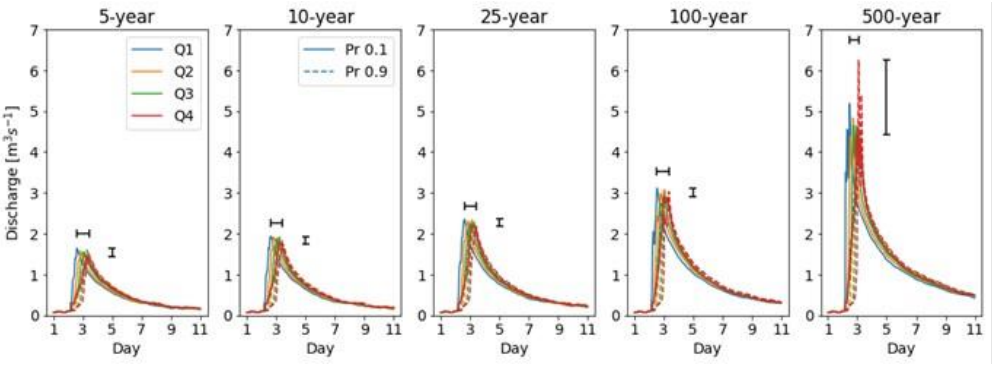

Figure 46. Discharge variability as simulated by MIKE SHE/MIKE 11 for a 24-hour event for various return periods. Error bars indicate uncertainty in maximum and minimum timestep and discharge values for the various quartiles and probabilities.

As expected, the simulated changes in discharge for various return periods, as shown in Figure 46, result in changes in the simulated amount of sediment transport. In Figure 47, the bottom panel shows the suspended solid concentration at the outlet. Increases in flow rate for increasing return period, leads to increased suspended solid concentrations, as for more locations critical flow velocities are exceeded resulting in channel bed erosion. Even for events with a 5-year return period, the simulated suspended solid concentration is double what is regularly observed within the basin (see Figure 39 and Figure 40) and peaks at around an average daily value of 100 mg l^{-1}. As return period increases, this value increases to almost 300 mg l^{-1} at a discharge of about 5 m^3 s^{-1} for the 500-year return period.

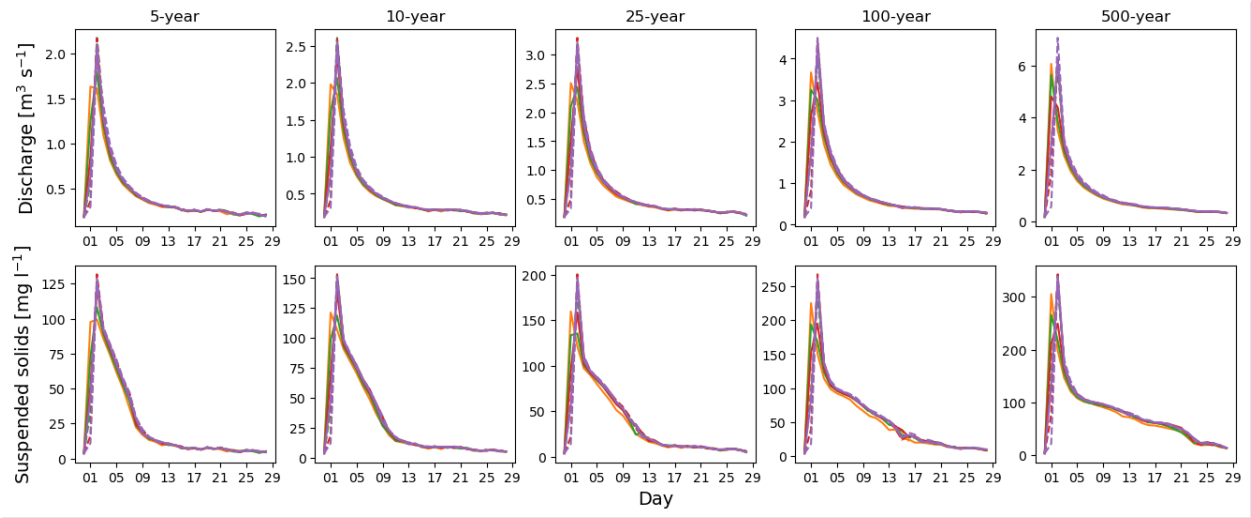

Figure 47. Simulated suspended solid concentrations using MIKE 11-AD for Tims Branch for location close to the outlet for 4 extreme precipitation events of 24 hours in duration with a return period of 5 years.

To gain an improved understanding of how this response varies throughout the basin and impacts local erosion and deposition, Figure 48 shows average overall impact of simulated sediment transport for various return periods. From the top panel it can be shown that predominantly only within the main channel, local flow velocities are high enough to exceed the critical velocity leading to erosion. As return period increases, the increase in flow rate leads to a longer period during which these critical velocities are exceeded. Furthermore, changes in cross-sections along the main branch impact flow velocities. Locations where flow velocities most often exceed critical

velocities are near the end of both Steed Pond and Beaver Pond 3. Although for the largest return periods, for a considerable stretch of the main channel, erosion-causing flow conditions are observed. The middle panel of Figure 48 shows the simulated suspended solid concentration, which generally increases downslope as well as with return period.

Lastly, the bottom panel of Figure 48 shows the amount of erosion and deposition for a given return period. Previously, Figure 45 showed that throughout Tims Branch both erosion and deposition occur. For 5- and 10-return periods some deposition is simulated on the north side of Beaver Pond 3 as well as along the main branch near the outlet. However, as return period increases almost everywhere south of Steed Pond, erosion is expected to occur. Furthermore, the northern part of Steed Pond and further upstream around Beaver Pond 2, where the majority of uranium was historically deposited, erosion is anticipated to be minimal, even at these extreme return periods. As such, contaminated sediments at these locations are anticipated to be stable, hardly impacting water quality conditions downstream. However, these results do show that the contaminated locations at the southern part of Steed Pond as well as within Beaver Pond 3 can be eroded during extreme flood events, impacting water quality conditions. The anticipated uranium concentrations of the water during these events will be a domain of focus for Year 4 of the DOE-FIU Cooperative Agreement.

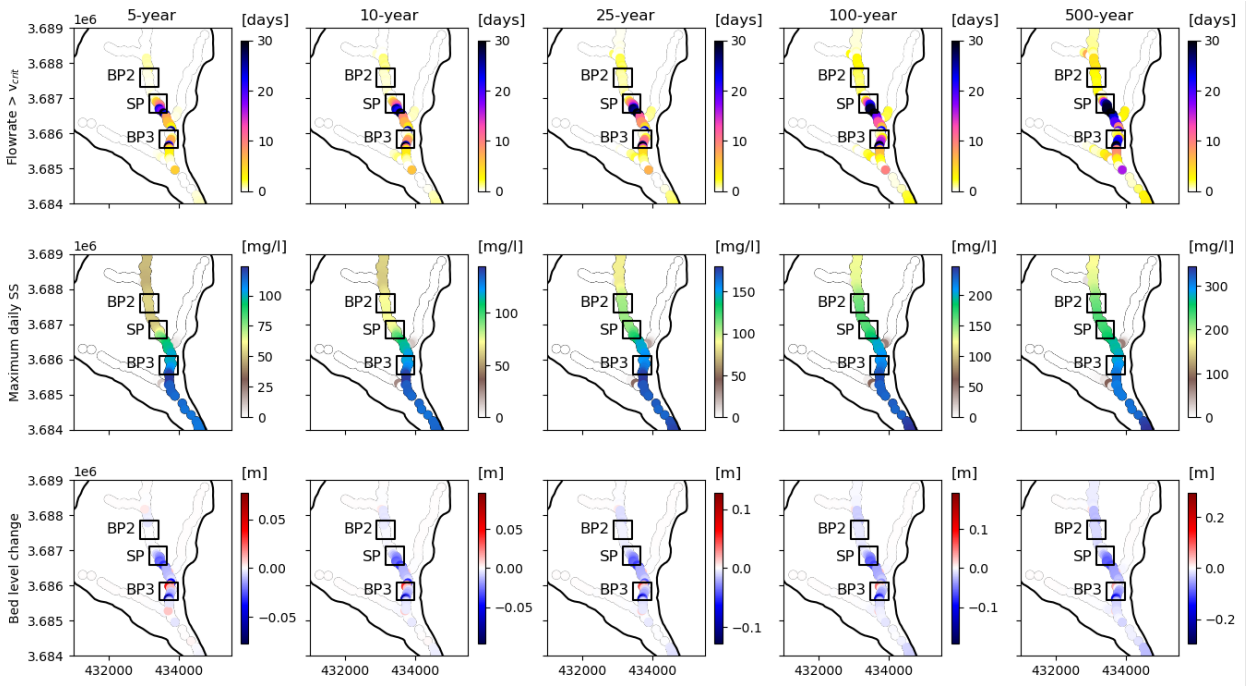

Figure 48. Flow and sediment transport response for various locations within Tim Branch as impacted by the intense precipitation event for various return periods. Top panel show the number of days that the critical flow velocity is exceeded. Middle panel shows the simulated suspended solid concentrations, while bottom panel indicates the simulated amount of erosion and deposition.

The results presented here for Subtask 3.1 show the long-term flow and sediment transport conditions as simulated for Tims Branch watershed. The main branch of this watershed has been contaminated with heavy metal pollution from historical DOE activities within the SRS A- and M-Areas. These contaminated particles were originally deposited along the main branch between Beaver Pond 2 and Steed Pond, but were able to freely move downslope after the removal of a dam at the exit of Steed Pond in 1984. The goal of this subtask is to evaluate whether long-term

changes in hydrological conditions effect the erosion channel bed contaminated particles and how these migrate downstream. Furthermore, as climate change is expected to result in the occurrence of more regular intense precipitation events, a second aspect of this work is to understand how intense flow events impact erosion and deposition.

The long-term simulation analyses presented above show that the majority of erosion occurs during intense flow events, with suspended solid concentrations quickly decreasing to near-zero as baseflow conditions are observed. This results in local changes in both erosion and deposition, where the majority of erosion occurs near the end and south of Steed Pond and further downslope where the channel bed is incised. Deposition is simulated within the braided reaches around Beaver Pond 3 and Railroad Pond. Over time, this has resulted in an increase in the amount of uranium-contaminated particles at these latter two locations, as has been observed by Kaplan et al. (2023).

Intense precipitation events with increasing return period are expected to result in higher flow rates and increases in the amount of erosion. Especially for the largest flow events at the 500-year return period, erosion is expected to occur almost everywhere within the main branch of Tims Branch, with the largest amounts occurring south of Steed Pond. As such, the more intense flow events, which are anticipated to occur more often due to climate change in the near future, are expected to result in increases in the amount of erosion thus impacting water quality conditions. However, both the long-term and event-based simulations show that at the locations where historically the majority of uranium-contaminated particles were deposited (between Beaver Pond 2 and Steed Pond), total erosion is small, limiting the amount of uranium contamination that can impair water quality. In the current work, uranium transport was not explicitly simulated. As such, the overall impact of erosion on uranium concentration in the water column is currently unknown, but will be a topic of focus in Year 4 of the DOE-FIU Cooperative Agreement.

3.1.2. Evaluate the uranium transport during storm events from contaminated sediments that are subject to erosion.

Subtask 3.1: References

Batson, V. L, Bertsch, P. M., & Herbert, B. E. (1996). Transport of anthropogenic uranium from sediments to surface waters during episodic storm events. *Journal of Environmental Quality*, *25*(5), 1129–1137.

Batson, V. L. (1994). *Surface water transport and distribution of uranium in contaminated sediments near a nuclear weapons processing facility*. Texas A&M University.

Evans, A. G., Bauer, L. R., Haselow, J. S., Hayes, D. W., Martin, H. L., McDowell, W. L., & Pickett, J. B. (1992). *Uranium in the Savannah River Site Environment*. Westinghouse Savannah River Co., Aiken, SC (United States).

Hayes, D.W. (1986). *Sediment transport studies in Tims Branch*. Rep. DPST-86- 468. E.I. du Pont de Nemours & Co, Savannah River Laboratory, Aiken, SC.

Kaplan, D. I., Smith, R., Parker, C. J., Baker, M., Cabrera, T., Ferguson, B. O., Kemner, K. M., Laird, M., Logan, C., & Lott, J. (2020). Uranium Attenuated by a Wetland 50 Years after Release into a Stream. *ACS Earth and Space Chemistry*, *4*(8), 1360–1366.

Kaplan, D. I., Smith, R. J., Parker, C. J., Roberts, K. A., Hazenberg, P., Morales, J., O'Loughlin, E. J., Boyanov, M. I., Weisenhorn, P., Kemner, K. M., and Powell, B. A. (2023). Natural Attenuation of Uranium in a Fluvial Wetland: Importance of Hydrology and Speciation, *Applied Geochemistry*, 155, 105718. Doi: 10.1016/j.apgeochem.2023.105718

Subtask 3.2: Model Development for Fourmile Branch with Specific Focus on the F-Area Wetlands

Subask 3.2: Introduction

The F-Area wetlands at the U.S. Department of Energy's (DOE's) Savannah River Site (SRS) has been a primary area of concern due to the presence of low-level radiological contamination in the groundwater, which originated from the disposal of 1.8 billion gallons of acidic, low-level radioactive waste from 1955 to 1988 in three unlined basins, known as the F-Area Seepage Basins. While most of the dispositioned radionuclides such as plutonium isotopes and cesium-137 sorbed to the basin soil, other mobile contaminants such as uranium (U) isotopes, strontium-90 (Sr-90), iodine-129 (I-129), technetium-99 (Tc-99), tritium (3H), and nitrate (NO_3^-) migrated through the vadose zone into the aquifer zone contaminating the groundwater. Over time the contaminant plume migrated downstream extending from the basins approximately 600 m downgradient, resurfacing at outcrops (seep lines) in the adjacent wetlands and entering the Fourmile Branch stream system (see figure below). As such, Fourmile Branch and its associated wetlands have been impacted by the outcropping of contaminated groundwater coming from the F-Area Seepage Basins.

The groundwater-surface water interface is the region where contaminated groundwater emerges to the surface, which is often one of the major ecological and human health risk exposure pathways. In the F-Area, I-129 is one of the main contaminants of concern. Over the years at several surface water stations (e.g., FAS-091 and FAS-092), there has been seasonal variation of I-129, in which high concentrations were detected during summertime while low concentrations were detected during winter/spring. These seasonal variations have not been observed at upstream groundwater wells, such as FSP-47A, where I-129 concentrations have remained fairly constant and lower since 2010. The spikes in I-129 concentrations observed at surface water stations during the summer suggest that there are processes (e.g., geochemical, microbial, physical) releasing I-129 from wetland soils to surface waters that are still not well understood. The concerns exist, therefore, with the stability of I-129 and other radioactive contaminants that have attenuated in organic rich seepline sediments as geochemical conditions slowly return to baseline conditions over the next few decades.

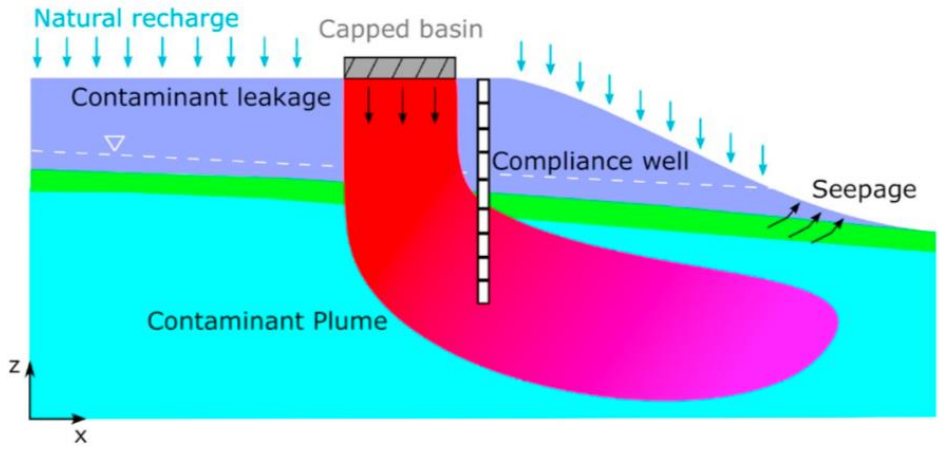

Figure 49. Schematic conceptual 2-D cross section of the F-Area focus domain and the existing residual contamination in the vadose zone and groundwater (from: Libera et al., 2019, JCH).

The F-Area Seepage Basins were closed and capped with a low-permeability material in 1988 after discharge operations ended. Furthermore, pump-and-treat remediation of contaminated groundwater was used to reduce to reduced dissolved phase contamination. In 2004, a funnel-and-gate system with groundwater flow barriers were constructed to decrease the groundwater gradient and enhance natural attenuation. Also, periodic base injections have been conducted at the gates to neutralize groundwater pH and cause the attenuation of uranium and Sr-90 by enhanced adsorption to mineral surfaces. Just upgradient of the base injection zones at the central gate, I-129 is being treated by injection of silver chloride particles. The particles react with I-129 that exist as iodide to form sparingly soluble silver iodide, removing I-129 from the groundwater. Currently, groundwater remains unnaturally acidic with high levels of various radionuclides and other contaminants upgradient of the funnel-and-gate.

Nowadays, remediation focuses on an enhanced monitored natural attenuation (MNA) approach, with periodically injecting a base solution to increase the sorption of cationic contaminants, making them less bioavailable. While these strategies are successful in sequestering the contaminants of concern, a long-term monitoring strategy is necessary at the zones of vulnerability of Fourmile Branch where there is potential for contaminant remobilization if changes in biogeochemical conditions occur that could potentially influence the release of contaminants.

Subtask 3.2: Objectives

FIU's aim is to develop a hydrological model for the Fourmile Branch riparian stream system near the SRS F-Area. This is critical for understanding the flow of contaminants to the down gradient stream. A detailed groundwater model was developed by the Advanced Long-Term Environmental Monitoring Systems (ALTEMIS) project using the Amanzi platform to model flow and reactive transport within the F-Area hillslope upstream of the seep line; however, the processes occurring below the model domain, including within the seep line within the riparian zone and river network, remains unclear. To understand the transport of contaminants from subsurface to surface and then to surface water, there is a need to improve the understanding of the groundwater-surface water dynamics occurring in the F-Area wetlands. FIU's aim is to extend the model developed by DOE by incorporating the seepline-riparian zone interface in the Advanced Terrestrial Simulator (ATS)-Amanzi model. This will enable more detailed understanding of seasonal-scale drying and wetting of the seepage face and riparian zone system and how it impacts contaminant transport.

For Year 3 FIU's objective was to also maintain close collaboration with SRNL and LBNL scientists and support the existing research being conducted in the SRS F-Area under the ALTEMIS project by developing a multi-year hydrological model simulation using ATS to better understand the flow of groundwater downslope through the funnel and gate system, entering the seep line, riparian zone, and river network. Specific focus was placed on seasonal variations in groundwater-surface water interaction within the seep line/riparian zone interface.

Besides understanding the small-scale hydrological response at the surface and subsurface and the interaction between the groundwater and Fourmile Branch surface water system of the F-Area hillslope, there is also an interest in understanding how seasonal-scale changes and long-term changes due to climate change impact the hydrological response as well as the transport of contaminants across Fourmile Branch watershed. Therefore, an additional objective of Subtask 3.2 is to developed a coupled hydrological-hydraulic model at the scale of Fourmile Branch watershed using MIKE SHE/MIKE 11. The development of this model follows a similar approach as the model developed for Tims Branch watershed in Subtask 3.1.

Subtask 3.2: Methodology

Subtask 3.2.1: Long-term simulation of the hydrological response of Fourmile Branch watershed

Developing a hydrological model that can simulate surface hydrology and estimate the flow components is essential in contaminant fate and transport modeling. Based on recent conversations with collaborators at Savannah River National Laboratory (SRNL) and Lawrence Berkeley National Laboratory (LBNL), for Year 3 it was decided to specifically focus on groundwater-surface water interactions within the F-Area wetlands, as well as the seasonal and yearly hydrological variability within the Fourmile Branch. FIU successfully created an initial version of the MIKE SHE/MIKE 11 model for Fourmile Branch with a 250 m pixel resolution using open-source data in combination with GIS and Python scripts. Previous literature research showed that the deeper aquifer systems do not drain into the Fourmile Branch river network. Therefore, only the upper two aquifer systems on top of the Gordon confining unit are defined within the model. A number of flow parameter values, such as lateral conductivity, were obtained using documentation provided by FIU's DOE collaborators. For the unknown parameters, the values originally estimated for the MIKE SHE/MIKE 11 Tims Branch model developed under Subtask 3.1 were used. The figure below shows the latest version of the MIKE SHE model for Fourmile Branch. The left panel shows green flags for all estimated parameters.

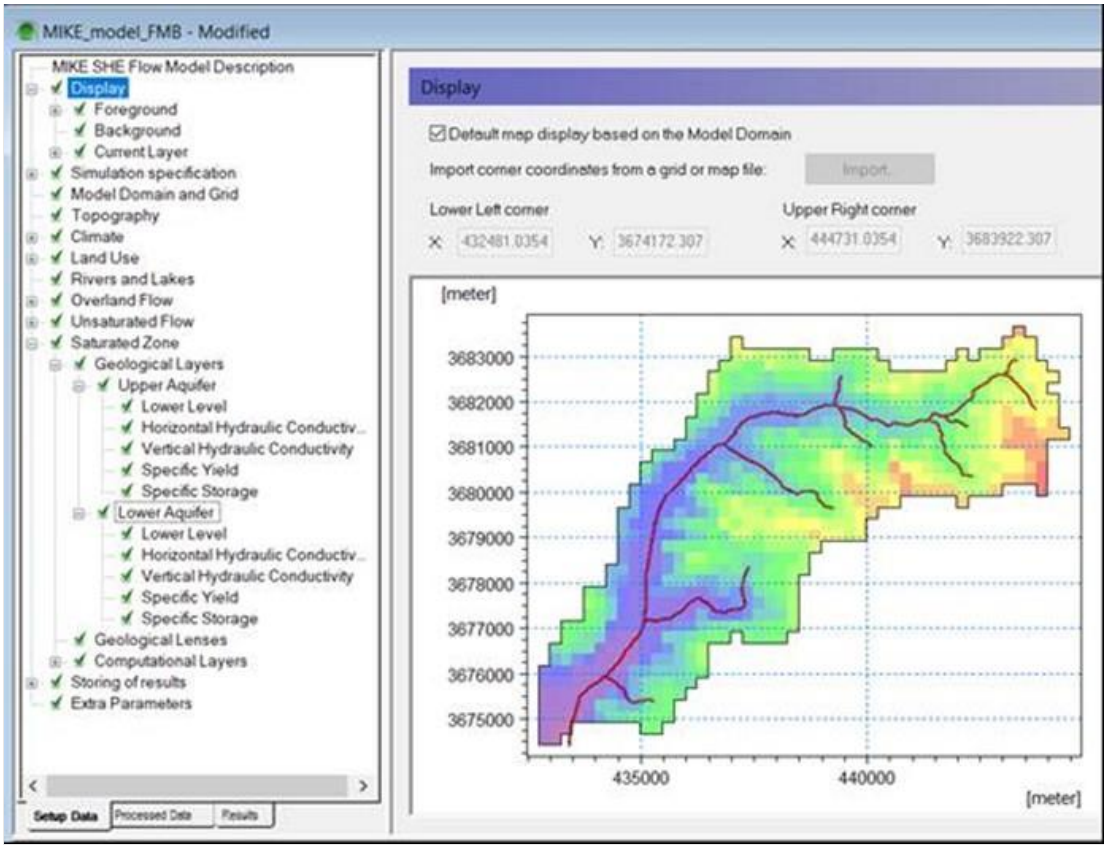

Figure 50. Overview of the MIKE SHE /MIKE 11 model for Fourmile Branch watershed.

Subtask 3.2.2 Development of a hydrological model for the groundwater-surface water interaction within the F-Area domain using Amanzi-ATS

The first phase of ATS work for FIU Year 3 was to develop a detailed understanding of the ATS model to establish an efficient process workflow and, in parallel, develop a "spinup" model to be used for the development of an integrated hydrology ATS model for the F-Area domain. A spinup model is used to establish an equilibrium state so that key hydrological variables, such as soil moisture, groundwater levels, and streamflow, reach a consistent and self-sustaining state. The spinup modeling was completed during a DOE Fellow internship at LBNL during the summer of 2023. The objective of this internship was to work under the ALTEMIS project and to develop understanding of the workflow, input requirements, and tools needed to perform hydrological simulations with a new version of ATS, version 1.3. In FIU Year 3, a transient model for the F-Area domain to show the seasonal variations and groundwater-surface water interactions was developed. A transient model differs from the spinup model as it includes temporal data that varies over time. The spinup data was used as the initial condition for transient conditions so that the model starts at a steady state.

The mesh of the F-Area domain was created with the Python module, Watershed Workflow. Watershed Workflow was developed by Oak Ridge National Lab (ORNL)and allows for geometrical and geophysical information about the site to be encoded into the ATS input file. Watershed Workflow allows for the incorporation of publicly available data into the mesh, such as digital elevation maps (DEMs), spatial variations in National Land Cover Dataset (NLCD) land cover types, Soil Survey Geographic Database (SURRGO) soil texture, and GLobal HYdrogeology MaPS (GLHYMPS) subsurface information. Watershed Workflow also contains a component that allows one to obtain daily atmospheric forcing (precipitation, temperature, radiation) from DayMet, a weather dataset provided by the National Aeronautics and Space Administration's (NASA's) Distributed Active Archive Center (DAAC) at ORNL.

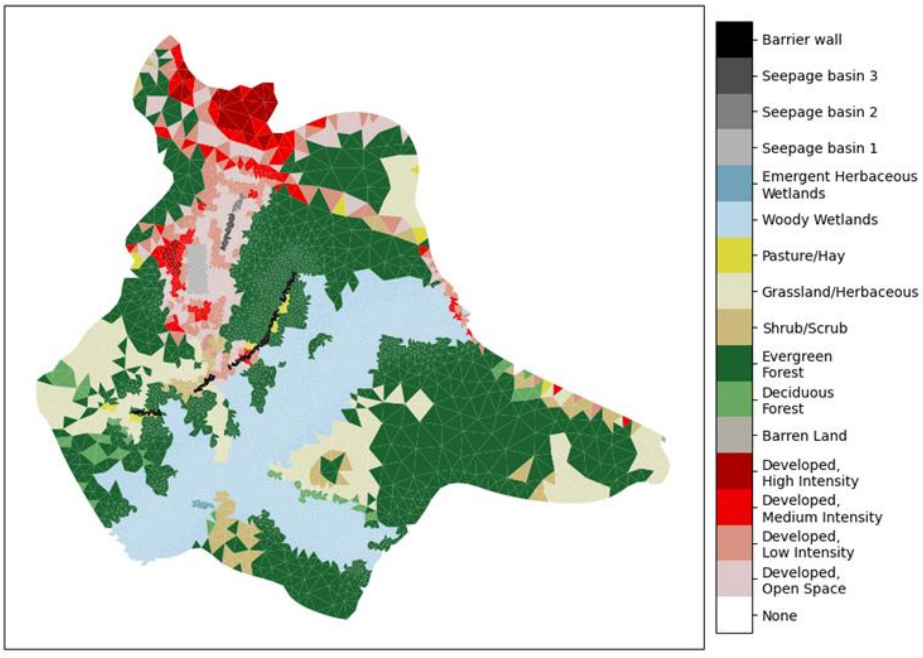

Figure 51. Plot of the F-Area mesh with the NLCD national land cover types, seepage basins, and the barrier wall displayed.

On the surface of the site, there are 13 NLCD land cover types, which are displayed in the above figure. In Year 3, FIU had extended the capabilities of Watershed Workflow, to include the existence of the seepage basins as well as the barrier wall into the mesh. In addition, more detail to the groundwater system was added through the inclusion of the upper two aquifers and the aquitard into the model mesh. The below figure shows the surface soil types provided by SSURGO as well as the 3 subsurface layers: the upper and lower aquifers and the tan clay confining zone. These surface and subsurface features were included in the ATS integrated hydrology model.

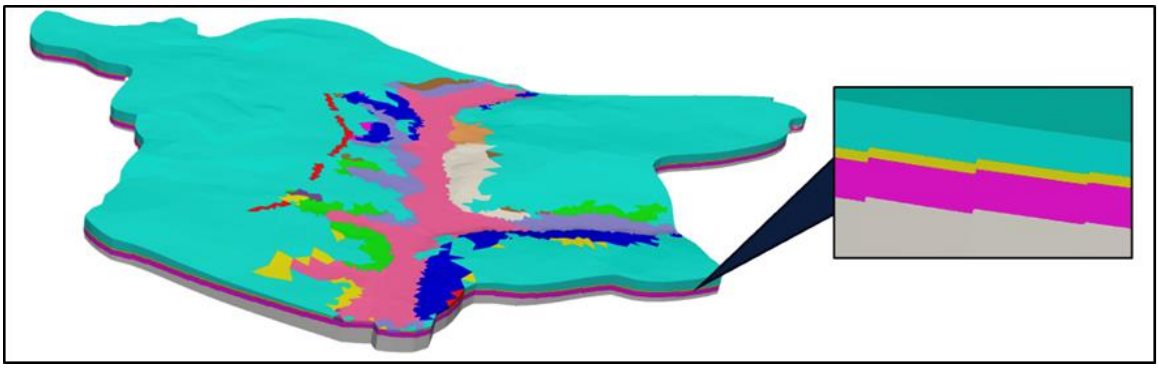

Figure 52. Top: SSURGO soil units, and barrier wall (red). Below SSURGO soil units: upper aquifer (blue), tan clay confining zone (yellow), and lower aquifer (pink) layers, assumed to be rested on top of impermeable layer (gray).

The output for Watershed Workflow is then used within an ATS input file. This input file is written in XML format and configures the set of coupled processes for the simulation at run time. This input file also defines all aspects of the hydrological model, such as meteorological data, geometric regions and mesh information, model parameter values, mathematical equations, and visualization output. FIU previously developed a Python script that enables automatic generation of the input file within Watershed Workflow.

The input file for this model uses the results from the spinup model developed during the summer internship in 2023 as the initial conditions. The transient model developed in FIU Year 3 includes meteorological forcings and evapotranspiration. With the transient model, the hydrological response of the F-Area due to precipitation can be assessed. Meteorological forcings for these years was obtained with Watershed Workflow for five years (January 1st, 2005 to December 31st, 2009). Watershed Workflow retrieves the daily atmospheric forcing (precipitation, temperature, radiation) from DayMet, which is a weather dataset provided by NASA's Distributed Active Archive Center (DAAC) at the Oak Ridge National Laboratory. Also needed for the model is the Leaf-Area-Index (LAI) for the major land cover types within the region. The LAI is time series-based and directly impacts the evapotranspiration of the model and therefore the entire water balance. The addition of the LAI will allow for more accurate evapotranspiration predictions and hydrology modeling. The LAI is obtained from MODIS satellite observations which are processed using Watershed Workflow in Python, which generates time series data for the major land cover types in an ATS readable format. In addition, a seepage face boundary condition was added to the surface flow in the input file. This boundary condition allows water (e.g., runoff) to leave the F-Area domain when saturation is present.

Subtask 3.2: Results and Discussion

Subtask 3.2.1: Long-term simulation of the hydrological response of Fourmile Branch watershed

The MIKE SHE / MIKE 11 model developed for Fourmile Branch watershed was used to simulate the hydrological response of the catchment for the period 1988-1992. This period was chozen as discharge observations of the main river network for a location near the outlet were available. For the simulations, the first two years were used for model spinup. After performing simulations within the initially chozen model parameter set, some of the lateral and vertical conductivity parameters of the groundwater layers were adjusted manually to improve the correspondence between the model and observational data.

The results obtained from this are shown in Figure 53. From this figure it can be concluded that we successfully developed a MIKE SHE / MIKE 11 model for Fourmile Branch using model parameter information predominantly available from public geographic data (i.e., soil, land surface, satellite observations) as well as by performing an initial calibration on some of the subsurface parameters of the groundwater system. See figure below.

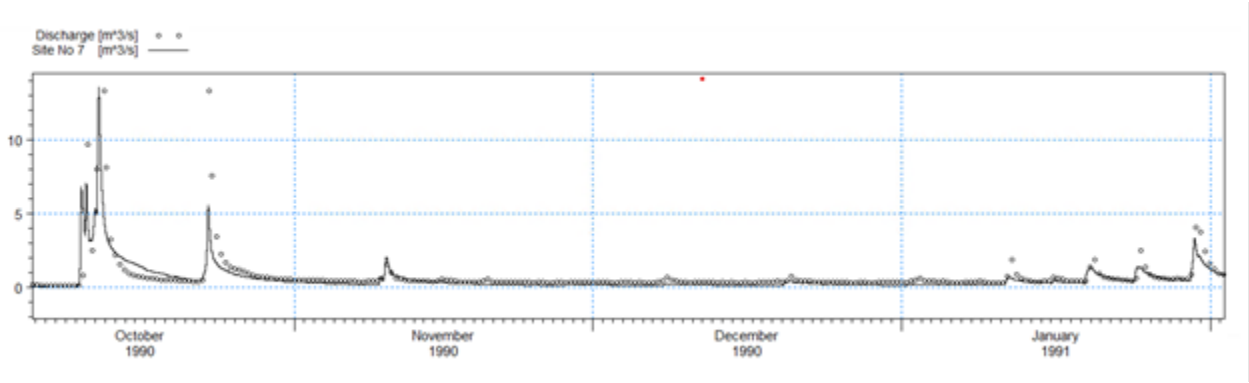

Figure 53: Correspondence between observed (dotted) and simulated (straight line) discharge of Tims Branch watershed near the basin outlet for the year 1990.

The results presented here only focus on the outlet and have not included any upstream information on both the river network as well as the hydrological response at the hillslope scale. This will become the focus of FIU Year 4, where we continue calibration to include upstream observations of surface water flow and groundwater levels, as well as perform detailed analyses on the water balance.

Subtask 3.2.2 Development of a hydrological model for the groundwater-surface water interaction within the F-Area domain using Amanzi-ATS

This sections shows the results from the ATS model. For the F-Area is subject to seasonal variation that affects the surface water and groundwater in the area. The results show seasonal variation and its effects on the surface water content (ponded water) and the subsurface infiltration. The figure below shows the actual precipitation (P) and snowfall (S) on each day for five years (2005 through 2009) to force the model. Furthermore, the ATS simulated outputs such as evapotranspiration (ET) and runoff (Q) are also shown. From this figure the wet and dry season can be seen. Precipitation intensities peak on average in summer, with evapotranspiration also being largest during this season. For example, the second largest precipitation event observed occurs around the 540th day (June 24th, 2006). The precipitation for this event was 0.055 m/d (55 mm/d) and the amount of

runoff ATS calculated was around 4 mm/d. The excessive amount of rainfall observed during this period also increased the simulated actual evapotranspiration flux of almost 3 mm/d. The evapotranspiration is also seasonal and effects the surface and subsurface water, as the evapotranspiration is near zero at the end and beginning of every year. The model also simulates the occurrence of one snowfall event (S) in January of 2005 although its overall impact on the water balance is small.

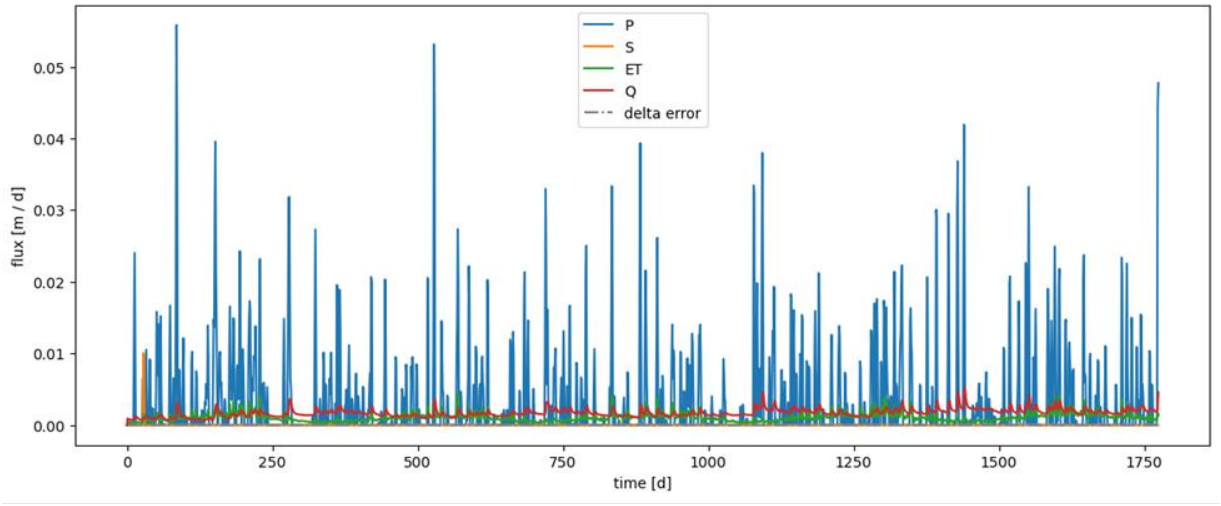

Figure 54. Graph of the water balance from the F-Area model with the flux (m/d) of rain, snow, evapotranspiration, runoff, and the error plotted versus time (d).

The figure below shows the simulated infiltration into the subsurface. The infiltration is frequently negative during rainfall events as the soil saturates, excess water runs downslope in the form of overland flow instead of infiltrating into the soil column.

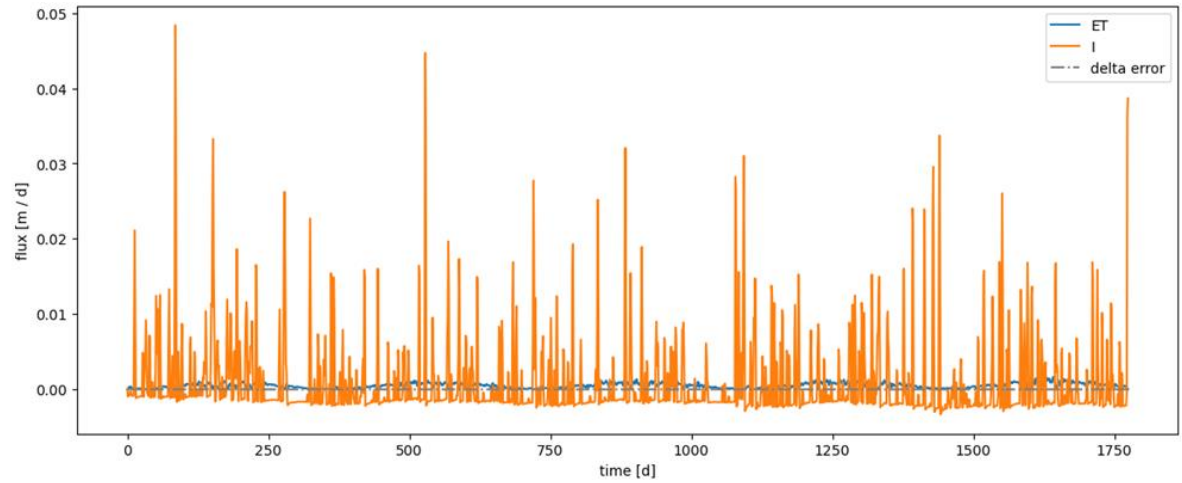

Figure 55. Plot of the flux (m/d) for infiltration (I) and evapotranspiration (ET) versus time (d).

To gain an improved understanding on soil moisture and surface flow variability of the F-area hillslope as simulated by ATS, in the following figure, the results are presented for a dry period on October 27th, 2005 and a wet period on July 13th, 2009.

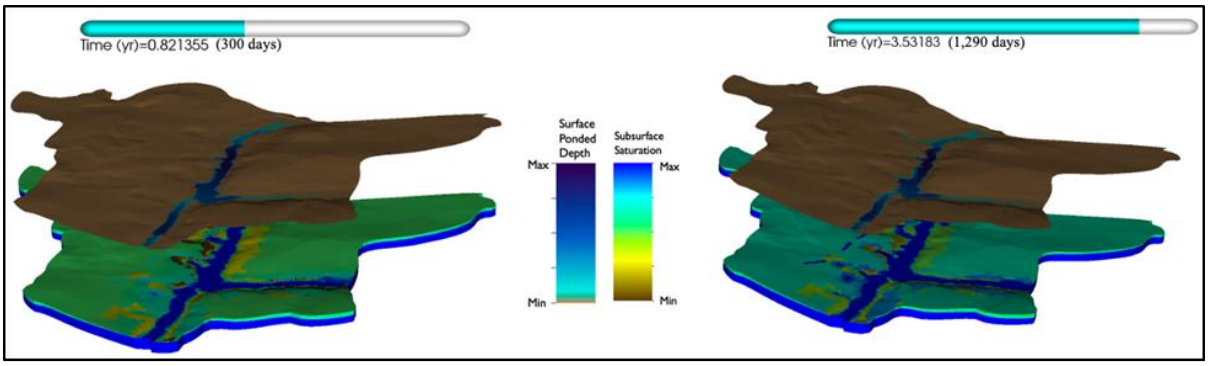

Figure 56. Image from a video simulation of the F-Area model on 300th day (left) and 1,290th day (right) (October 27th, 2005, and July 13th, 2009) in which surface ponded water depths are shown with a color table.

The surface layer was given a customized color scheme that shows the ponded depth of water along the surface after precipitation. The brown represents no ponded water at the surface, while the darker blue colors indicate ponding. The surface layer elevation was also transformed upward in the z-direction to better show the subsurface infiltration and the presence of the river network in the domain. On the left, even in the dry season where less precipitation is present, the river basin contains ponded water in the stream and the subsurface is saturated in certain areas where more permeability soil types are present. There is consistently water flowing through the wetland according to this model. For the example on the right, it can also be observed that during the wet period the extent of the saturated domain surrounding the river network extends a bit more upslope especially in the direction of the barrier wall. On the surface, the ponded water slightly increases, and the river extent expands.

In June of 2006, an intense precipitation event occurred within the domain and the impact is seen in the figure below.

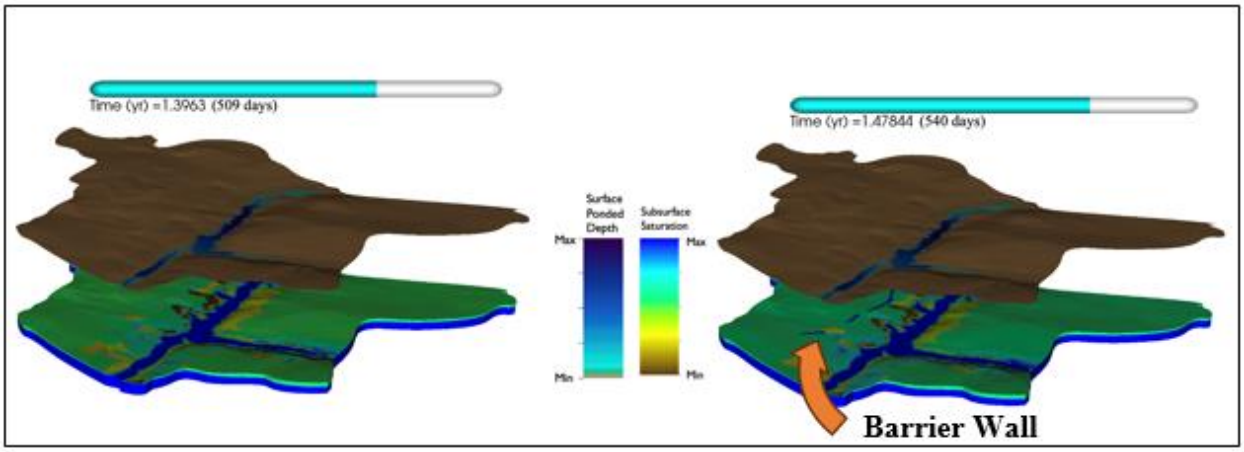

Figure 57. Image from a video simulation of the F-Area model on 509th day (left) and 540th day (right) (May 24th, 2006, and June 24th, 2006) in which the surface ponded water depths are shown with a color table.

The surface ponded depth and subsurface saturation were visualized for the 509th day (May 24th, 2006) and the 540th day (June 24th, 2006). After the rainfall event, the model calculated a high subsurface infiltration at the location of the barrier walls within the F-Area as well as around the river network. Heavy precipitation may cause an increased flow of water and water content around the barrier walls in the domain, yet more investigation is needed to determine the interaction between the barrier wall and the water content. How these changes in moisture conditions impact

water quality conditions in groundwater and surface water will be the focus of interest for the future.

Subtask 3.2: Conclusions

Training of DOE Fellows and FIU staff on the ATS model was provided by LANL and LBNL scientists. The initial version of the developed MIKE SHE / MIKE 11 is able to simulate the hydrological response at the catchment scale. Furthermore, the detailed ATS model, developed for the F-area hillslope response, represents essential details relating to soil textures, meteorological forcings, and subsurface information. The ATS model makes use of a high-resolution mesh and an advanced process kernel tree, which allows for the calculation of runoff, evapotranspiration, and infiltration. The ATS model developed in FIU Year 3 has stability by using the spinup model as the initial conditions for the transient model. Overall, the preliminary ATS model does show that seasonal precipitation influences the subsurface saturation and surface flows.

Subtask 3.2: References

Amanzi. (2023). GitHub. Retrieved from https://amanzi.github.io/ats/index.html

Coon, E. T., Moulton, J. D., & Painter, S. L. (2016). Managing complexity in simulations of land surface and near-surface processes. Environmental modelling & software, 78, 134-149.

Coon, Ethan T., and Pin Shuai. “Watershed Workflow: A toolset for parameterizing data-intensive, integrated hydrologic models.” Environmental Modelling & Software 157 (2022): 105502.: https://doi.org/10.1016/j.envsoft.2022.105502

Livingston, D. (2020). TINerator API Reference. Los Alamos National Laboratory.

TASK 5: REMEDIATION RESEARCH AND TECHNICAL SUPPORT FOR WIPP

Subtask 5.2: Fate of Actinides in the Presence of Ligands in High Ionic Strength Systems

Subtask 5.2: Introduction

The Waste Isolation Pilot Plant (WIPP) is a deep geologic repository for permanent disposition of transuranic waste (TRU). It is characterized by high ionic-strength porewater (up to 7.4 M). Every 5 years recertification of the WIPP is required to demonstrate that the long-term performance of nuclear wastes stored in the WIPP repository complies with Federal regulations and is protective of human health and the environment. Thus, a comprehensive understanding of the fate and transport of actinides in a high ionic-strength brine environment laden with metal chelating ligands is critical to developing a robust risk assessment model that addresses the low-probability scenario of potential brine inundation and contaminant release due to human intrusions. The potential release of actinide (An) from the WIPP environment is ranked in the following order: plutonium (Pu) ~ americium (Am) > uranium (U) >> thorium (Th) and neptunium (Np). In addition to uranium [U(VI)] (the largest inventory in treated TRU waste) the most relevant actinide oxidation states considered for safety assessment calculation for the WIPP and other deep geologic waste repositories are An(III) and An(IV). Sorption retards migration of actinide to the environment by allowing longer transport time resulting in decay of larger portions of actinide inventory. It is normally expressed in terms of partition coefficient (K_{dc}), which is a measure of distribution of actinides between the immobile solid phase(s) and mobile aqueous phase(s). However, previous studies have shown that actinide can form strong complexes with organic ligands such as EDTA, resulting in an increased solubility compared to the organic ligand-free system. A majority of these studies considered the formation of only binary An-L complexes (L = organic ligand) in acidic conditions. In neutral to hyperalkaline pH conditions the formation of tertiary An(IV)-OH-L complexes is predicted.

The current PA for the WIPP recommends a K_{dc} range of 20 – 400 mL/g for Pu(III) and Am(III) (Brush and Storz, 1996). These previous models heavily relied on data derived from experiments that often did not fully cover WIPP-relevant conditions (Brady et al., 1996; Brush and Storz, 1996; Perkins et al., 1999). Strong chelators that have been previously identified in the WIPP, such as EDTA and oxalate (Dunagan et al., 2007), have been accounted for in the current PA models (PAIR-2018, Brush, 1990). Additional ligands of interest include degradation products such as gluconate, a cement additive, (Askarieh et al. 2000), which has been identified in the hyperalkaline conditions expected in cementitious repositories (Gaona et al., 2008). Currently gluconate and other similarly structured ligands are not considered in WIPP risk assessments due to the expected low impact under WIPP conditions. Structurally similar to gluconate, isosaccharinate is an important byproduct of alkaline degradation of cellulose that is considered a major concern in many PAs of nuclear waste repositories. However, sorption of gluconate and other similarly structured ligands and WIPP-relevant minerals (e.g., iron oxide, a corrosion product of steel containers) have not been well studied. Thus, current batch sorption experiments under realistic WIPP conditions will provide an improved understanding of actinide interaction with corrosion

products and organic ligands. Moreover, updated sorption data will indirectly support future risk assessment models through reduction of uncertainty associated with these models.

Subtask 5.2: Objectives

The overarching objective of this task is to provide updated sorption data via batch studies that shed light on the behavior of actinides and lanthanides in the presence of complexing ligands in WIPP-relevant conditions. To indirectly support future PA models, the potential impact of isosaccharinate (ISA) in the presence of corrosion products (iron oxide mineral) in WIPP conditions will be investigated.

Research Questions to be addressed:

1. *How do relevant ligands/chelators impact sorption of the actinides at ionic strengths relevant to the WIPP environment?*
2. *What potential impact do isosaccharinate and corrosion products (iron oxide mineral) have on the transport of actinides and lanthanides in source-term models?*
3. *What impact do competitive ions (e.g., $Ca^{2+}$and Na^{+}) from the various WIPP-specific brines have on the transport of actinides and lanthanides in the presence of relevant ligands?*

Subtask 5.2: Methodology

Further details on the methodology can be found in the draft manuscript titled *"Remediation Research and Technical Support for the Waste Isolation Pilot Plant"* authored by Johnbull Dickson, Yelena Katsenovich, Juliet Swanson included in Appendix D.

Subtask 5.2: Results and Discussion

Further details on the experimental results can be found in the draft manuscript titled *"Remediation Research and Technical Support for the Waste Isolation Pilot Plant"* authored by Johnbull Dickson, Yelena Katsenovich, Juliet Swanson included in Appendix D.

Subtask 5.2: Conclusions

FIU presented experimental results for this subtask titled *"Gluconate and Magnetite Control on Actinide Transport in WIPP High Ionic-Strength Brines"* on the ABC Salt Workshop 2023, Santa Fe, NM, June 15-16, 2023. The oral presentation by Johnbull Dickson was co-authored by Yelena Katsenovich, Leonel Lagos, Juliet Swanson and Donald Reed. In addition, a draft manuscript on the FIU Year 3 results was developed and included in Appendix D.

Subtask 5.2: References

Baston, G. M. N., J. A. Berry, K. A. Bond, M. Brownsword, and C. M. Linklater (1992), Effects of Organic Degradation Products on the Sorption of Actinides, Radiochim Acta, 58-9(2), 349-356, doi: https://doi.org/10.1524/ract.1992.5859.2.349.

Brady, P. V., H. W. Papenguth, and J. W. Kelly (1999), Metal sorption to dolomite surfaces, Appl Geochem, 14(5), 569-579, doi: Doi 10.1016/S0883-2927(98)00085-7.

Brown, G. O., D. A. Lucero, and W. G. Perkins (1999), Column Experiments for Radionuclide Adsorption Studies of the Culebra Dolomite: Retardation Parameter Estimation for Non-Eluted Actinide Species*Rep. SAND98-1005; Other: ON: DE00002672 United States 10.2172/2672 Other: ON: DE00002672 SNL English*, Sandia National Laboratories, Albuquerque, NM, and Livermore, CA.

Brush, L. H., and L. J. storz (1996), Revised Ranges and Probability Distributions of Kds for Dissolved Pu, Am, U, Th, and Np in the Culebra for the PA Calculations to Support the WIPP CCA*Rep.*, Albuquerque, New Mexico.

Colàs, E., M. Grivé, I. Rojo, and L. Duro (2011), Solubility of ThO2·xH2O(am) in the presence of gluconate, Radiochim Acta, 99(5), 269-273, doi: 10.1524/ract.2011.1837.

Colàs, E., M. Grivé, I. Rojo, and L. Duro (2013), The Effect of Gluconate and EDTA on Thorium Solubility Under Simulated Cement Porewater Conditions, Journal of Solution Chemistry, 42(8), 1680-1690, doi: 10.1007/s10953-013-0054-2.

Gaona, X., V. Montoya, E. Colas, M. Grive, and L. Duro (2008), Review of the complexation of tetravalent actinides by ISA and gluconate under alkaline to hyperalkaline conditions, J Contam Hydrol, 102(3-4), 217-227, doi: 10.1016/j.jconhyd.2008.09.017.

Lagos, L. E., Y. Katsenovich, R. Gudavalli, A. Lawrence, and M. Mahmoudi (2018), Environmental remediation science and technology - Year-end technical report*Rep.*, Applied Research Center, Florida International University, Miami, Florida.

Mayant, C., B. Grambow, A. Abdelouas, S. Ribet, and S. Leclercq (2008), Surface site density, silicic acid retention and transport properties of compacted magnetite powder, Physics and Chemistry of the Earth, Parts A/B/C, 33(14-16), 991-999, doi: 10.1016/j.pce.2008.05.011.

Reed, D. T., and M. Altmaier (2013), Proceedings of the Third International Workshop on Actinide and Brine Chemistry in a Salt-Based Repository (ABC-Salt III), Los Alamo National Laboratory, Santa Fe, New Mexico.

Sawyer, D. T. (1964), Metal-Gluconate Complexes, Chemical Reviews, 64(6), 633-643, doi: 10.1021/cr60232a003.

Stein, C. L. (1985), Mineralogy in the Waste Isolation Pilot Plant (WIPP) facility stratigraphic horizon*Rep. SAND-85-0321; Other: ON: DE86000571 United States 10.2172/5203761 Other: ON: DE86000571 NTIS, PC A03/MF A01. SNL English*, Medium: ED pp, Sandia National Labs., Albuquerque, NM (USA).

Tits, J., E. Wieland, and M. H. Bradbury (2005), The effect of isosaccharinic acid and gluconic acid on the retention of Eu(III), Am(III) and Th(IV) by calcite, Appl Geochem, 20(11), 2082-2096, doi: 10.1016/j.apgeochem.2005.07.004.

TASK 6: HYDROLOGY MODELING OF BASIN 6 OF THE NASH DRAW NEAR THE WIPP

The Waste Isolation Pilot Plant (WIPP) is the nation's only deep geologic waste repository in operation which isolates transuranic waste 2,150 feet underground within the Salado Salt Formation. This karst region formed from the dissolution of soluble rocks such as limestone, dolomite, and gypsum. Scientists and researchers are concerned about the long-term vulnerability of this karst topography and thus the eventual integrity and performance of the WIPP due to the influence of characteristic surface features, such as sinkholes, swallets, and karst valleys on groundwater recharge over time. The Rustler Formation which lies above the Salado Formation contains three fluid-bearing zones, the Rustler-Salado contact residuum, the Culebra dolomite and the Magenta dolomite, of which the Magenta and Culebra are of primary concern as they extend over the WIPP site. Just west of WIPP is the Nash Draw, which is an enclosed basin made up of thirty internally drained sub-basins identified from topography and field surveys. Nash Draw developed through solution and erosion of upper Permian rocks creating an array of surface features, including sinkholes, swallets, and karst valleys, and thus serves as an ideal area for this study with similar topography and representative surface hydrological features as that which overlies the WIPP.

This task therefore involves the development of a high-resolution digital elevation model (DEM) of Basin 6 of the Nash Draw to more accurately delineate surface hydrological features, as well as the development of hydrological models using the DOE-developed Advanced Simulation Capability for Environmental Remediation (ASCEM) modeling toolset to improve the current understanding of the regional water balance, particularly the relation between the Culebra recharge and the intense, episodic precipitation events typical of the North American monsoon. This relationship is essential for understanding the rate of propagation of the shallow dissolution front, and the impact of land-use changes around the WIPP facility and Nash Draw on water levels and chemistry in compliance-monitoring wells.

Subtask 6.2: Model Development

Subtask 6.2: Introduction

The proposed work to develop a groundwater model (GWM) for Basin 6 of the Nash Draw near the WIPP. After evaluating various open-source surface hydrological models (among others: Community Land Model (CLM), WRF-Hydro) it was decided to make use of the Advanced Terrestrial Simulator (ATS) to simulate the near-surface hydrological response (i.e. infiltration and evapotranspiration) and how this impacts groundwater recharge.

ATS is an ecosystem-based, integrated, distributed hydrology simulator that is built on the underlying multi-physics framework provided by Amanzi, the high-performance computing simulator developed in the ASCEM program used for environmental applications to provide flexible and extensible flow and reactive transport simulation capability. The output of the ATS model includes predictions of infiltration rates over selected regions of interest, such as sinkholes, and groundwater recharge, and hence ensembles of ATS simulations facilitate sensitivity and uncertainty analysis of groundwater and surface water flows.

The first phase of this task is to develop a detailed understanding of the ATS-Amanzi model as well as identification of available relevant hydrological data (as obtained from Subtask 6.1), followed by the development of a coupled ATS-Amanzi model to enable simulation of regional scale groundwater recharge and assess the role of small-scale hydrological features (e.g. sink holes, brine lakes and gullies).

Subtask 6.2: Objectives

The objective of the proposed task is to develop a groundwater model for Basin 6 of the Nash Draw near the WIPP site using the ASCEM toolset coupled with the Advanced Terrestrial Simulator (ATS) to account for the surface and near-surface processes. These models will be used to compute the water balance across multiple scales and to reduce uncertainties in recharge estimates and propagation of the shallow dissolution front.

Subtask 6.2: Methodology

During FIU Year 3, FIU expanded on the development of an ATS model of the Basin 6 study domain using the data derived from Subtask 6.1. Hydrological, climate and topography datasets were collected from various national database platforms and incorporated in the model mesh using the Python library Watershed Workflow. Watershed Workflow was developed by Oak Ridge National Lab (ORNL) and allows for geometrical and geophysical information about the site to be encoded into the ATS input file. Newly added to the model in FIU Year 3 was spatial variations in NLCD land cover types, SURRGO soil texture, and GLHYMPS subsurface information), as well as daily atmospheric forcing (precipitation, temperature, radiation) obtained from DayMet. In FIU year 2, the modeling workflow was established during a student summer internship at Los Alamos Laboratory. In FIU Year 3, this workflow was expanded on with the incorporation of a spinup model to be used for the development of a multi-year ATS simulation for Basin 6. A spinup model is used to establish an equilibrium state so that key hydrological variables, such as soil moisture, groundwater levels, and streamflow, reach a consistent and self-sustaining state.

Subtask 6.2: Results and Discussion

After completing the development of the spinup model, FIU initiated the development of multi-year simulations of the hydrological response within Basin 6 due to meteorological events. The dates chosen for this model were January 1st, 2013, to December 31st, 2015. These three years (2013, 2014, and 2015) were chosen because it contained both a sustained drought and an intense flooding event. This allows us to investigate how extreme events can impact the Nash Draw. The multi-year model developed in FIU Year 3 includes meteorological forcings and evapotranspiration. With the multi-year model, the hydrological response of the basin due to precipitation can be assessed. Also incorporated in the model is the Leaf-Area-Index (LAI) for the major land cover types within the region. The LAI is time series-based and directly impacts the evapotranspiration of the model and therefore the entire water balance. The addition of the LAI allows for more accurate evapotranspiration predictions and hydrology modeling.

The graph below shows the actual precipitation (P) and snowfall (S) on each day for three years to force the model. Furthermore, the ATS simulated outputs such as evapotranspiration (ET) and runoff (Q) are also shown. The biggest precipitation events occurred around day 200 and day 630, corresponding to July 19th, 2013, and September 22nd, 2014. As discussed above, overflow was recorded in Basin 6 in September of 2014. ATS also simulates surface runoff around this period.

The amount of runoff ATS calculated peaked around 0.014 m/d, corresponding to about 3.88 m3/s. The excessive amount of rainfall observed during this period also increased the simulated actual evapotranspiration flux of almost 5 mm/d.

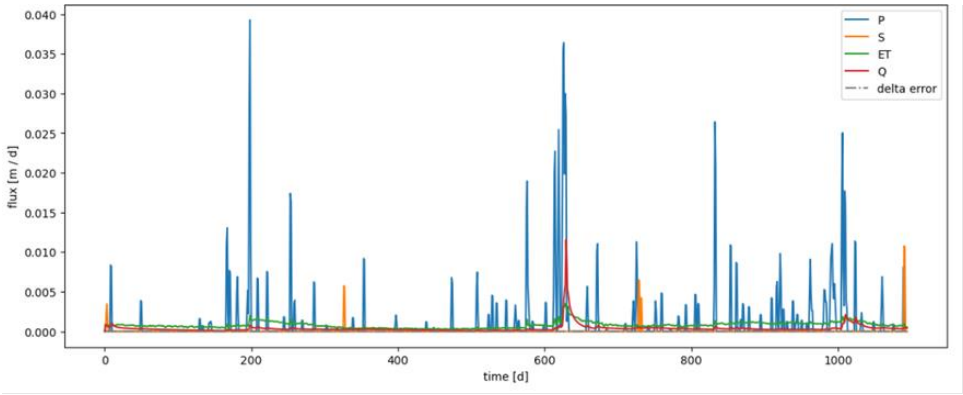

Figure 58. Graph of the water balance from the Basin 6 multi-year model with the flux (m/d) of rain, snow, evapotranspiration, runoff, and the error plotted versus time (d).

The model also simulates the occurrence of a number of significant snowfall events (S). These snowfall events typically occur in January. When significant, these snowfall events can impact groundwater recharge, in the case sufficient runoff is produced after melt, but the actual extent is currently unknown.

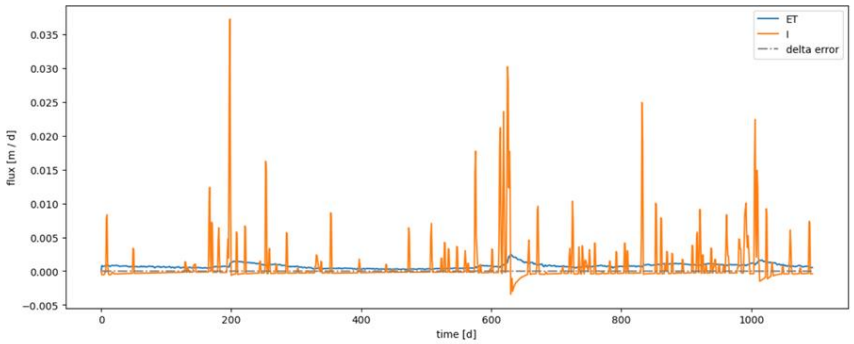

Figure 59. Plot of the flux (m/d) for infiltration (I) and evapotranspiration (ET) versus time (d).

The figure above shows the simulated infiltration into the subsurface. After the heavy rainfall events around days 200 and 630, the infiltration becomes negative. During these heavy rainfall events, the soil may become saturated quickly, leading to the excess water running downslope in the form of overland flow instead of infiltrating into the soil column. During the snowfall events, like on day zero, there is a large amount of infiltration, which may be attributed to the snow melt.

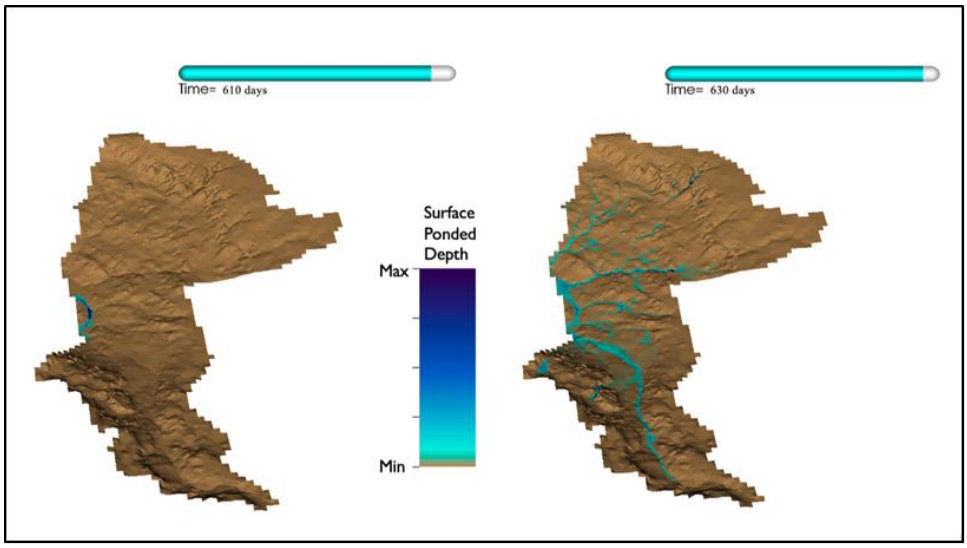

Figure 60. Image from a video simulation of the Basin 6 multi-year model on 610th day (left) and the 630th day (right) (September 2nd, 2014, and September 22nd, 2014) in which the surface ponded water depths are shown with a color table.

The overflow from this precipitation event between the 610th day and the 630th day (September 2nd, 2014, and September 22nd, 2014) is visualized with VisIt in the figure above. The surface layer was given a customized color scheme that shows the ponded depth of water along the surface after precipitation. The brown represents no ponded water at the surface, while the darker blue colors indicate ponding. The surface layer elevation was also scaled upward in the z-direction, to show the elevation changes in Basin 6 and the presence of the river network. These figures show that after a heavy precipitation event, the overland flow migrates downslope towards the main river network. It is anticipated that within the riparian reaches, the majority of groundwater recharge occurs (as water converges). Furthermore, within these locations the majority of sinkholes are observed. The amount of recharge within these domains will be focused on in future contributions.

Subtask 6.2: Conclusions

During FIU Year 3, the model presented has improved significantly since the first preliminary integrated surface/subsurface model of Basin 6 that was developed in FIU Year 2. An updated model mesh has been generated using the Python library, Watershed Workflow. Watershed Workflow has allowed for model advancements relating to soil textures, meteorological forcings, and subsurface information. The updated model version developed in FIU Year 3 also makes use of a much higher model resolution. The current model also contains an advanced process kernel tree, which allows for the calculation of evapotranspiration, which was not present before. The model developed in FIU Year 3 is more stable, by including a spinup model in the methodology before running multi-year transient simulations.

Training of DOE Fellows and FIU staff on the ATS model was provided by LANL scientists. The next step will be to follow the established workflow for development of an integrated surface/subsurface model of Basin 6, explicitly representing surface features such as sinkholes, swallets and brine lakes, which are anticipated to increase infiltration and can potentially impact the regional groundwater recharge. In FIU Year 3, FIU researchers collected soil samples and

installed pressure transducers in May of 2023 as part of task 6.3. The data collected from this fieldwork is currently being evaluated and will be used to calibrate and validate the ATS model for Basin 6. These analyses will be focused on in Year 4 of the DOE-FIU Cooperative Agreement. Once finalized, the model will be used to evaluate the long-term impact of changes in climate on the regional hydrology surrounding the WIPP domain, so DOE-EM scientists can better predict the rate of halite dissolution and propagation of the shallow dissolution front in order to quantify the potential impact on the WIPP repository performance.

Subtask 6.2: References

Amanzi. (2023). GitHub. Retrieved from https://amanzi.github.io/ats/index.html

Beauheim, R. L. (2009). Collection and integration of geoscience information to revise the WIPP hydrology conceptual model. In *Approaches and challenges for the use of geological information in the safety case for deep disposal of radioactive waste*.

Chaturvedi, L. (1993). WIPP-related geological issues. In Carlsbad Region, New Mexico and West Texas, New Mexico Geological Society Forty-fourth Annual Field Conference, Carlsbad, NM (pp. 331-338).

Coon, E. T., Moulton, J. D., & Painter, S. L. (2016). Managing complexity in simulations of land surface and near-surface processes. Environmental modelling & software, 78, 134-149.

Coon, Ethan T., and Pin Shuai. "Watershed Workflow: A toolset for parameterizing data-intensive, integrated hydrologic models." Environmental Modelling & Software 157 (2022): 105502.: https://doi.org/10.1016/j.envsoft.2022.105502

Corbet, T. F., & Knupp, P. M. (1996). *The role of regional groundwater flow in the hydrogeology of the Culebra Member of the Rustler Formation at the Waste Isolation Pilot Plant (WIPP), southeastern New Mexico* (No. SAND-96-2133). Sandia National Lab, Albuquerque, NM (United States).

Freedman, V. L., Agarwal, D., Bensema, K., Finsterle, S., Gable, C. W., Keating, E. H., Krishnan, H.. Lansing, C., Moeglein, W., Pau, G. S. H., Porter, E., Scheibe, T. D. *Akuna: An Open Source User Environment for Managing Subsurface Simulation Workflows.* American Geophysical Union, Fall Meeting 2014.

Goodbar, A. K., Powers, D. W., Goodbar, J. R., & Holt, R. M. (2020). Karst and sinkholes at Nash Draw, southeastern New Mexico (USA).

Hart, D. B., McKenna, S. A., & Beauheim, R. L. (2009). *Calibration of the WIPP culebra transmissivity fields* (No. SAND2009-7334C). Sandia National Lab.(SNL-NM), Albuquerque, NM (United States); Sandia National Laboratories,, Carlsbad, NM.

Hayes, A. (2019). *Culebra Hydrologic Model in WIPP Performance Assessment* (No. SAND2019-4432PE). Sandia National Lab.(SNL-NM), Albuquerque, NM (United States).

Kollet, S., Sulis, M., Maxwell, R. M., Paniconi, C., Putti, M., Bertoldi, G., ... & Sudicky, E. (2017). The integrated hydrologic model intercomparison project, IH-MIP2: A second set of benchmark results to diagnose integrated hydrology and feedbacks. Water Resources Research, 53(1), 867-890.

Livingston, D. (2020). TINerator API Reference. Los Alamos National Laboratory

Sampson, K., & Gochis, D. (2018). *WRF Hydro GIS Pre-Processing Tools, Version 5.0 Documentation.* Boulder, CO: National Center for Atmospheric Research, Research Applications Laboratory.

Wehbe, Y., Temimi, M., Weston, M., Chaouch, N., Branch, O., Schwitalla, T., Wulfmeyer, V., Zhan, X., Liu, J. and Al Mandous, A. (2019). *Analysis of an extreme weather event in a hyper-arid region using WRF-Hydro coupling, station, and satellite data.* Natural Hazards & Earth System Sciences, 19(6).

Yucel, I., Onen, A., Yilmaz, K. K., & Gochis, D. J. (2015). *Calibration and evaluation of a flood forecasting system: Utility of numerical weather prediction model, data assimilation and satellite-based rainfall.* Journal of Hydrology, 523, 49-66.

Zeitler, T. R. (2016). *WIPP Performance Assessment* (No. SAND2016-8142PE). Sandia National Lab.(SNL-NM), Albuquerque, NM (United States).

Subtask 6.3: Fieldwork and Data Collection to Support Hydrological Model Calibration and Validation (NEW)

Subtask 6.3: Introduction

No in situ observations of soil texture, organic content and soil physical properties are currently available for Basin 6. Also, no in situ observation of surface flow nor information on locations where surface flow occurs is available. However, this information has an important impact on the flow of water throughout the subsurface. Instead, information derived from soil pits nearby or from large scale soil texture datasets are available, but it is currently unknown how representative these datasets are for Basin 6. This newly developed subtask deals with obtaining soil samples from various depths and locations within Basin 6 and evaluating these data within the lab. This ensures that site specific hydrological parameter values for the unsaturated zone are developed. Furthermore, site specific observations of locations where surface flow occurs as well as the magnitude are needed to evaluate the performance of the ATS model developed in Subtask 6.2.

Subtask 6.3: Objectives

The objective of this subtask it to obtain detailed soil texture information for various locations and at various depths within Basin 6 of the Nash Draw. This information can subsequently be used to estimate the various hydrological flow parameters within the unsaturated zone as used by ATS. Furthermore, these texture observations will be used to evaluate the quality of large-scale publicly available soil texture datasets (i.e., STATSGO2, SSURGO and SoilGrids). Also, depending on available resources, FIU proposes to make some initial efforts to obtain information on the location of surface flow as well as its magnitude that can help to assess the performance of the ATS model developed in Subtask 6.2.

Subtask 6.3: Methodology

In April of FIU Year 3, FIU began reviewing the soil sampling procedures and drafting a work plan in preparation for the fieldwork planned in Basin 6 during the summer. A meeting was held on May 15, 2023 with the DOE collaborator from the Carlsbad Field Office, Dr. Anderson Ward, to discuss FIU's itinerary and work plan. FIU prepared a detailed field and laboratory workplan and Vendors were identified for the soil sampling equipment and water level data loggers that will be required as shown below.

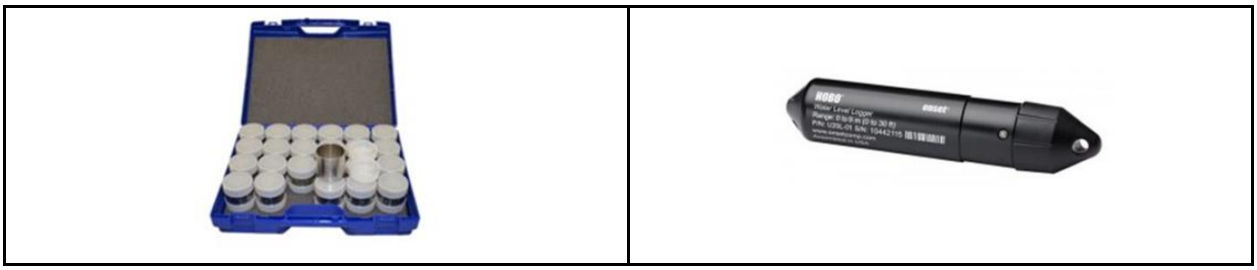

Figure 61. Eijkelkamp soil sampling rings (left) and HOBO water level data logger (right).

Key locations were also identified for collection of the soil samples and deployment of the piezometers for recording water level data. Using ArcGIS tools in ArcMap, a ~1 km line transect

was plotted which intersects three verified karst features (sinkholes and swallets). Several soil sampling locations were then plotted along this transect. GIS shapefiles of the transect line, soil sampling and piezometer locations were created, and the geographic coordinates recorded.

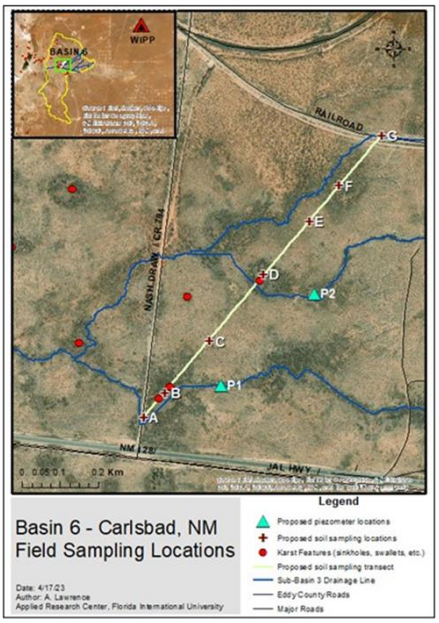

Figure 62. GIS map of proposed field sampling locations in Basin 6.

The HOBO U20L water level data loggers (piezometers) that will be deployed in Basin 6 were also tested to ensure they were operational and providing accurate readings. The battery life and data storage were determined as this is important as it defines how long the HOBO units can be left in the field to collect data. If the time interval is five minutes, then the units can be left in the field for 75 days (about 2 and a half months) before they run out of data storage. The battery life is five years, which is good for this fieldwork campaign.

Subtask 6.3: Results and Discussion

From May 29 – June 1, 2023, an FIU team, comprised of a senior research scientist and a DOE Fellow, traveled to New Mexico to perform fieldwork in Basin 6 of the Nash Draw just west of the WIPP which included:

- Deployment of 5 HOBO U20L water level loggers (pressure transducers) within the Basin 6 study area:
  - Location #1 → Sinkhole within sinkhole cluster.
  - Location #2 → Largest sinkhole within the Location #1 cluster.
  - Location #3 → A site of ponding water at the end of an upstream flow path.
  - Location #4 → The upstream flow path of Location #3.
  - Location #5 → Site near Location #2 placed above surface to monitor atm. pressure.
- Collection of 48 soil samples at various strategic locations within the Basin 6 study area:
  - Samples were collected at depths from surface to 120 inches below the surface.

Fieldwork support was provided by Dr. Anderson Ward from the DOE Carlsbad Field Office as well as Dennis Powers, a Consulting Geologist and subject matter specialist on the Nash Draw hydrogeology.

In Figure 63an image of the setup for the first pressure transducer at Location #1 is seen. The pressure transducer is within the PVC pipe being held by a non-stretch wire. This location is a sinkhole within a cluster of sinkholes, measuring approximately 14 feet from the surface. At Location #1, soil samples were taken at depths ranging from the surface to 14 feet. A variety of colors and textures were observed within these samples.

Figure 63. Pressure transducer Location #1.

In Figure 64an image of the setup for the second pressure transducer (Location#2) is seen. This location is the largest sinkhole within a cluster of sinkholes, measuring over 20 feet from the surface. Near this sinkhole is the location of the fifth pressure transducer, which monitors the atmospheric pressure. This unit will be used to determine water level changes recorded by the loggers deployed at all the other locations.

Figure 64. Pressure transducer at Location #2.

In Figure 65 an image of the soil variation near the sinkhole in Location #1 is seen. The soil samples at this location were taken along the sinkhole wall and showed variation in color, from red to white, which seemed to correlate with the amount of gravel present. Soil samples were collected

at other locations in a similar manner, along the sinkhole walls where the various soil horizons could be clearly seen and easily accessible for sampling.

Figure 65. Soil variation near Location #1.

An Excel spreadsheet was created for the soil samples that contained the box number (#1 or #2), sample number (#1-#24), location coordinates of the sample, the depth of the sample below the surface, and any comments or descriptions about the sample and its location. An Excel sheet was also created for the pressure transducers that contained the location number (#1-5) of the transducer, location coordinates, transducer serial number, dimensions of the sinkhole or feature of interest within which the transducers were placed, and the description. The soil sample and transducer locations were predetermined prior to going in the field and plotted along a transect line using ArcGIS, however many of these locations had to be altered as they were found to be in accessible due to heavy brush, sinkholes, and presence of wild animals.

In August of FIU Year 3, FIU completed more fieldwork in August. Senior Research Scientist, Dr. Pieter Hazenberg, visited Basin 6 to collect data from the six pressure transducers placed in the field during the May-June fieldwork excursion. These pressure transducers contain data on the water level for two sinkhole locations and a stream that leads into a depression for June, July, and the beginning of August (one transducer in the stream and another in the depression). The beginning steps were taken to analyze the data obtained from the pressure transducers, as the data was downloaded from the units and uploaded to the HOBO unit software that came with the transducers. The transducers will continue to collect data in Basin 6 into FIU Year 4. The following figure shows the results from the summer of the pressure transducers. The graph displays the date and temperature variations for each location.

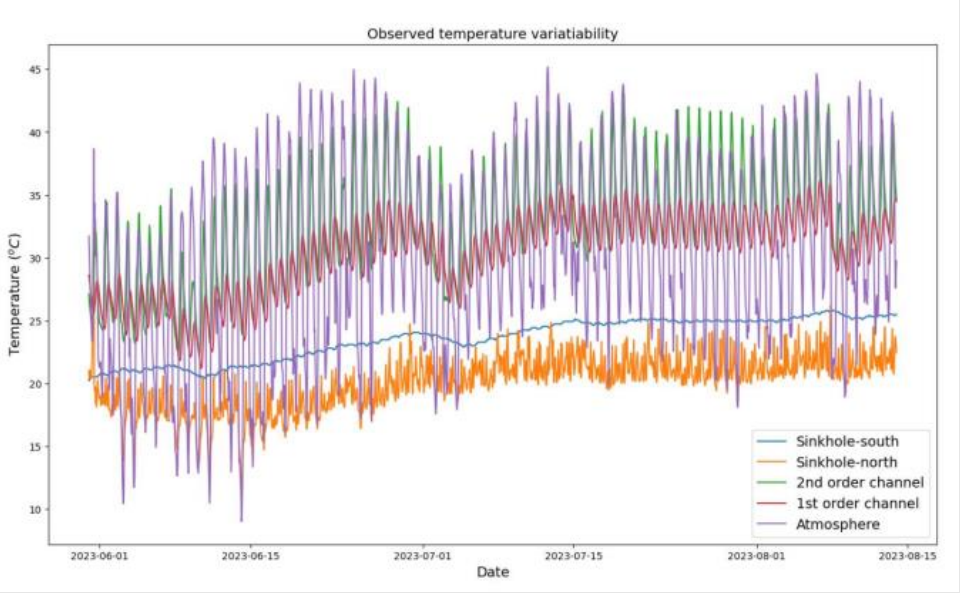

Figure 66. Temperature variation at each pressure transducer location for the months of June through August 2023 collected in FIU Year 3.

In addition, preliminary steps were taken to analyze the soil samples within in the FIU-ARC Soil & Groundwater laboratories. DOE Fellow, Aubrey Litzinger, who will be conducting the soil analysis work, worked on completing the training required to perform soil analysis experiments in the laboratories. The standard practices for soil analysis were also reviewed and the equipment needed for the analysis was also noted.

Subtask 6.3: Conclusions

In FIU Year 3, FIU researchers collected soil samples and installed pressure transducers in May of 2023 as part of task 6.3. The data collected from this fieldwork is currently being evaluated and will be used to calibrate and validate the ATS model for Basin 6. Deliverable 2022-P2-D4, identify soil parameters from in situ observations and lab analysis, and a draft report on soil parameter variability for Basin 6 will be completed in the first quarter of Year 4. Completion of this milestone was delayed due to an unexpected reduction in personnel. A total of 48 soil samples were obtained from Basin 6 and various lab analyses will be performed to obtain the soil parameters of interest.

Subtask 6.3: References

Goodbar, A., Powers, D., Goodbar, J. and R. Holt (2020). Karst and sinkholes at Nash Draw, southeastern New Mexico (USA). DOI: 10.5038/9781733375313.1026.

TASK 7: ENGINEERED MULTI-LAYER AMENDMENT TECHNOLOGY FOR MERCURY REMEDIATION ON THE OAK RIDGE RESERVATION

Task 7: Introduction

This research advances the development of sorbent-based technology in support of but not duplicative of ORNL and DOE-EM mercury remediation efforts on the Oak Ridge Reservation. Specifically, this task comprises of exhaustive evaluations of an in-situ multi-layer amendment technology for mercury remediation within the East Fork Poplar Creek (EFPC), a highly contaminated stream in Oak Ridge, Tennessee.

From 1950 to 1963 approximately 128,000 ± 35,000 kg of mercury (Hg) from the headwaters in the Y-12 National Security Complex (NSC) was released to East Fork Poplar Creek, resulting in contamination of floodplain soils, surface water and streambed sediment. Despite remedial actions in the early 1980s that significantly reduced Hg inputs to EFPC, it is still classified as an impaired waterbody due to elevated concentrations of Hg in soil, water, and biota.

Furthermore, the significant repository of mercury (~57 tons) in the HRD (fine-grained, dark-colored layer enriched in recalcitrant form of mercury) poses environmental concerns and warrants targeted remedial actions for reduction of mercury levels in EFPC.

While sorbent amendments are effective at sequestering mercury, they are less effective at reducing methylmercury and mercury bioavailability for methylation. Moreover, fouling problems of sorbents can lead to potential leaching of constituents and particles into waterbodies, thereby severely limiting their applications for Hg sequestration. Mercury fate and transport in EFPC are controlled by its strong interaction with dissolved organic matter (DOM) which renders Hg^{2+} binding to sorbents and removal from water column problematic and less effective. It has been shown that DOM can outcompete mercury for sorption sites on amendment materials such as activated carbon (AC) and biochar, decreasing the overall effectiveness of these materials for mercury. The reduction in overall effectiveness is attributed to AC-DOM interaction rather than the direct interaction between AC and Hg. Despite ubiquitous use of amendments for in-situ sequestration of organic contaminants, large-scale application of sorbents for mercury remediation is uncommon. Furthermore, widespread use of mercury sorbents may be cost-prohibitive and less effective in the presence of DOM.

Task 7: Objectives

While many sorbents have been shown to sorb heavy metal contaminants, the specific goal of this study is to evaluate the effectiveness of a suite of low-cost, sustainable sorbents for removal of mercury in the presence of DOM. Thus, this research evaluates the effectiveness of an engineered treatment technology consisting of multi-layer reactive sorbents/amendments (MRA) contained between two to several geotextile layers (mats) for enhanced removal of mercury and methylmercury from the EFPC ecosystem (soil, ground/surface water and biota). Proposed experiments will aid in evaluating the performance characteristics of the MRA technology for design considerations and site-specific deployment. Furthermore, this work will foster close collaboration between Florida International University and the Oak Ridge National Laboratory scientists.

This technology will aid DOE EM in meeting its priority mission of reducing mercury concentration to below regulatory targets within EFPC and mitigating contaminant export from demolition of contaminated buildings in the East Tennessee Technology Park (ETTP).

Task 7: Methodology

Further details on the methodology can be found in the draft manuscript titled *"Engineered Media for Mercury Removal in the Presence of Dissolved Organic Matter"* authored by Johnbull Dickson, Caridad Estrada, Yelena Katsenovich, Leonel Lagos, Alexander Johs, Eric Pierce included in Appendix D.

Task 7: Results and Discussion

Further details on the experimental results can be found in the draft manuscript titled *"Engineered Media for Mercury Removal in the Presence of Dissolved Organic Matter"* authored by Johnbull Dickson, Caridad Estrada, Yelena Katsenovich, Leonel Lagos, Alexander Johs, Eric Pierce included in Appendix D.

Task 7: Conclusion

FIU presented experimental results for this subtask during the DOE-FIU Cooperative Agreement Annual Research Review in August 2023. In addition, a draft manuscript on engineered media for mercury removal was developed *titled "Engineered Media for Mercury Removal in the Presence of Dissolved Organic Matter".* This paper was authored by Johnbull Dickson, Caridad Estrada, Yelena Katsenovich, Leonel Lagos, Alexander Johs, Eric Pierce included in Appendix D.

The achievements of Subtask 7 also include a poster presented by DOE Fellow, Caridad Estrada, at the 2022 DOE Fellows Poster Exhibition (Figure 67) and Waste Management 2023 Symposia during the student poster session (Figure 68).

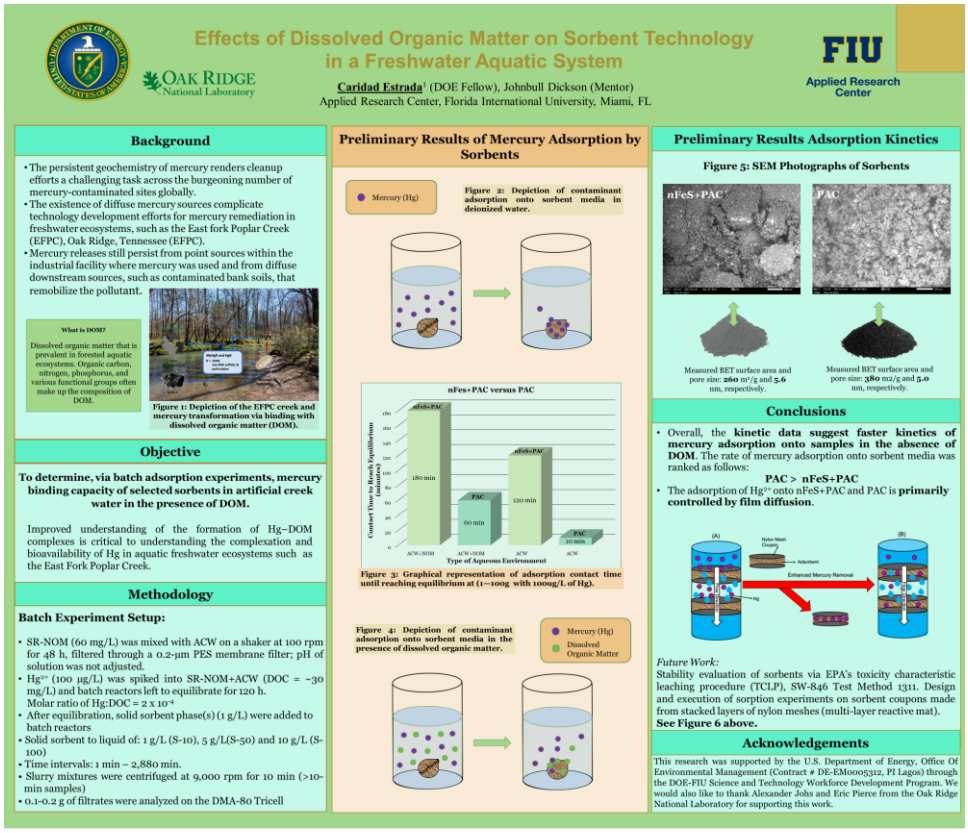

Figure 67. Poster presented by DOE Fellow, Caridad Estrada, at the 2022 DOE Fellows Poster Exhibition.

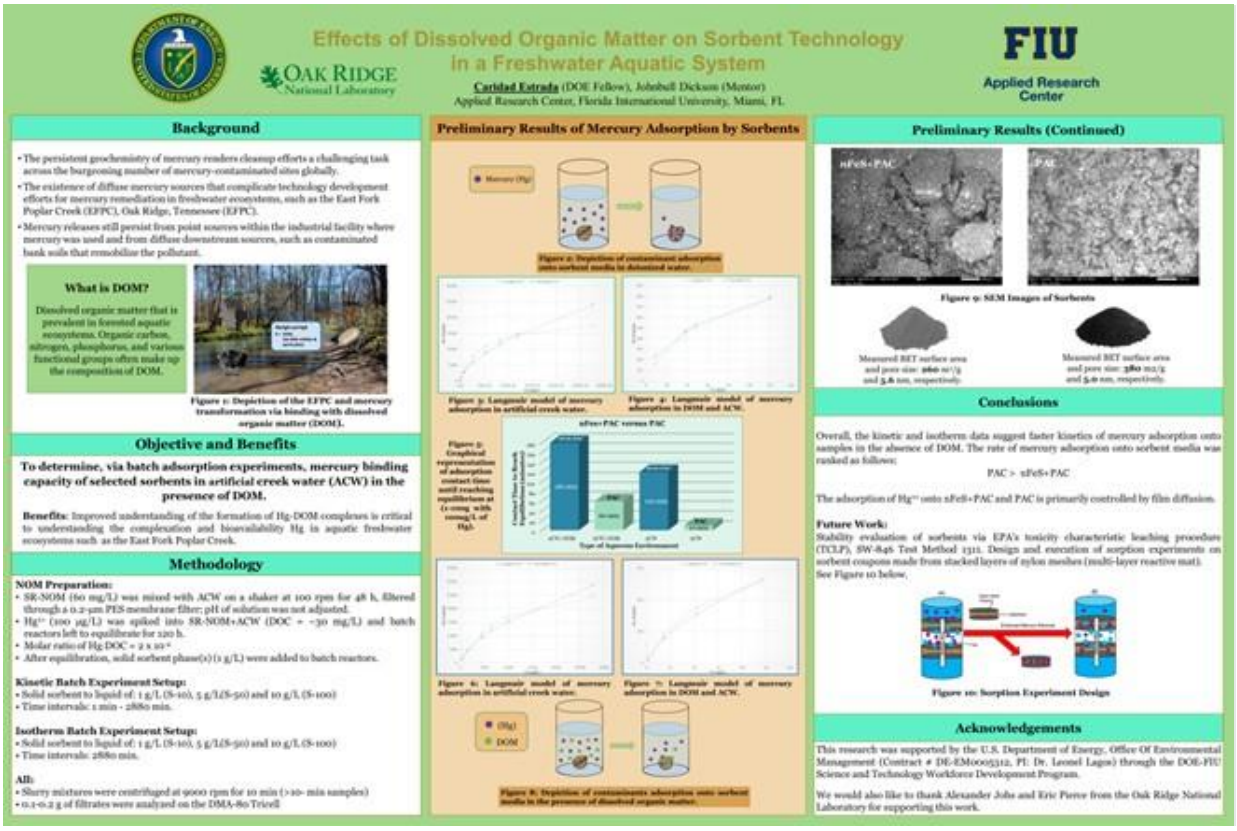

Figure 68. DOE Fellow Caridad Estrada's poster presented at the upcoming Waste Management 2023 Symposia during the student poster session.

Task 7: References

Futsaeter, G., and S. Wilson (2013), The UNEP Global Mercury Assessment: Sources, Emissions and Transport, E3S Web of Conferences, 1, 36001, doi: 10.1051/e3sconf/20130136001.

Kocman, D., M. Horvat, N. Pirrone, and S. Cinnirella (2013), Contribution of contaminated sites to the global mercury budget, Environmental Research, 125, 160-170, doi: https://doi.org/10.1016/j.envres.2012.12.011.

Southworth, G. R., M. S. Greeley Jr, M. J. Peterson, K. A. Lowe, R. H. Ketelle, and S. B. Floyd (2010), Sources of Mercury to East Fork Poplar Creek Downstream from the Y-12 National Security Complex: Inventories and Export Rates*Rep. ORNL/TM-2009/231*, Medium: ED pp, Oak Ridge National Lab. (ORNL), Oak Ridge, TN (United States); Oak Ridge Electron Linear Accelerator.

CONFERENCE PARTICIPATION, PUBLICATIONS, AWARDS & ACADEMIC MILESTONES

Peer-reviewed Publications

Katsenovich, Y., Maria, A., Williams, J., Kandel, S., Boglaienko, D., P. Emerson, H., and T.G. Levitskaia. Reductive Removal of Pertechnetate and Chromate by Zero Valent Iron under Variable Ionic Strength Conditions. *Journal of Hazardous Materials*, v. 445, March 2023, p.130546.

Kaplan, D. I., R. J. Smith, C. J. Parker, K. A. Roberts, P. Hazenberg, J. Morales, E. J. O'Loughlin, M. I. Boyanov, P. Weisenhorn, K. M. Kemner, and B. A. Powell, 2023: Natural attenuation of uranium in a fluvial Wetland: Importance of hydrology and speciation, Applied Geochemistry, 155, 105718, doi: 10.1016/j.apgeochem.2023.105718.

Mariah S. Doughman, Kevin E. O'Shea, Nikolla P. Qafoku, Hilary P. Emerson, James E. Szecsody, Kenneth C. Carroll, Yelena P. Katsenovich, 2023. Impact of chromium (VI) as a co-contaminant on the sorption and co-precipitation of uranium (VI) in sediments under mildly alkaline oxic conditions (accepted in the *Journal of Environmental Management*)

Yelena Katsenovich, Angel Almaguer, Nikolla Qafoku, Jim Szecsody, Hilary Emerson, and Leonel Lagos, *"Re-oxidation Behavior of Technetium-99 and Uranium Immobilized by Strong Reductants"*. Proceedings of the Waste Management Symposia 2023, February 26- March 2, 2023, Phoenix, AZ

Phuong Pham, Hansell Gonzalez-Raymat, Ravi Gudavalli and Leonel Lagos, *"Remediation of Iodine-129 at Savannah River Site's Wetland by Organoclays Amendment (23270)"*. Proceedings of the Waste Management Symposia 2023, February 26- March 2, 2023, Phoenix, AZ

Johnbull Dickson, Yelena Katsenovich, Juliet Swanson and Donald Reed, *"The Impact of Gluconate and Magnetite on Actinide Mobility in High Ionic-Strength Matrices of the WIPP"* – Proceedings of the Waste Management Symposia 2023, February 26- March 2, 2023, Phoenix, AZ.

Conference Presentations

Oral Presentations (presenter is underlined)

Yelena Katsenovich, Angel Almaguer, Nikolla Qafoku, Jim Szecsody, Hilary Emerson, and Leonel Lagos, *"Re-oxidation Behavior of Technetium-99 and Uranium Immobilized by Strong Reductants"*. Waste Management Symposia 2023, February 26- March 2, 2023, Phoenix, AZ

Phuong Pham, Hansell Gonzalez-Raymat, Ravi Gudavalli and Leonel Lagos, *"Remediation of Iodine-129 at Savannah River Site's Wetland by Organoclays Amendment (23270)"* –.Waste Management Symposia 2023, February 26- March 2, 2023, Phoenix, AZ

Johnbull Dickson, Yelena Katsenovich, Leonel Lagos, Juliet Swanson and Donald Reed *"Gluconate and Magnetite Control on Actinide Transport in WIPP High Ionic-Strength Brines"* (Oral Presentation). ABC Salt Workshop 2023, Santa Fe, NM, June 15-16, 2023.

Poster Presentations (presenter is underlined)

Mariah Doughman, Yelena Katsenovich, Leonel Lagos, Kevin O'Shea, Hilary Emerson, James Szecsody, Nikolla Qafoku. Impact of Chromium (VI) as a Co-mingled Contaminant on the Attenuation Mechanisms of Uranium (VI) in Hanford Formation Sediment. Waste Management 2023, Phoenix, AZ, March 2023.

Johnbull Dickson, Yelena Katsenovich, Juliet S. Swanson, Donald T. Reed. The Impact of Gluconate and Magnetite on Actinide Mobility in High Ionic-Strength Matrices of the WIPP Waste Management 2023, Phoenix, AZ, March 2023.

Aubrey Litzinger (DOE Fellow), David Moulton, Pieter Hazenberg, Angelique Lawrence, Ravi Gudavalli, and Leonel Lagos, *"Development of an Integrated Hydrological Model for Basin 6 near the Waste Isolation Pilot Plant (WIPP) Using the Advanced Terrestrial Simulator (ATS)"* (WMS2023 Poster)

Caridad Estrada (DOE Fellow), Johnbull Dickson "Effect of Dissolved Organic Matter on Sorbent Technology in a Freshwater Aquatic System" (Poster Presentation), WM2023 Conference February 26-March 2, 2023, Phoenix, Arizona, USA.

Phuong Pham (DOE Fellow) "Characterization of Savannah River Site's Wetland Soils at Different Depth Intervals" (*Posters: Roy G. Post Scholarship 2023 Winners*), WM2023 Conference February 26-March 2, 2023, Phoenix, Arizona, USA.

DOE Fellows prepared and presented posters at DOE Fellows poster exhibition and competition:

- Constructing an Integrated Hydrology Model for Basin 6 of the Nash Draw near the Waste Isolation Pilot Plant (WIPP) - **Aubrey Litzinger**
- Effects of Dissolved Organic Matter on Sorbent Technology in a Freshwater Aquatic System - **Caridad Estrada**
- Impact of Chromium (VI) as a Co-mingled Contaminant on the Attenuation Mechanisms of Uranium (VI) in Hanford Formation Sediment - **Mariah Doughman**
- Insights into the Sorption and Release Mechanisms of I-129 Occurring at SRS Wetlands - **Phuong Pham**
- Understanding Groundwater-Surface Water Interchange in the F-Area Wetlands of Fourmile Branch Watershed - **Stevens Charles**

Awards

DOE Fellow, Aubrey Litzinger, who supports the research on Tasks 3 and 6 was voted "DOE Fellow of the Year". In addition, Dr. Ravi Gudavalli, who leads Project 2 Task 2 as well as Projects 4 & 5, received the "Mentor of the Year" award.

Figure 69. DOE Fellow, Aubrey Litzinger, being awarded "DOE Fellow of the Year" during the Annual DOE Fellows Induction Ceremony held in November 2022 at FIU's Modesto Maidique Campus.

Figure 70. Dr. Ravi Gudavalli being awarded "Mentor of the Year" during the Annual DOE Fellows Induction Ceremony held in November 2022 at FIU's Modesto Maidique Campus.

Academic Milestones

DOE Fellow Phuong Pham successfully passed her Ph.D. defense. Her dissertation is titled *"Removal of Heavy Metals and Radionuclides from the Environment using Environmentally Friendly Sorbents"*. Upon graduation at the end of the spring 2023 semester, Phuong joined Savannah River National Laboratory as a Postdoctoral Associate.

DOE Fellow Stevens Charles graduated with bachelor's degree in environmental engineering and participated in the Fall 2022 graduation ceremony at FIU's Modesto Maidique Campus (MMC). Stevens was admitted to graduate school to earn a Master of Science degree in Environmental Engineering at the University of Georgia (UGA).

DOE Fellow Mariah Doughman was awarded the MSIPP program's one-year fellowship at PNNL. She is planning to graduate from FIU with a PhD in Chemistry in 2024.

ACKNOWLEDGEMENTS

Funding for this research was provided by U.S. DOE Cooperative Agreement #DE-EM0005213. FIU's Applied Research Center would like to acknowledge the commitment of DOE-EM to this specific Environmental Remediation Science and Technology project and to all the collaborators at DOE-EM HQ and the National Labs for support of the research being conducted as part of the Cooperative Agreement. The partnership between DOE EM and FIU has also resulted in the development and training of outstanding minority STEM students that will benefit this country as a whole.

APPENDIX A

The following documents are available at the DOE Research website for the Cooperative Agreement between the U.S. Department of Energy Office of Environmental Management and the Applied Research Center at Florida International University:
https://doeresearch.fiu.edu/SitePages/Welcome.aspx

FIU Year 3 Annual Research Review Presentations:

1. FIU Research Review - Project 1
2. FIU Research Review - Project 2
3. FIU Research Review - Project 3 - D&D IT ML
4. FIU Research Review - Project 4 & 5
5. FIU Research Review - Project 4 - DOE Fellow Aris Duani Rojas
6. FIU Research Review - Project 4 - DOE Fellow Aubrey Litzinger
7. FIU Research Review - Project 4 - DOE Fellow Brendon Cintas
8. FIU Research Review - Project 4 - DOE Fellow Bryan Torres
9. FIU Research Review - Project 4 - DOE Fellow Carolina Trummer
10. FIU Research Review - Project 4 - DOE Fellow Joel Adams
11. FIU Research Review - Project 4 - DOE Fellow Josue Estrada
12. FIU Research Review - Project 5 - DOE Fellow Shawn Cameron
13. FIU Research Review - Wrap Up - Project 1
14. FIU Research Review - Wrap Up - Project 2
15. FIU Research Review - Wrap Up - Project 3 – D&D IT ML
16. FIU Research Review - Wrap Up - Project 4
17. FIU Research Review - Wrap Up - Project 5

APPENDIX B

A peer-reviewed journal manuscript has been drafted by DOE Fellow Mariah Doughman. The manuscript is titled *"Comparison of batch versus column methods for analysis of the impact of chromium (VI) as a co-contaminant on the sorption of uranium (VI) in sediments under mildly alkaline oxic conditions"*. Once published, this manuscript will be made available to DOE via OSTI pending any copyright restriction.

APPENDIX C

Draft manuscript titled *"Tracking the effect of Ca on the dissolution of Re and B from the borosilicate glass"*.

APPENDIX D

Draft manuscript titled *"Remediation Research and Technical Support for the Waste Isolation Pilot Plant"* authored by Johnbull Dickson, Yelena Katsenovich, Juliet Swanson.

APPENDIX E

Draft manuscript titled *"Engineered Media for Mercury Removal in the Presence of Dissolved Organic Matter"* authored by Johnbull Dickson, Caridad Estrada, Yelena Katsenovich, Leonel Lagos, Alexander Johs, Eric Pierce.